

# Assessing alongshore variability of intertidal channels at Noordwijk by means of LiDAR measurements

by

Xander Joosse

to obtain the degree of Master of Science

at the Delft University of Technology,

to be defended publicly on Thursday August 26, 2021 at 15:30.

Student number:	4273184
Project duration:	September 1, 2020 – August 26, 2021
Thesis committee:	Dr. ir. S. E. Vos, TU Delft, supervisor
	Dr. ir. S. de Vries TU Delft
	Dr. R. C. Lindenberg, TU Delft
	Dr. ir. A. J. H. M. Reniers TU Delft



# Abstract

In order to understand the long term behavior of intertidal ridge-runnel systems high resolution spatial and temporal data covering extended periods of time is needed. Such datasets are still rare but are becoming more available through the usage of remote sensing technologies such as Argus and Terrestrial Laser Scanning.

A three month period (Feb – April 2020) with data obtained by laser scanning at the beach of Noordwijk, the Netherlands, has been analysed to evaluate the alongshore variability of rip channels. During this period varying weather conditions occurred. The timeseries consist out of snapshots taken around the occurrence of the lowest tidal water level each day, containing elevation data of an 1km alongshore section of the beach. Each scan in this timeseries is processed in order to remove noise, objects and correct for time dependent rotations. The spatial gaps in the scans present in the data as the result of flowing or standing water are interpolated using a 2D grid interpolation method.

The analysis is done using two different methods: a 1D-method using alongshore elevation transects, and a more advanced 4D-Object-by-Change based upon elevation changes over time. The 1D-method detected 44 rip channels that existed for multiple days, with an average alongshore migration rate of 1.55 m/day. The average spacing between rip channels was found to be 131 meters. The 4D-OBC detected less rip channel when compared to the 1D-method but did capture other morphological features such as runnels.

A comparison of the alongshore migration rates and the dominant wave and wind directions that during this period showed a correlation between wind and wave direction and the direction of the alongshore migration direction, however some exceptions are visible. Comparing this research to similar research and literature did show differences in the migration rates and rip spacing. These are explained by the different nature of both datasets (2D vs 3D) and methodology used in the detection of rip channels.





# Preface

This thesis is the result of almost a year of work doing research, programming, writing, having discussions and much more. During this period, working on a full-time individual project, I have developed myself into a more complete person acquiring new knowledge and skills. Working from home during the pandemic proved challenging with accommodating ups and downs.

Reflecting on the past year shows me how much I have learned on doing your own scientific research. Looking back on my progress made throughout the year I would have done a few things different. It is easy to get stuck at certain points in your research and loosing the overview of the bigger picture. This becomes particularly clear when working on the final stages of the Thesis. There are things I would have like to research further and in more detail, while there are also things that feel like they have been a waste of time. In the end I am proud of what I have achieved this year, even though there is still room for improvements.

Enjoy the read.

## Acknowledgments

I would like to take this opportunity to say a word of gratitude to all the people that have helped to get at this point. Starting with the people involved in guiding me through the graduation process.

First, I would like to thank my daily supervisor Sander Vos. Creating time every week for almost a year talking about and discussing my work steered me in the right direction. I'm great full that you made this time for me. I would also like to thank the other committee members, Ad Reniers, Sierd de Vries and Roderik Lindenbergh for their valuable input during our meetings. Furthermore, I would like to thank Katharina Anders for her time helping me understand her methodology and even providing me with some custom adjustments I have used in this research.

Of course, a special thanks has to go out to my family. Without the support of my parents and sister I would never been in this position. Their interest in my field of study and research taught me to explain the interesting topics of coastal engineering to people of other disciplines.

Furthermore, a word of gratitude towards all the roommates I have lived with in the past years. We have had some amazing times, varying from spending nights in the university library to going on memorable holidays. Having all of you around me during, especially during the pandemic, helped me out a lot.

Finally, an acknowledgment to all the amazing people I have met during my years of study. It have been some amazing years and I am grateful to have been able to spend this time in Delft with all of you.

*Xander Joosse  
Delft, August 2021*



# Contents

<b>1</b>	<b>Introduction</b>	<b>1</b>
1.1	Background . . . . .	1
1.2	Problem definition . . . . .	2
1.3	Objective . . . . .	3
1.4	Thesis outline . . . . .	3
<b>2</b>	<b>Literature Study</b>	<b>5</b>
2.1	The coastal region . . . . .	5
2.2	Intertidal morphology . . . . .	6
2.2.1	Intertidal bar formation and migration . . . . .	7
2.2.2	Rip channel spacing and migration . . . . .	10
2.3	3D behaviour of intertidal zone . . . . .	10
2.4	Permanent Laser scanning . . . . .	11
2.4.1	Basic working of a laser scanner . . . . .	11
2.4.2	Limitations and errors . . . . .	11
<b>3</b>	<b>Study Area</b>	<b>15</b>
3.1	Study site: Noordwijk aan Zee . . . . .	15
3.2	Data availability . . . . .	16
3.3	Data selection . . . . .	16
3.3.1	Period selection . . . . .	16
3.3.2	Interval selection . . . . .	18
3.4	Wave data . . . . .	19
<b>4</b>	<b>Methodology</b>	<b>21</b>
4.1	Data Preparation . . . . .	21
4.1.1	Time dependent rotations and reduction of data points . . . . .	22
4.1.2	Validation time dependent rotations . . . . .	23
4.2	Post processing . . . . .	26
4.2.1	Noise and object removal . . . . .	26
4.2.2	Local reference system . . . . .	26
4.2.3	Merging and rasterising data . . . . .	27
4.3	Spatial interpolation of intertidal area . . . . .	27
4.3.1	Radial basis function interpolation . . . . .	28
4.3.2	Comparison with GPS data . . . . .	29
4.4	1D Alongshore analysis . . . . .	31
4.4.1	Cross-shore location . . . . .	31
4.4.2	Channel detection . . . . .	31
4.5	4D-Objects-By-Change analysis . . . . .	33
4.5.1	4D-Objects-by-change method . . . . .	33
4.5.2	Application Noordwijk data set . . . . .	35
<b>5</b>	<b>Results 1D- and 4D-Analysis</b>	<b>37</b>
5.1	1D Alongshore analysis results . . . . .	37
5.2	Improved 1D alongshore analysis . . . . .	39
5.2.1	Varying cross-shore location . . . . .	39
5.2.2	Extended channel detection . . . . .	41
5.2.3	Classification of channels over time . . . . .	42
5.2.4	Improved 1D alongshore analysis results . . . . .	45

5.3	4D-Object-by-change analysis results . . . . .	47
5.3.1	Adjustments to 4D-OBCs method . . . . .	47
5.3.2	4D-OBCs Results. . . . .	49
5.4	Comparison between 1D- and 4D- Analysis . . . . .	51
<b>6</b>	<b>Discussion</b>	<b>53</b>
6.1	Data selection . . . . .	53
6.2	Data processing . . . . .	53
6.2.1	Noise and object removal . . . . .	53
6.2.2	Time dependent rotations . . . . .	54
6.2.3	Data rasterization. . . . .	54
6.2.4	Spatial interpolation . . . . .	54
6.3	Analysis . . . . .	55
6.3.1	1D methods. . . . .	55
6.3.2	4D methods. . . . .	56
6.4	Comparison with existing research and literature. . . . .	58
6.4.1	Comparison with previous research . . . . .	58
6.4.2	Comparison with literature . . . . .	59
6.5	Added value of laser scan data in the intertidal zone. . . . .	61
<b>7</b>	<b>Conclusion</b>	<b>63</b>
<b>8</b>	<b>Recommendations</b>	<b>65</b>
8.1	Improvements to results . . . . .	65
8.2	Continuation of research . . . . .	66
	<b>Bibliography</b>	<b>67</b>
<b>A</b>	<b>appendix A</b>	<b>71</b>
<b>B</b>	<b>appendix B</b>	<b>75</b>

# Introduction

## 1.1. Background

The Dutch coastline mainly exists out of sandy beaches and dunes as its primary coastal defence. On sections of these beaches distinctive morphological features can be seen, such as the intertidal ridge-runnel systems. These systems are continuously switching between being emerged and submerged as a result of the tidal cycle. A section of such a beach, located at Noordwijk (the Netherlands) can be seen in Figure 1.1. On this picture a typical ridge-runnel system is seen, on the left a runnel can be seen retaining water, this water flows back towards the sea (on the right) through rip channels. The dry sections of sand separating the runnel from the sea are referred to as intertidal bars or runnels.



Figure 1.1: Photograph of the beach at Noordwijk, the Netherlands during low tide (13 April 2021). On the right side of the image the sea is visible. On the left side standing water inside of a so called runnel is visible. Water is flowing from the runnel back toward the sea through a rip channel. The dry section of beach between the water masses are referred to as intertidal bars or ridges. (own image)

Sandy beaches have a self restoring mechanism. Beaches tend to erode during storm conditions where the submerged bar system migrates offshore and the beach profile flattens. During periods of low and mild wave activity sediment is transported back onshore, and a corresponding bar movement is observed. This is often referred to as the winter- and summer-profiles of beaches, and is relative well understood. However, the intertidal bar system shows more variability and is suggested to be an importance restoring mechanism on sandy beaches due to the large amounts of suspended sediments being transported in this area. Little is known about the 3D variability of these restoring mechanisms

even though research related to these features started as early as the nineteenth century [1]. Improved understanding of the development of intertidal bar systems is beneficial for coastal management as these features are a key factor in controlling beach elevation levels and play an important role in the sediment budget.

King and Williams published an article in 1949 containing a part of this early research and additional observations. In this paper a distinction is made between bar forming at non-tidal beaches, so called 'barred beaches', and tidal beaches named 'ridge and runnel' beaches [2]. From this point onwards, a lot of research has been conducted in order to gain more insights in the morphodynamics of beaches. However, most research mainly focusses around the developments of the cross shore movement of (semi) submerged ridges [3] and does not include the 3D variability in temporal and spatial behavior of these features.

In order to obtain more insight in the temporal and spatial behavior of intertidal features new measurement techniques are being used in the field of coastal monitoring. Permanent laser scanning allows to monitor morphology changes of beaches on time scales varying from hours up to years providing high resolution spatially data.

## 1.2. Problem definition

With the increasing popularity of building with nature solutions for coastal protections it becomes more important to monitor the behavior of the natural protections over time. In order to obtain a good insight in the temporal changes within the intertidal zone there is a need for high resolution temporal (small time intervals) and large spatial scale (xyz) data. Such data is relative rare as most previous research consisted out of high resolution temporal data but on a small scale, or vice versa.

Most research focuses on understanding the processes and morphologic response on the time scale of storm events and post storm recovery [4]. This research is confined to a specific location and short time periods (a few tide cycles) [5]. In these researches point or line measurements are used to construct 2D cross sections along the shore at a set interval, resulting in a spatially sparse dataset. The spatial sparse nature of this data lacks the ability to capture the spatial variability in wave and current fields, bathymetry, and beach morphology necessary to understand and properly characterize many of these processes [6].

Other research that spans large spatial area's often lacks the temporal resolution needed for detailed analysis. An example is the LiDAR based coastal surveying campaigns done by Miles et al. [7]. They used 17 years of yearly airborne LiDAR data to monitor the alongshore variability of a multi-bar ridge-runnel system. This research is promising but uses a temporal interval of months and therefore still lacks the temporal interval required for a more detailed analysis. Image capturing systems such as the Argus [6, 8, 9] and high resolution satellite spot imagery [10] have been used to capture morphologic changes on longer time scales with higher temporal resolution (daily interval). These imaging methods yield promising results but cant provide any accurate elevation data of the intertidal zone. Furthermore, the spatial resolution is still limited as a single pixel within the image represents around an 1x1m area [9].

In order to understand the long term behavior (months up to years) of intertidal bar systems, knowledge is required of the nearshore morphodynamic system. Such knowledge is best obtained from analysis of long time series of morphology and forcing conditions, rather than from short intensive field experiments [4]. The CoastScan project aims to provide measurements on varying spatial and temporal scales [11]. The current permanent laser scan (PLS) setup at Noordwijk provides topographic data in an accuracy range of centimeters on a hourly basis.

## 1.3. Objective

This thesis aims to validate the use of terrestrial laser scanning (TLS) for coastal monitoring of the intertidal zone. The application of TLS could provide data at the spatial and temporal scales required to analyse the intertidal zone in more detail. A measurement campaign at the beach near Noordwijk (The Netherlands) using a permanent laser scanner setup started collecting data of a 1km alongshore beach stretch at an hourly interval. The measurements started in July 2019 and are still ongoing up till this date.

The main research question of this thesis is formulated based around this dataset and is formulated as follows:

**How does the alongshore variability of channels in the intertidal zone develop on a time scale of months at a 1km section of the beach at Noordwijk**

In order to be able to answer this question a subset of research questions are formulated. The sub questions are focussed on the processing and analysis of the laser scan data and combining them with additional information sources. These additional questions are:

- How can rip channels be observed in the laser scan data?
- What is the temporal interval required to monitor alongshore morphological changes in the intertidal zone?
- How can rip channels be tracked in space and time?
- How do the result compare to previous research and literature?

## 1.4. Thesis outline

In order to formulate an answer to the research questions stated in the previous section, the thesis will be divided into 7 chapters (see Figure 1.2). The chapters are listed below, a brief summary of the expected content of these chapters is provided.

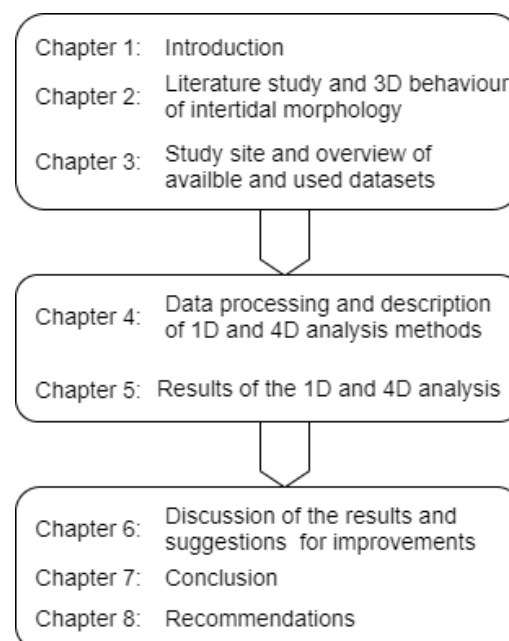


Figure 1.2: Overview of the structure of the thesis.

After the introduction the reader is familiarised with the topic of intertidal morphology. Chapter 2 describes the layout of the intertidal area and the processes that shape this region. Furthermore, relevant studies done covering the topic of alongshore variability are discussed. This is followed by the introduction of the study site and data availability at Noordwijk, done in Chapter 3. In this chapter the first sub question regarding the temporal interval is answered.

In the next chapter the methodology used for the analysis is explained. Starting with the processing of laser scan data, followed by the explanation for the detection of channels in the two analysis methods that are used, answering the second sub research question. In Chapter 5 the results of both analysis methods are provided and a comparison between the two is given.

The final part of the thesis consists out of the discussion of the results, explaining the limitations and how they can be improved. Based on the results a comparison is made between existing research and literature, answering the final sub research question. The conclusions and the answer on the research question, are presented in Chapter 7. The thesis ends with a chapter covering recommendations on how to follow up this research.



## Literature Study

In this chapter a study of the intertidal area is provided in order to describe the processes that dominate the formation and migration of the morphological features. The chapter continues with describing the 3D variability of the intertidal zone based on previous research. Finally a brief introduction into laser scanning is provided in order to familiarise the reader with the technology and its limitations.

### 2.1. The coastal region

Figure 2.1 shows a schematic cross-sectional view of the coastline present at the study site near Noordwijk, the Netherlands. In this figure the area that are important for this research are indicated. The horizontal dashed lines represent the Mean High Water Spring (MHWS) and Mean Low Water Spring (MLWS), the area of the beach located in between those lines is referred to as the intertidal zone. Within the intertidal zone morphologic highs, referred to as intertidal bars or ridges, and morphologic lows, consisting out runnels and channels, are located.

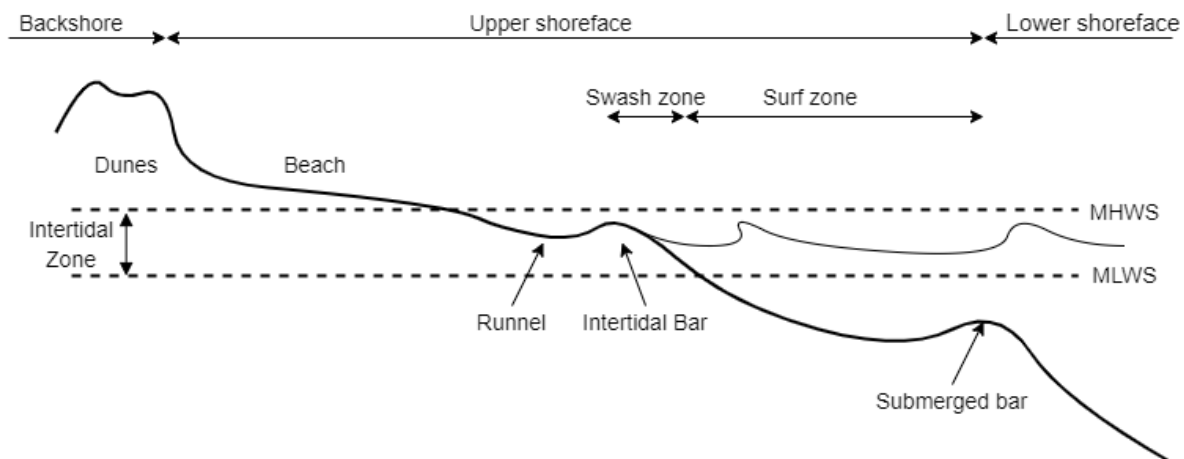


Figure 2.1: Cross sectional view of the coast.

During low tide the intertidal area is emerged and as the tide rises it gets submerged, this area corresponds to the location of the swash zone, which is defined as the region of the beach profile where there is intermittent fluid coverage or the time varying region extending from the point of bore collapse on the beach face to the maximum uprush limit [12]. The swash zone is characterized by strong and unsteady flows, high turbulence levels, large sediment transport rates and rapid morphological change [13]. The effect of swash zone processes on the beach slope is dependent on the equilibrium profile. When the beach face is flatter than the equilibrium profile the uprush transports more sediment than the backwash, resulting in a onshore transport and steepening of the beach profile. In case of a steep

profile, the backwash dominates the sediment transport and the profile becomes less steep. These processes are from importance for the behaviour of intertidal bars, and are discussed next in section 2.2. The subtidal zone which is permanently submerged as it is below the mean low water spring (MLWS) level. In this region submerged bars are present that can move under the influence of wave conditions. In the surf zone wave breaking starts to occur inducing turbulence in the water column. The sediments are stirred up and are transported by means of suspended and bed load.

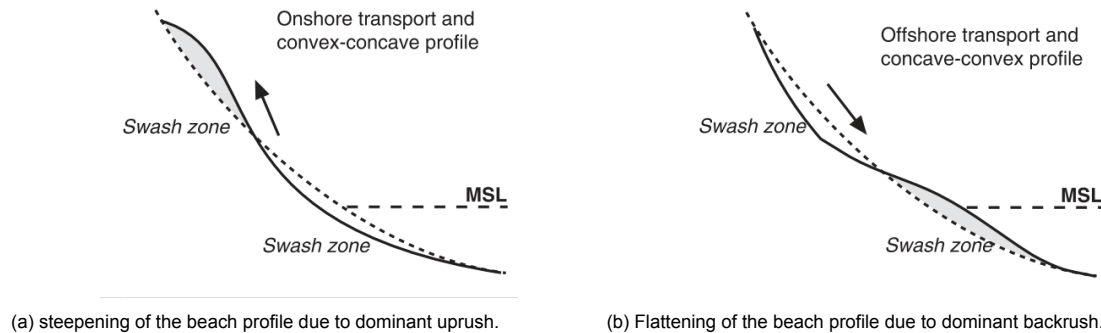


Figure 2.2: Beach face response to changing wave conditions. From Masselink and Puleo [12].

During energetic conditions, such as storms, submerged bars tend to move offshore as the offshore directed sediment transport due to undertow is dominant. This is explained by the higher and longer waves that are present during storms, increasing the orbital motion velocities at the bed and stirring up more sediments. During periods of milder waves, submerged bars tend to move onshore [14]. This can be explained by the non-linear relation between flow velocities and the sediment transport [15]. This process is also visible on seasonal time scales and is referred to as the summer- and winter-profiles. During the summer wave conditions tend to be milder and the onshore sediment transport is dominant while during winter wave conditions are more energetic and an offshore sand transport is present. The effect of this seasons on the cross shore beach profile is shown in Figure 2.3.

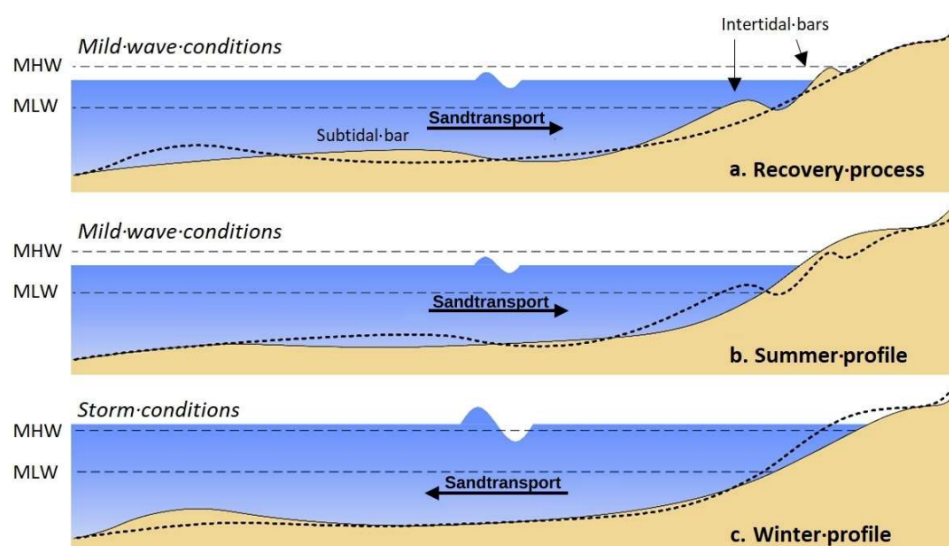


Figure 2.3: Cross-shore variability during different stages. The dashed line indicating the beach profile at the previous stage. From Vos et al. [11].

## 2.2. Intertidal morphology

Within the intertidal zone two different types of morphology can be observed. The first one are morphological highs, referred to as intertidal bars, and secondly morphological lows, referred to as runnels and channels. Intertidal bars are morphological highs situated between the mean low and high water spring levels on tidal beaches with a tidal range larger than 1m. They are aligned parallel or under

a small angle (see Figure 2.7) to the shore and may be dissected by shore oblique rip channels at quasi-regular intervals [16]. Between the intertidal bars and emerged zone shore parallel runnels can be observed. The runnels and channels facilitate the return flow of the water that overtops the intertidal bars introducing a 3D factor in the intertidal morphology.

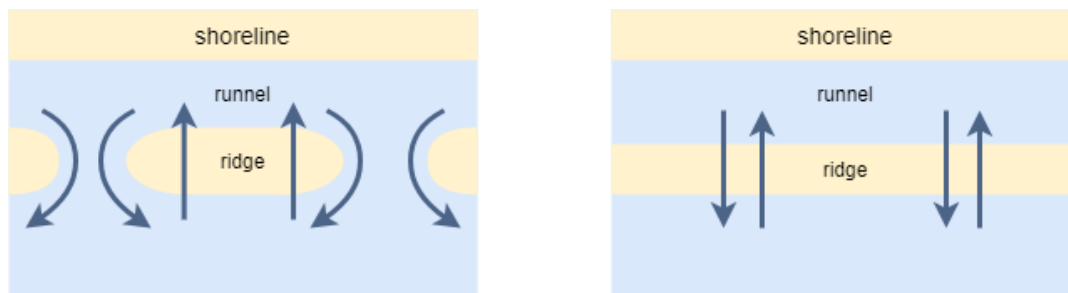


Figure 2.4: Left: Return flow trough rip channels. Right: Return flow over top of the ridge crest.

Intertidal bars are referred to in literature by various terms such as ridges, sand waves, and swash bars. Ridge-runnel systems are important for the beach recovery after storms and play an important role in the coastal sediment budget [5]. The formation of ridge and runnel morphology has not yet been resolved. The complicated sediment transport processes that drive the ridge-runnel dynamics are only poorly understood [5, 17]. Ridges and runnels are considered to be permanent features on beaches [2, 18], this does not mean that the morphology does not respond to changes in the wave conditions. The problem in determining the origin of ridges and runnels is in the permanent nature of the morphology [17]. Masselink [17] summarized three factors that contribute to the permanency of these intertidal formations. The first reason provided states that because of the large tidal range the morphological relaxation times are long. The effect of these long relaxation times is that there is not sufficient time to reach an equilibrium situation. Due to the changing tide, the hydrodynamic processes are only constant for a limited time. The second explanation is provided by King. Ridge-runnel systems are generally found along beaches that are located at a fetch limited coastlines. Fetch limited beaches are sheltered from extreme wave conditions, therefore extreme wave conditions that could flatten the ridge morphology are non existing. A third explanation, proposed by Wijnberg and Kroon [4], suggest that the offshore submerged bar morphology protects the intertidal ridge-runnel system. Wave breaking occurs on the lower part of the beach profile, protecting the upper beach from erosion.

### 2.2.1. Intertidal bar formation and migration

The formation of intertidal bars is not yet resolved but several hypothesis have been suggested. King and Williams [2] suggested that intertidal ridge formation is the result of waves trying to form an equilibrium in the swash zone. However, other studies disagree on the fact that ridges originate from the swash zone, or that they originate from the surf zone. Hine [19] monitored the berm development of beaches in which three stages are distinguished: neap-berm formation, ridge-runnel formation and berm-ridge formation. This works suggest that bar formation starts in the subtidal zone and moves onshore, forming an ridge-runnel system to finally process up on the beach to reinforce the berm. Research from Masselink and Anthony [20] found that the highest ridges occur just above mid-tide water level where the tidal non-stationarity is greatest. These findings suggest that ridges are the result of a combination of swash- and surf zone process acting across the intertidal zone.

van Houwelingen et al. [21] stated that intertidal bars are subjected to swash, surf and shoaling processes. The importance of each of these processes varies over time and is related to the water depth and time of inundation of the bars. The tidal water level is of importance for the evolution of the intertidal bars. During low tide the the swash processes dominate the evolution with a net onshore transport of sediments. Uprush deposits sediments on the beach slope resulting in accretion while backwash erodes sediments from the beach resulting in a offshore directed sediment flux. However, its a order of magnitude smaller than the onshore directed sediment flux, hence the net onshore transport [22]. When the uprush overtops the intertidal ridges the backwash is directed onshore as well and is deposited on the back slope of the ridge, reinforcing the formation process. During high tide, the intertidal bar becomes submerged and surf zone processes start to take over and a offshore sediment trans-

port is initiated. The tidal water level and the height of the ridges influence wave breaking, Guedes et al. [23] concluded that the influence of tidal water level, and its relation to wave breaking, might be a major process in controlling swash hydrodynamics on barred beaches under mild conditions. The morphological changes of bars under surf zone processes and swash action is relative similar. Surf zone processes are more prevalent and therefore have the largest influence on beach morphology. Swash action is significant when the (high) tide level is located on the intertidal bar. The influence of shoaling waves has an insignificant role in affecting intertidal bar morphology [21]. These findings are inline with the previous formulated hypothesis of Masselink and Anthony [20].

Onshore ridge-runnel migrations takes place when the ridge crest is overtopped by waves and the suspended sediments are deposited inside the runnel. The relative low flow velocities inside the runnel allow for sediments to settle, resulting in an onshore movement. As water levels inside the runnel increases, a return flow is initiated resulting in an outflow of water and sediments out of the runnel. The offshore directed return flow of water can occur over the top of the ridge crest or trough so called rip channels as shown in Figure 2.4 [5]. Ridge-runnel migration can be in the order of meters per day for slip-face bars, low-amplitude ridges and sand waves tend to migrate slower [16].

A conceptual model describing the cross-shore intertidal bar behavior along the Dutch coast is proposed by Vos et al. [24] describing 4 development stages: formation, migration, growth and destruction. In this model three different regimes is distinguished, being the run-up regime (during low water), the overwash regime (during rising or falling tidal levels) and the submersion regime (during high water). These regimes combined with mild or energetic wave conditions result in one of the four development stages. Figure 2.5 illustrates this conceptual model.


Development stage		A. Formation	B. Migration	C. Growth	D. Destruction
Wave conditions		Mild	Mild	Mild	Energetic
	1 <b>Run-up regime</b> <i>Sand transport dominated by swash zone processes</i>	Formation, if:  • Mild wave conditions • Significant tidal range		Horizontal growth	
	2 <b>Overwash regime</b> <i>Intertidal bar dominated by swash zone</i>		(Fast) onshore migration	Horizontal+ vertical growth	Destruction
	3 <b>Submersion regime</b> <i>Intertidal bar dominated by surf zone processes</i>				(Fast) destruction

Figure 2.5: Table illustrating the conceptual model describing the formation, migration, growth and destruction based upon the prevailing regime, from Vos et al. [24].

Different types of intertidal bars are observed in the field. The different types of bars are classified based on their morphology, Masselink et al. [16] divided them into three types (Figure 2.6): Slip-face bar, Low-amplitude ridges and Sand waves. The morphologic characteristics of these different types are summarized in Table 2.1. On the Dutch coast mainly slip-face bar systems are observed [4]. The orientation of these bars can vary from shore parallel to shore oblique, as can be seen in Figure 2.7.

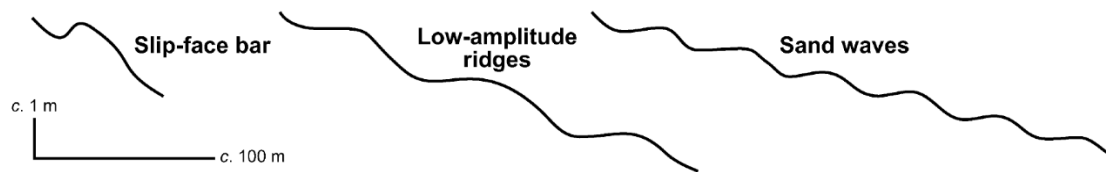


Figure 2.6: Diagram illustrating the three main intertidal bar types, from Masselink et al. [16].

	Slip-face bars	Low-amplitude ridges	Sand waves
Intertidal slope (degrees)	Gentle (2)	Very gentle (1)	Sub-horizontal (<0.5)
Seaward slope of bar (degrees)	Steep (3-6)	Intermediate (2-4)	Gentle (1-3)
Cross-shore shape	Strongly asymmetric	Weakly asymmetric	Symmetric
Height	>1 m	0.5-1 m	<0.5 m
Bar spacing	200 m	100 m	50 m
Number of bars	1	2-6	>6

Table 2.1: Morphologic characteristics of intertidal bars. From Masselink et al. [16].



Figure 2.7: Slip-face ridges near Noordwijk, The Netherlands. (a) Shore oblique slip-face ridges (May 26, 1995). (b) Shore parallel slip-face ridges (Dec 28, 1997). From Wijnberg and Kroon [4].

### 2.2.2. Rip channel spacing and migration

Rip channels are present on barred sandy coasts and appear as cross-shore features that facilitate off-shore directed flows to drain the runnel located behind the intertidal bar morphology. The development of rip channels over time is a topic that is still being researched extensively and several hypothesis have been proposed. A satisfactory predictor for the development of rip channel spacing and growth has not yet been proposed [25].

A hypothesis of self-organization has been suggested by Deigaard et al. [26], stating that rip channels emerge as a response to the random perturbations within the initial sea bed bathymetry as an result of the self-organizing nature of the coastal system. These self-organizing hypothesis are derived by means of numerical models. The self-organizing model states that the alongshore rip spacing increases with an increase in flow resistance, wave length and wave height. Furthermore, it is suggested that rip spacing depends on the cross-sectional area of a trough and the distance between the bar crest and shoreline [26]. Other research, conducted by Calvete et al. [25], suggests a relation between rip spacing and the water depth over the intertidal bar crest. Field observations do often not match with the suggested relations for the development or rip channels [27].

Another hypothesis suggests a coupling between the intertidal bar morphology and the submerged bar morphology. It is stated that the rip channels within the outer submerged bar allow for higher waves to reach the intertidal morphology resulting in wave height variability and set-up gradients. A cell circulation pattern is created and rip channels on the intertidal bar are present out of phase with the submerged rip channels. Quartel [9] used 15 months of Argus video observations at Noordwijk aan Zee (the Netherlands) researching this relation between the subtidal- and intertidal-bar rip spacing. This research revealed a coupling between the subtidal- and intertidal-bar spacing and a coupling with hydrodynamic parameters. The number of rip channels increases with incident wave height, the migration of channels was found to match the anticipated direction of the alongshore current.

Besides the differences between the hypothesis and the field observations an additional issue is addressed by Brander and Cowell [28]. Brander and Cowell [28] state that the lack of highly descriptive definitions of of geometric dimensions of rip-channels (width, relief, depth and cross-sectional area) make comparisons between research difficult and subjective. They relate this issues to the problem of obtaining measurements within the surf-zone.

### 2.3. 3D behaviour of intertidal zone

The 3D behaviour of intertidal bars has gained interest of the research community in recent years. Long term 3D bar evolution is challenging to study due to the difficulties in obtaining high resolution measurements over large temporal and spatial scales [7]. When studying the 3D variability of intertidal bar systems a difference is made between the ridges, runnels and rip channels. The processes dominating the formation and migration of ridges differ from those that influence the location of the runnels and rip channels [29]. Ridges are commonly dominated by cross shore processes in the surf- and swash-zone while runnels are dominated by shore parallel processes such as currents [21, 29].

Most studies in the intertidal zone focus on the development of the bar system, however the importance of the runnel system can not be discarded as these are important to the sediment distribution in the intertidal zone. The 3D variability of the intertidal zone is dependent on the dominance of cross- and along-shore processes over each other, combined with the seasonal variation in wave-energy conditions [21]. Only limited research and monitoring has been done at time scales from months up to years. This can be directly related to the difficulties of conducting measurements in the intertidal zone. New survey techniques such as LiDAR provide 3D information on coastal morphology which traditional survey methods can not obtain.

The long term monitoring of bar systems is necessary because long term wave non-linearities influencing the sediment transport impacting bar evolution can make bar behaviour hard to predict. The non-linearities in the underlying hydrodynamic and sediment transport processes are not cancelled out on the larger and longer scale of sandbars, but continue to affect the predictability of long term trends in sandbar behaviour. [30]

Miles et al. [7] studies 17 years of airborne LiDAR data of a multi barred beach on the northwest coastline of England. The temporal spacing between the surveys varied from three months up to ten months with a gap of nine years. Miles et al. [7] stated that a substantial amount of alongshore variability can be seen and that the cross-shore drainage channels show more variability than the bars themselves. The research concluded that a pattern of onshore migration is clear, narrowing and steepening of the bars was observed and was related to the effects of wave shoaling. The researchers acknowledge that the temporal irregularity of their data limits the analysis and suggest a bi-annually LiDAR survey (winter and summer respectively) close to low spring tide would improve the research.

Other surveying systems such as Argus that make use of shore based optical observations are used to obtain information about nearshore morphology, estimations of bathymetry, beach slopes and to quantify shoreline changes over time [6, 31]. However, Argus can not provide highly accurate data on beach elevations or water surfaces. Quartel et al. [8] developed an object-oriented extraction technique to extract beach morphology from video images, as provided by the Argus system. Using a maximum likelihood classification the data segmentation for dry, wet and water areas is done. The paper shows a proof of a concept that can be used for tracking of morphologic features but does not provide an analysis of these features. However, the workflow presented provides insights than can be applied to LiDAR data.

## 2.4. Permanent Laser scanning

Permanent laser scanning is a new and promising tool to observe and analyse natural variations at short time-scales for extended periods of time in order to monitor coastal processes [11, 31]. The CoastScan project is an example of the application of this new technology. A measurement campaign of 8 months has been done at Kijkduin and currently a measurement campaign is done at the beach of Noordwijk. The project makes use of a Riegl VZ-2000 long range 3D LiDAR (Light Detection and Ranging) scanner that is located on top of the hotel at Noordwijk. The position of the laser scanner does not changed during the period of the measurements, this is a so called Permanent Laser Scanning (PLS) set up. This PLS executes a scan once every hour of the day.

### 2.4.1. Basic working of a laser scanner

Laser scan measurements are based on three basic attributes of laser light: unobscured light travels in a straight line, the velocity of light travelling in space is known, and the light produced by laser is typically only a single wave length light and is therefore easy to detect [32]. Using the principle of time of flight the distance to an object can be determined. The distance is calculated by the speed of light multiplied by the travel time divided by two. Multiple pulses are used to measure the distance of one point, by applying a least squares fitting the reliability is improved. The measured distance is combined with the horizontal and vertical angle of the scanner to create a 3D point cloud. This process is often not done by the scanner itself but by means of a computer program due to the computational power required for this conversion.

### 2.4.2. Limitations and errors

Terrestrial laser scanners can provide accurate measurements on elevation data, effected by equipment, setup and processing. However, the quality laser scanning is affected by noise. Soudarissanane et al. [33] assessed the quality of individual points in a point cloud. Four main factors can be distinguished: scanner mechanism, atmospheric conditions and environment, object properties and scanning geometry. These four factors are discussed in more detail.

The first source of errors is related to the scanner mechanism. This factor includes errors as the result of hardware, calibration, and settings. Internal rotations of the mirror and axis misalignments induce measurement errors that increase over distance. Additional errors can be induced by small deformation within the frame or building on which the scanner is mounted [11] These errors can be eliminated in the post processing of the data by use of reference objects. Secondly, the atmospheric conditions and environment such as humidity, temperature and pressure variations can influence to quality of the measurements. Water particles in the air can reflect or diffract the light. Furthermore the time of day at which the scan is taken further influences the quality, the different lighting intensities influence the reflection of the laser light on the surfaces.

Friedli et al. [34] studied atmospheric refraction of terrestrial laser scanning on long range. The deflections caused by atmospheric refraction can be in the order of a few decimeters over a distance of a kilometer. Figure 2.8 illustrates the findings of the research. Vertical beam deflection is the dominant factor for errors in measurements on a distance of kilometers. Furthermore, Friedli et al. [34] concluded that correction for this vertical refraction is not possible and suggest that scans should be taken in a window where atmospheric disruptions are minimal.

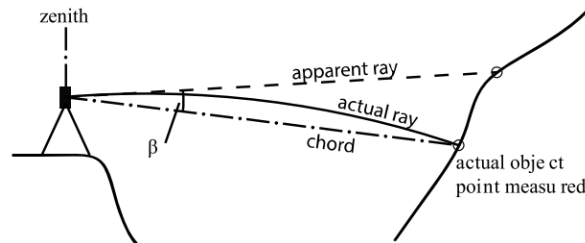


Figure 2.8: Vertical refraction of a laser ray as a result of atmospheric refraction, from Friedli et al. [34].

The third factor is related to object properties. The surface of objects have different reflectivity and roughness properties, the reflection depends on the relation between these properties and the wavelength of the scanner. Finally, the scanning geometry, the placement of the scanner relative to the area of interest influences the local point density and incidence angle. Laser light is divergent, meaning that the footprint of the laser beam increases over distance (Figure 2.9). Even though the lasers used for the practice of scanning have a small divergence the size of the footprint increases resulting in a lower point density over distance. This effect results in a lower accuracy.

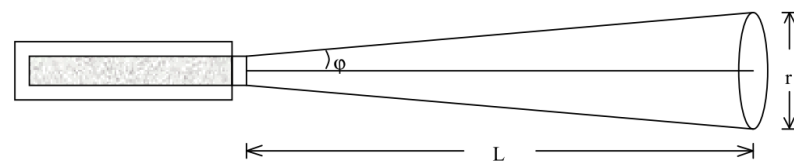


Figure 2.9: Laser beam divergence, from Angelopoulou and Wright [32].

By selecting a favourable location for the scanner the incidence angle can be lowered resulting in a smaller footprint. An increase of the footprint results in a weaker return signal. Figure 2.10 shows the differences of the footprints and its energy distribution between a perpendicular laser ray and an laser ray that hits the surface under an angle. This topic has been studied in more detail as part of the CoastScan measurement campaign at Kijkduin (the Netherlands) by Vos et al. [11]. In their work the influence of distance, incidence angle and horizontal angle on the laser footprint size and shape is researched. Figure 2.11 shows these effects on the footprint, furthermore a reduction of point density over distance is observed.



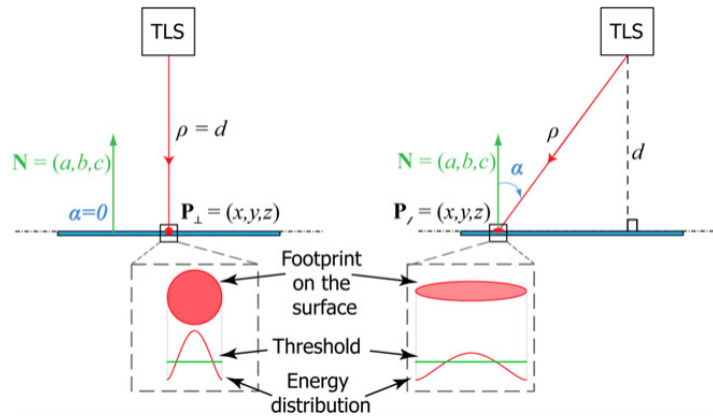


Figure 2.10: Influence of angle of incidence on reflection and shape change of footprint, from Soudarissanane et al. [33].

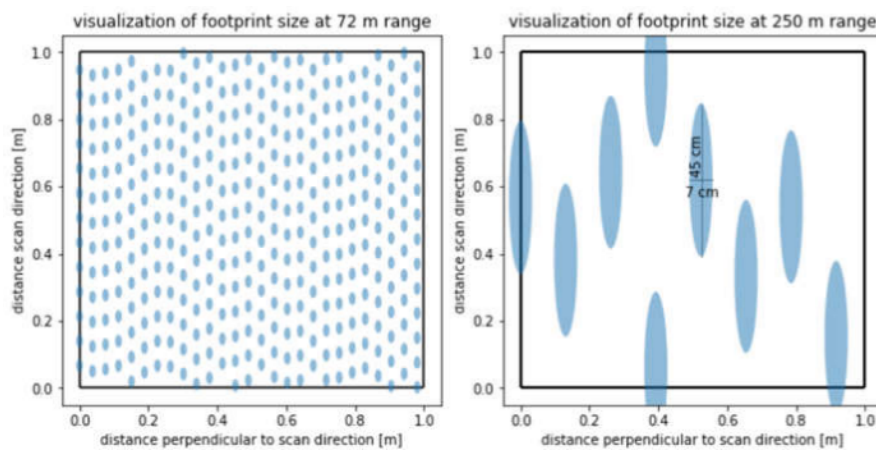


Figure 2.11: Influence of angle of incidence, horizontal angle and distance on the shape and size change of footprint. A change in point density is visible. From Vos et al. [11].



# 3

## Study Area

This chapter provides information on the study site and the data used in the research. A description of the laser scanner measurement setup is provided and an oversight of the state of the coastline at the site is given. The process regarding the period selection and interval of data that will be analysis is elaborated upon.

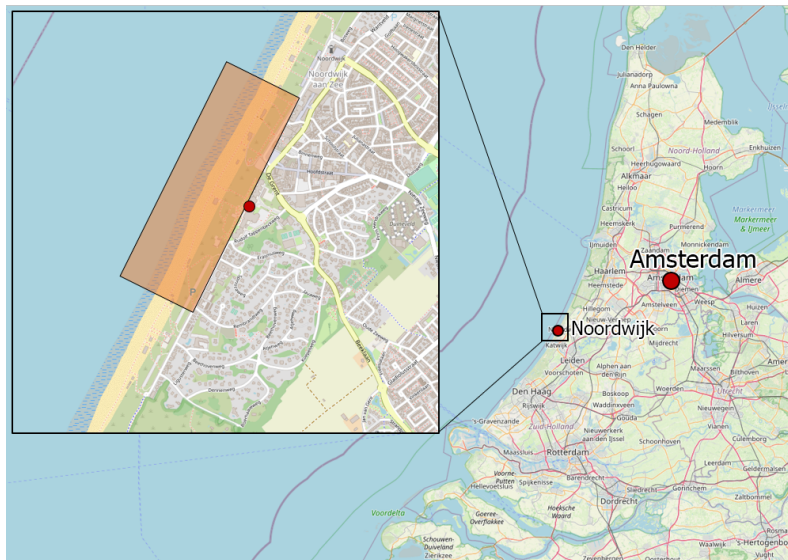
### 3.1. Study site: Noordwijk aan Zee

The study site is located at the coast of Noordwijk, South-Holland the Netherlands. Figure 3.1a shows an overview of the study site showing to location of the laser scanner (red dot) and the area covered by the scanner (orange box). The area is part of the central Dutch coastline and faces the semi-enclosed North Sea. It is located in between two inlets, the harbour of Rotterdam and the Noordzeekanaal, which allows access to the harbour of IJmuiden and Amsterdam.

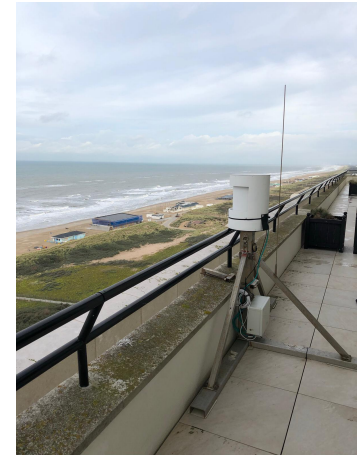
Data gathering at this site started in July 2019 as part of the CoastScan project [3]. A laser scanner is mounted on the balcony of hotel Huis ter Duin and gathers laser scans of the beach and dunes on a hourly interval. Theses scans cover about 1km of the beach in longshore direction. Figure 3.1b shows the setup of the laser scanner on the balcony of the hotel. The mount of the scanner is clamped to the building in order to reduce movement of the equipment. The CoastScan project uses a Riegl VZ2000 scanner placed in a protective housing to protect it from the environment.

The coastline in this area is characterized by two well developed subtidal bars and the presence of one intertidal bar [35]. During low energy conditions a secondary intertidal bar can form on the existing intertidal bar morphology [9]. The beach is classified as microtidal with semi-diurnal tidal cycle. Meaning that is has a limit tidal range and low-high water twice every 24:50h. The tidal range has maximum of 1.8m during spring tides and a minimum of 1.4m for neap tides [36] . The tidal flow along the Dutch coastline results in a net northwards directed longshore sediment transport. Furthermore, the beach consists out of well sorted sediment with grain sizes between 250 - 350  $\mu\text{m}$  (Van Bemmelen CE. 1988)

On the upper part beach are several permanent structures located. During high energy wave conditions, such as winter storms, artificial sand dunes are constructed in front of these building in order to protect them.



(a) Location of the study site.



(b) Laser scanner setup at the balcony of hotel Huis ter Duin.

Figure 3.1: Overview of study site and location of the laser scanner at Noordwijk beach (The Netherlands).

## 3.2. Data availability

The data used in this research is obtained from three sources. A brief summary of the contents of each dataset and its source are listed below.

- **Laser scan data:** laser scan data of the beach at Noordwijk is available through the CoastScan project, this dataset is not public accessible. Data gathering started in July 2019 and continues up to this at the time of writing. The continuous hourly data has interruptions during periods where equipment malfunctioned or maintenance was done.
- **Weather data:** data on the topic of wind velocities and directions, rainfall and hours of sun per day were acquired from the public accessible database of the KNMI (The Royal Netherlands Meteorological Institute). The data is obtained from the KNMI weather station located at Hoek van Holland, roughly 30km away from the study site. This measurement station is chosen due to its location along the Dutch coastline and relative close proximity to the study site.
- **Tidal data:** tidal data is used for the selection of period of low tide. The tidal data is obtained from the public accessible dataset of Rijkswaterstaat (Ministry of Infrastructure and Water Management) at the measurement station at harbour of Scheveningen. This station is located about 20km to the South of Noordwijk.
- **Wave data:** information on the daily average significant wave height, wave period and direction are obtained from Rijkswaterstaat. This information is obtained by a wave buoy located at the shipping lane the IJgeul (roughly 25km off shore from IJmuiden (the Netherlands)). This wave data is used for the correlation between the alongshore movements and forcing conditions.

## 3.3. Data selection

The selection of data for analysis is based on weather data and is done in two steps. First, a time window is chosen in such a way that multiple weather conditions occur during this time frame. With a period for analysis established the time interval at which the data is analysed is chosen.

### 3.3.1. Period selection

Previous research on the topic of permanent laser scanning has pointed out the influence of weather and atmospheric conditions on the quality of the data [34]. The presence of water particles in the air are one of the most important influences on the data quality. Days with significant amounts of rain or fog can be expected to provide poor data quality or in some cases no data at all. In order to assess the impact of quality differences on the developed methodology a period of varying weather types is

selected for analysis. The period containing the months February, March and April shows a variation of different weather types and is therefore selected for further analysis. In Figures 3.2 and 3.3 this selection is indicated by section between the red dashed lines. During the selected period there is no scan data available from April 6th up to April 13th due to malfunctioning of the equipment.

Figure 3.2 show the daily data of rain and sunshine conditions during the period of January up till June 2020. The top graph shows the rainfall hours per day and the bottom graph shows the amount of sunshine expressed in percentage of maximum possible hours of sunshine. The first half of the selected period, February and the first half of March, experienced large amounts of rainfall and only limited hours of sun. In contrast, during the second half of the selected period there was almost no rainfall and many days with more than 90% sun.

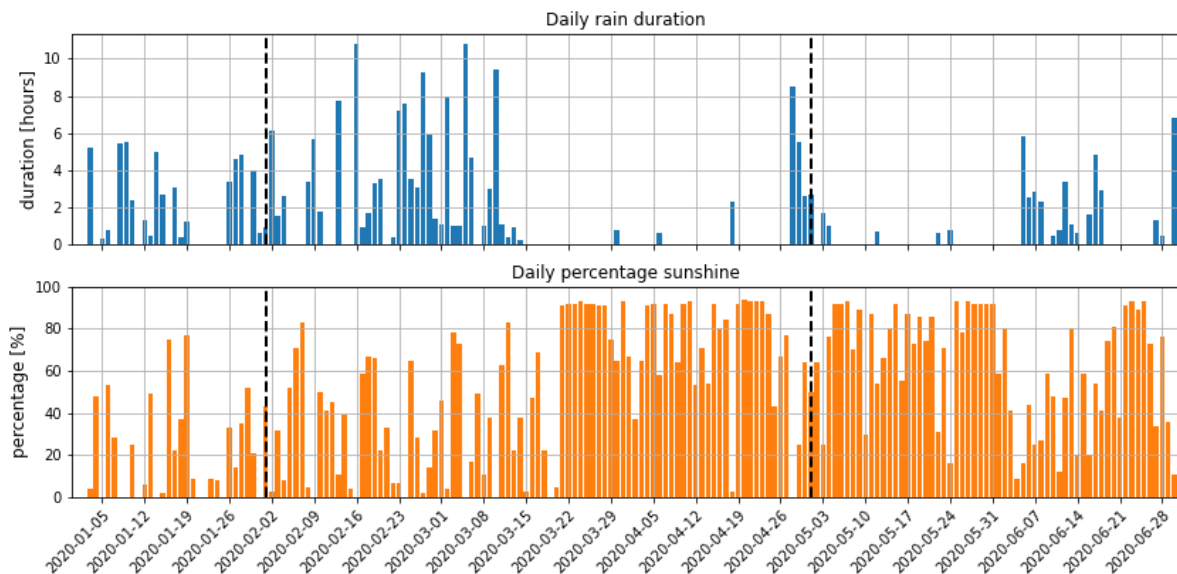


Figure 3.2: Weather data of KNMI weather station at Hoek van Holland for period January - June 2020. Vertical dashed lines indicated the selected period (February - April) Top figure displays the summation of hours where rainfall occurred for each day. Bottom figure displays the daily percentage of sunshine between sunrise and sundown for each day during this period.

Figure 3.3 visualizes the wind data for the same period. In the top figure wind velocities are shown, a distinction between the daily mean velocities (blue) and the maximum velocities during the day (green) are made. The bottom figure shows the corresponding daily averaged wind direction expressed in degrees (180 degrees is South, 360 degrees is North). The wind velocity and direction are important to take into account due to their influence on the water level. Wind directions directed onshore, in between South-West and North-West, result in an increase of the water level which directly impacts the area of the intertidal zone that is visible on the laser scan data. On the other hand an offshore directed wind results in a water level set down and therefore a larger part of the intertidal area becomes visible on the scan.

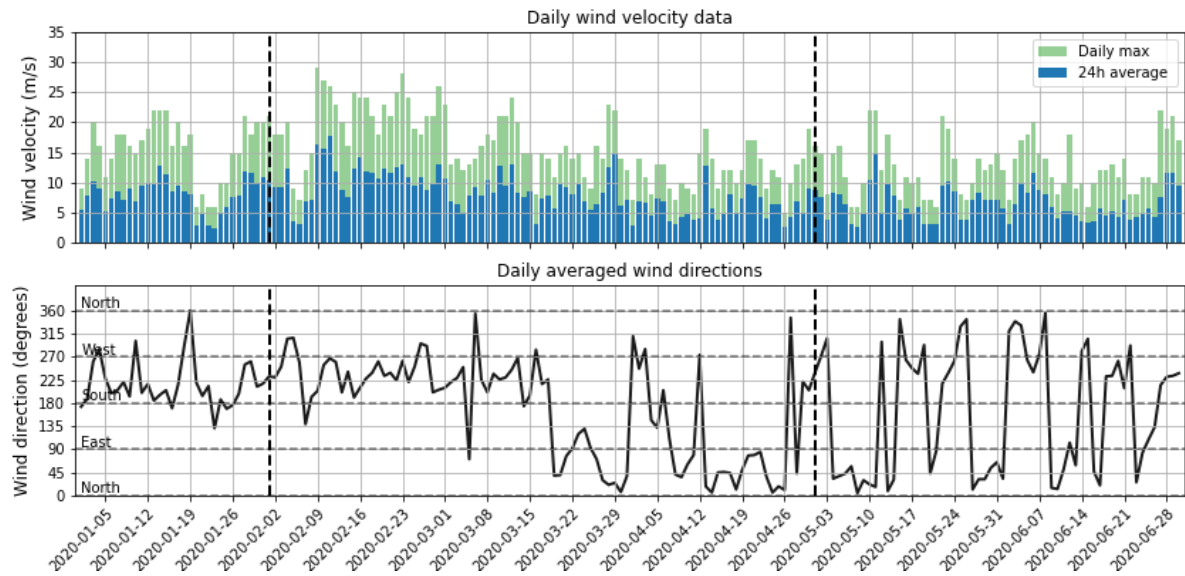


Figure 3.3: Wind data of KNMI weather station at Hoek van Holland for period January - June 2020. Vertical dashed lines indicated the selected period (February - April) Top figure displays the maximum and averaged wind velocities for each day. Bottom figure displays the dominant wind direction for each day.

### 3.3.2. Interval selection

The interval at which scans are assessed is determined based upon the tidal cycle. As stated in the previous section, the permanent laser scanning set up provides data on a hourly interval. However, due to the nature of the intertidal zone only few of the scans taken each day cover the area of interest. Only during the periods of low water sections of the intertidal area become visible. The semi diurnal tidal cycle results in two moments of low water each day with different amplitudes, this can be seen in Figure 3.4. The difference between these can be as large as 30cm which can result in significant lower coverage of the area. The difference in amplitude is not constant and varies during the tidal cycle.

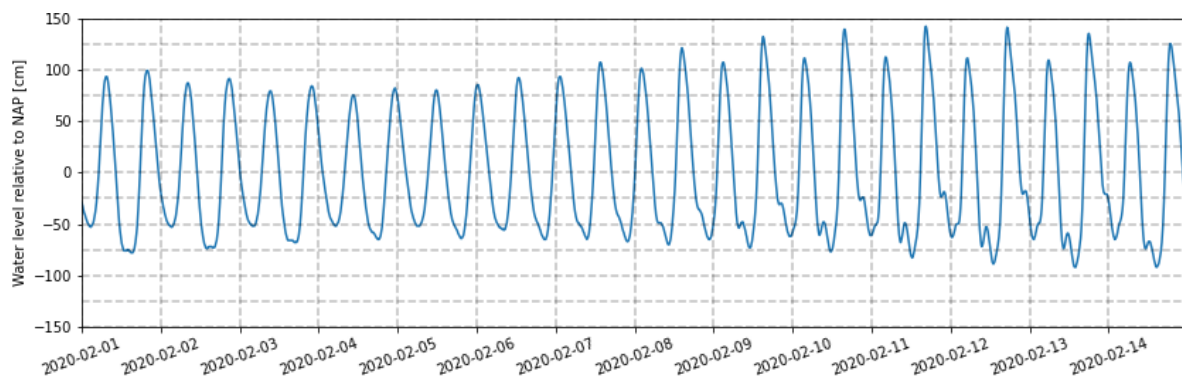


Figure 3.4: Tidal amplitudes during period 1 up to 14 February 2020, showing clear differences within the amplitudes for successive tidal cycles.

The moment at which the lowest water occurs does often not coincide with the time at which the hourly scans are taken. By combining two scans, one taken before and one taken after the moment when the lowest water occurs, the coverage of the area is maximised. This approach results in a maximum time gap of 30 minutes between low water and the timestamp of the scan. The differences in the morphology of the two consecutive scans that are combined can be argued to be negligible compared to the timescale of weeks up to months that is being researched.

### 3.4. Wave data

The wave data is obtained from a wave buoy located at the shipping channel (the IJgeul) near the harbour of IJmuiden. This wave buoy is located 25 km offshore, the water depth at this location around 20 meters. Measurement on wave height, wave period and wave direction are done in a 10 minute interval, these values are averaged on a daily interval for the application in this research. Figure 3.5 shows the daily average significant wave height ( $H_s$ ) and the corresponding wave period. Figure 3.6 shows the daily averaged wave direction.

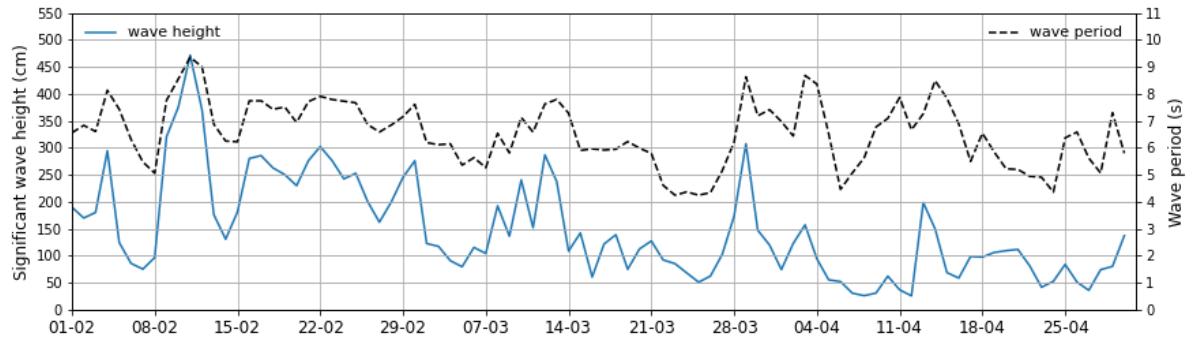


Figure 3.5: Daily averaged wave heights (blue line) and corresponding wave period (dashed black line) for the period February - April 2020.

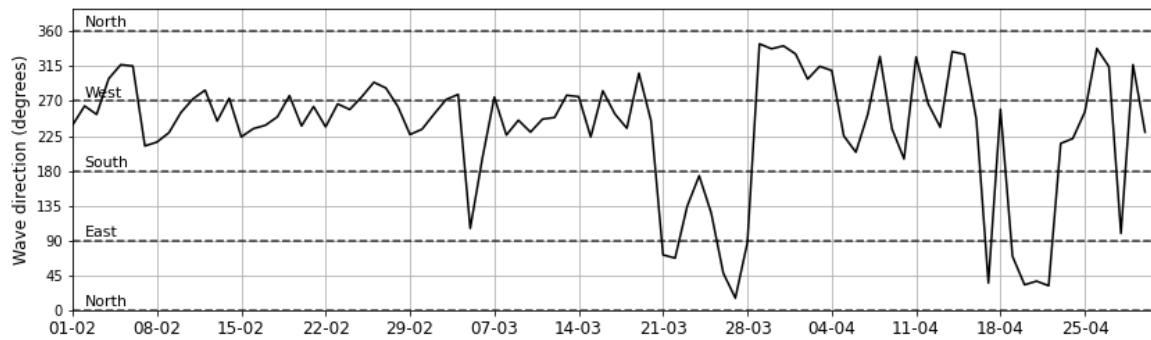


Figure 3.6: Daily averaged wave direction for the period February - April 2020.





# Methodology

This chapter describes the workflow of processing laser scan data. Furthermore, it explains the methodology used for the two analysis that are done in this research.

## 4.1. Data Preparation

Before an analysis can be done is is needed to process and validate the data obtained from the laser scanner. Figure 4.1 shows the basic infrastructure for the storage of the data obtained by the laser scanner. The hourly output of the scanner is stored on the data servers of the TU Delft. The data which is determined to be used in the previous chapter has to be manual selected from the server and downloaded.

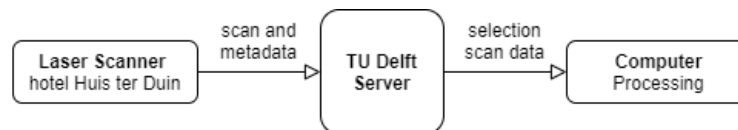


Figure 4.1: Scheme of the workflow

In Figure 4.2 visualises the workflow of processing and validating the data. For each of the steps in this diagram a brief explanation is given.

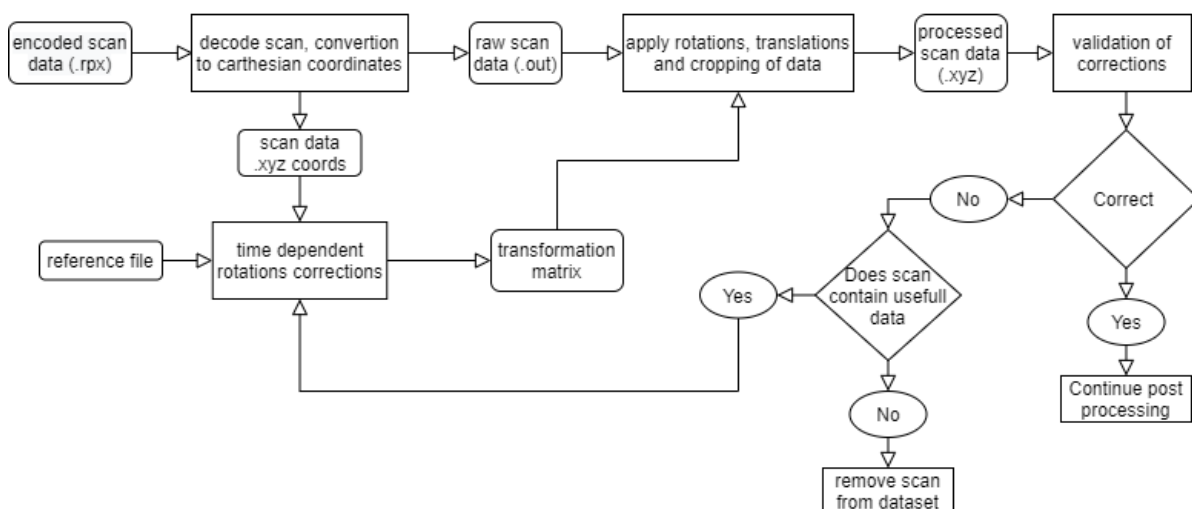


Figure 4.2: Workflow of the processing of laser scan data.

### 4.1.1. Time dependent rotations and reduction of data points

The laser scanner describes a point in space by means of two angular rotations and a distance, which is determined by the travel time of multiple laser pulses and the speed of light. For each data point several attributes are provided, such as reflection, amplitude, range and deviation. *Riegl Decode* allows for basic filtering of these attributes and is used to filter based on reflection. Previous research using the same laser scanning equipment has shown that reflection values larger/smaller than -20dB can be classified as noise and are removed in this first step. The program converts the file that is outputted by the scanner to xyz-coordinates.

Due to weather conditions such as strong winds movement of the equipment is possible resulting in a tilt of the scanner. These deviations are small but result in significant errors at longer ranges, these errors are in the order  $\mathcal{O}(0.1m)$ . Another source of rotational errors is present as a result of rotations in the equipment itself. The laser scanner makes use of a very fast rotating mirror, this mirror rotates along a horizontal axis and has tight tolerances but is not perfect. In order to correct these errors a time dependent rotation matrix can be derived by comparing the data with a reference scenario, using this matrix data is rotated. The process behind the time dependent rotations consists out of three steps (see Figure 4.4) and is explained in more detail below.

A scan from 11-07-2019 is used as reference data, this scan is manually corrected to be as accurate as possible. From the reference data and the data that needs to be corrected (from now on referred to as 'moving data') three area's are selected in which the objects can be considered immovable. These area's are: a part of Hotel Huis ter Duin, Breakers Beach House and a building to the south side of the Hotel. Figure 4.3 shows the location these three area's. Currently only two of those area's are used in the correction method, being the Breakers Beach House and the section of a wall and roof of a building in the south.



Figure 4.3: Three reference area's used for the correction of time dependent correction, indicated by the red boxes.

In the first step of the corrections an iterative closest point (ICP) algorithm is applied. Down sampling of the point clouds is needed to reduce the overhead of the calculations. The algorithm pairs points based upon shortest distance between the moving data point cloud to the reference point cloud. Using a root mean square point to point distance metric minimisation, an estimation for the combination of rotation and translation is made. Applying the rotations and translations and repeating this, iterative, process a transformation matrix is returned. The ICP algorithm does not yield a perfect result and minor adjustments are needed. Therefore two more steps are applied, both steps lean on the same concept of a difference in the centre location of the objects.

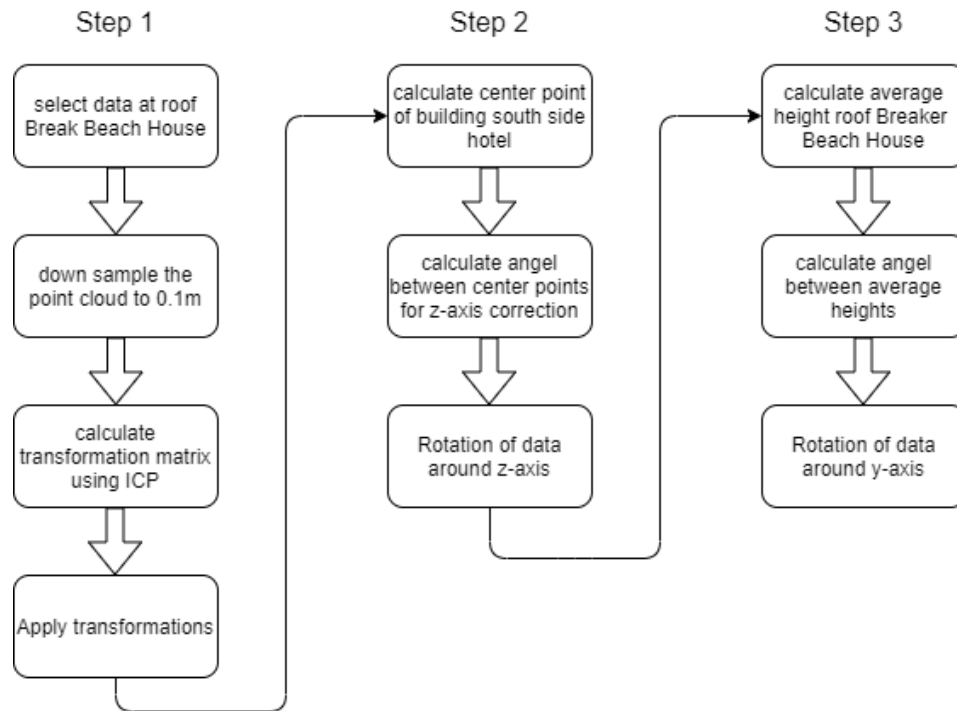


Figure 4.4: The workflow for the time dependent rotations correction, consisting out of three main steps.

Step 2 compares the centre location of the wall of the building south of the hotel. This step checks the difference in the z-values (elevation) at this point. Calculating the vertical angle between the centre points of the reference data and the moving data and the laser scanner an angular rotation is applied. In the last step, step 3, the same concept is applied to the roof of the Breakers Beach House. Using the centre point of the roof a rotational correction in the y-axis is applied.

Besides the corrections and translations the data size is reduced by cropping the scan to the area of interest. This research is focussed around the intertidal zone and a large area of the data in the scan is irrelevant and can be removed. This was not yet possible in earlier steps as the data in those areas was required for the detection of the time dependent rotations. Cropping the data to the intertidal zone reduces the amount of data points significant. A full scan contains just shy of 8 million data points where the cropped version is just below half a million, a reduction around 90% of the original data points is achieved.

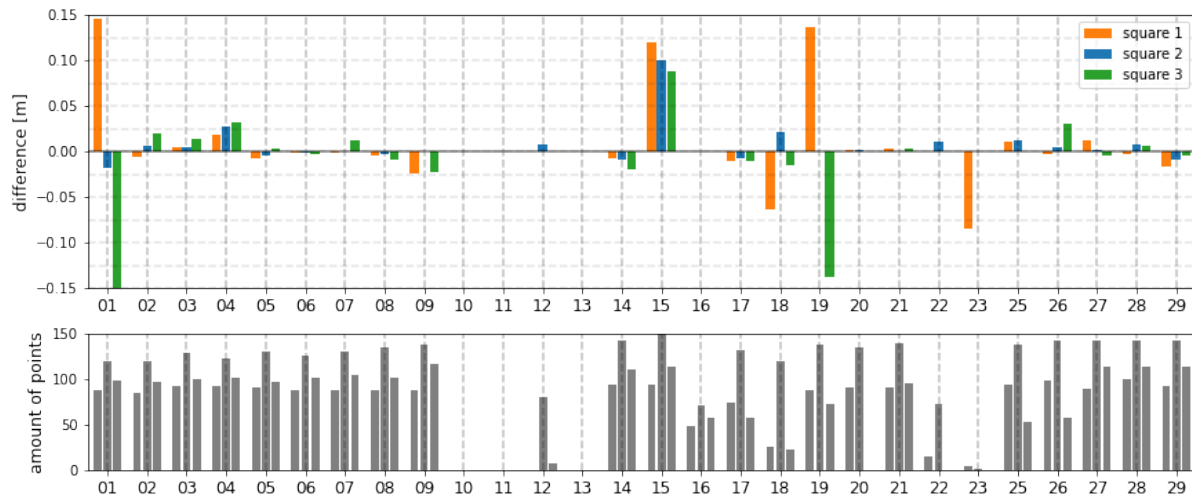
#### 4.1.2. Validation time dependent rotations

Validation of the rotations is done by comparing average height profiles in three sections on the beach between two consecutive scans for each day. These three sections are located, from the perspective of the scanner, on the left-, middle-, and right-side. Comparing the heights at three different locations allows for evaluation of the plane in which the data points are located. For example, if the average height on the left side are to lower and on the right side to higher while they are matching in the middle it can be concluded that the entire scan is tilted around the y-axis (cross-shore direction).

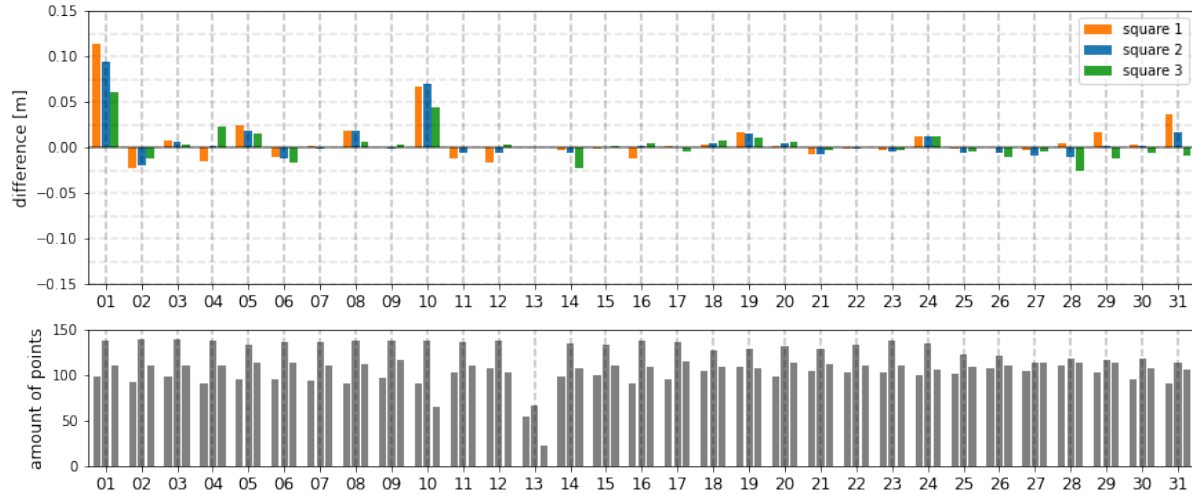
Figure 4.5a, 4.5b and 4.5c display the results of the height comparison between two consecutive scans at one day for the three area's on the beach for the months February, March and April respectively. In each figure the these height differences are combined with the amount of points that are located in each area. In some cases the height error can be related to the limited amount of data availability in the area. From the Figures a few distinctive outliers can be observed, however, it becomes clear that for most of the scans within an acceptable range of a few centimeter. The outliers can be classified as three different error types related to tilt, elevation and data availability.

- **Tilt:** elevation profile on the left side contradicts the elevation profile of the right side. This error can be observed in the data on 1 and 19 February, in both cases the left side of the beach shows an increased average height whereas the right side shows a decreased average height.
- **Elevation:** the elevation of the entire scan is increased or decreased. This type of error can be observed in the data on 15 February ,and 1 and 10 March.
- **Data availability:** the average height comparison shows a deviation combined with only limited data points used for the comparison. This can be observed in the data on 18 and 23 February. During the end of April (25 up to 30) a pattern is visible where the deviations in square 2 (the middle) are larger than on the sides, this is related to the limited amount of data points in this square compared to the two outer squares.

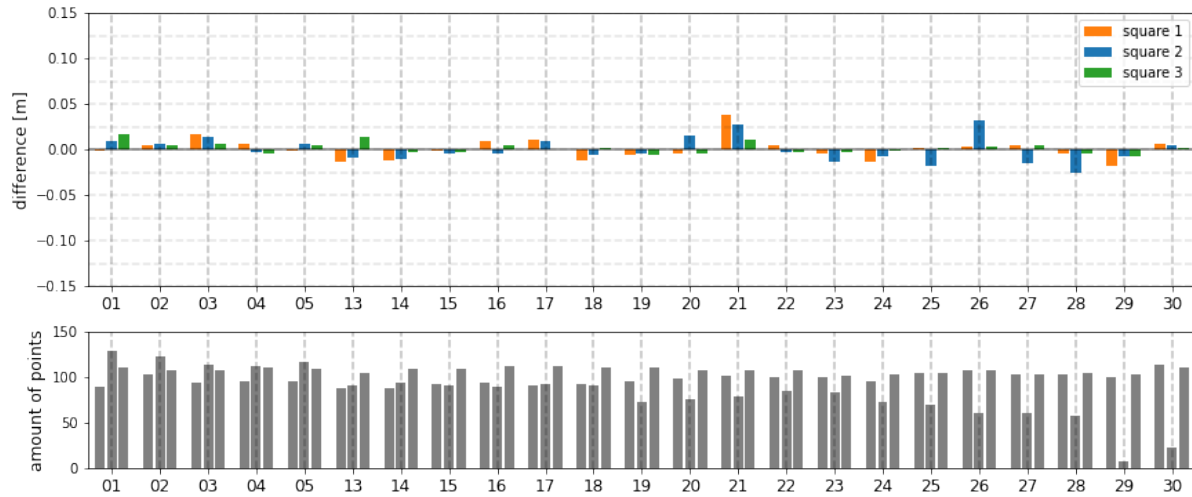
The limited amount of processed data containing errors are manually assessed to determine if they need to be corrected or that they can be dropped. Not all scans contain relevant information of the intertidal zone. In the case that the considered scan does contain relevant information but contains an error in the time dependent rotation correction a manual correction can be applied.



(a) Height differences for consecutive scans from one day for three areas on the beach during February.



(b) Height differences for consecutive scans from one day for three areas on the beach during March.



(c) Height differences for consecutive scans from one day for three areas on the beach during April.

Figure 4.5: Comparison between height profiles in the three squares for consecutive scans for each day during the period February - April. For each month, the top figure shows the differences in mean elevation for the data points within the relevant squares. The bottom figure shows the summation of data points used for this comparison.

## 4.2. Post processing

With the data converted to the correct format and corrected for deviations in the rotations several post processing steps are applied to prepare the data for analysis. These steps consist out of removal of noise and objects, creating a local reference frame, merging and rasterising data. This section elaborates on each of these steps.

### 4.2.1. Noise and object removal

The first step in the post processing consists out of the removal of noise. Noise removal is done by means of statistical outlier removal (SOR). The SOR filter removes points based upon the distance from a point to its  $k$ -neighbouring points in a comparison of the average distance between points in the entire point cloud. It rejects points that are located farther than this average distance ( $\mu$ ) plus a set times the standard deviation ( $n \cdot \sigma$ ). Both parameters can be set and adjusted to fit the dataset. It was found that a value of  $n=20$  and  $\sigma=2.0$  resulted in the best removal of noise for this dataset.

$$\text{max distance} = \mu + n \cdot \sigma \quad (4.1)$$

Noise removal does not take care of the removal of temporal objects such as people, animals or vehicles. In order to remove objects the LasGround filter is applied. This filter determines a plane that fits the general shape of sections in the point cloud and rejects points that are located too far from this plane. This concept is commonly used in processing airborne lidar in order to distinguish between ground and objects such as buildings and trees.

### 4.2.2. Local reference system

Besides the time dependent transformations a global transformation is applied to convert the coordinates from the local reference system of the laser scanner to the in the Netherlands commonly used Rijksdriekhoek (RD) system which is a cartesian coordinate system. From the RD system an additional translation is done to create a local reference system in which the data will be analysed. This is achieved by rotating the data around the origin of the laser scanner with an angle equal to the shore angle at this site, which is 62.7 degrees from the horizontal axis (Figure 4.6b). The origin of the local reference system is defined in the lower left corner. Figure 4.6a shows the orientation of the local reference frame. The shore parallel axis, also referred to as the alongshore direction, corresponds with the x-axis of the reference frame and the cross-shore direction corresponds with the y-axis. The local reference system is chosen to be located just in front of the permanent buildings present on the beach and stretches 150 meters in the cross-shore direction, and 1200 meters in the alongshore direction. The zero point of the local reference system is located at  $x,y=(89029,472598)$  in the Rijksdriekhoek coordinate system.

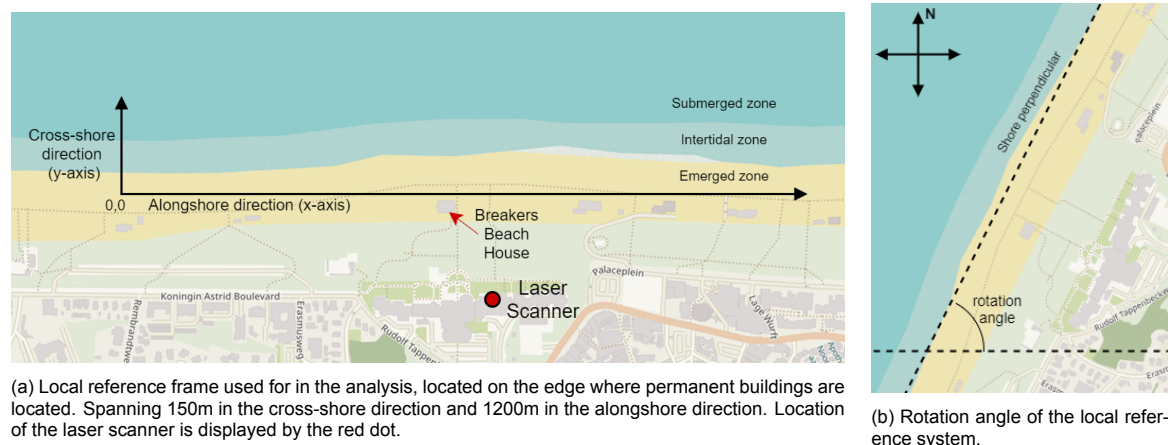


Figure 4.6: Local reference frame.

### 4.2.3. Merging and rasterising data

The final step in the process is rasterizing the point cloud to a 2D data grid. The grid has 1x1m grid cells and is 1200x150m in along- and cross-shore directions respectively, resulting in a total of 180.000 grid points. Rasterizing the data allows to evaluate a single point in space over time (elevation space-time array) which is a requirement for the 4D Objects By Changes analysis that will be conducted. Rasterizing of data can be done in different ways. A nearest neighbour approach and an area averaged approach are both considered.

The nearest neighbour approach searches the nearest point in the point cloud based on x,y distance for each point in the grid. The values of the nearest point are translated to location of the grid point. This method works fine but raises questions on how well this single point represents the entire 1x1m grid cell. For example, it could be possible to have around 30 single data points within this 1x1m. Using a single value, only based on its distance, could provide with a poor representation of the actual elevation profile in this grid cell.

The area averaged method takes into account all the data points within an range of the grid point. By taking the mean elevation of all data points within the area of this grid point the representative value is determined. This method has the additional benefit of smoothing out remaining outliers in the elevation data.

Figure 4.7 displays a section of the 2D grid comparing the different rasterization methods, the colours in the figure are an indication of elevation. The left figure shows the data from the point cloud and is used as reference for comparison. The middle figure corresponds to the nearest neighbour approach and the right figure is the result of the area averaged approach. Comparing these two with the reference case it seems both methods result in an accurate representation of the elevation profile, however, the nearest neighbour approach shows a more pixelated result. The area averaged approach shows a smoother elevation surface, similar to the reference situation. Furthermore, the area averaged approach has a better representation of the contours of the full point cloud. Combined with the additional benefit of taking all data points in to consideration and being less sensitive to remaining outliers, it is chosen to use the area averaged approach for to create the 2D data grids.

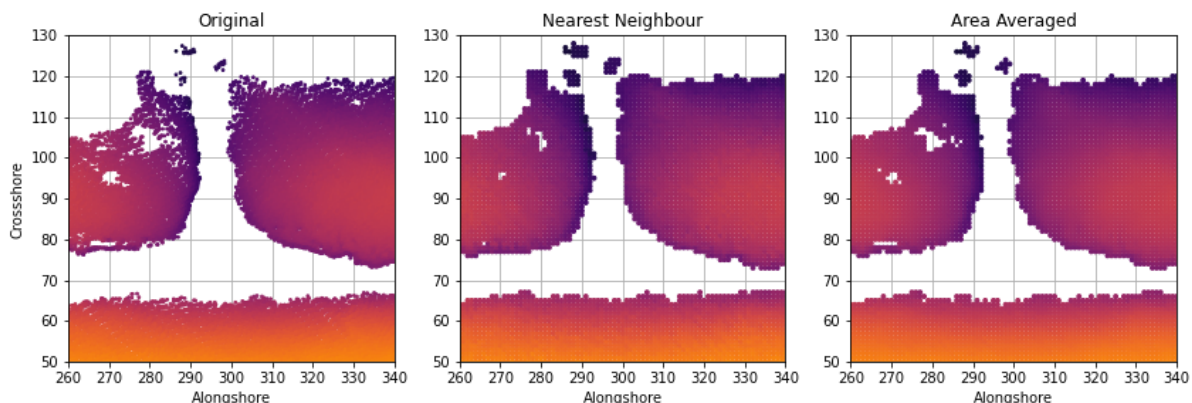


Figure 4.7: Comparison of a section of surface elevation between the full point cloud (left), the nearest neighbour approach (middle) and the area averaged approach (right).

## 4.3. Spatial interpolation of intertidal area

During the lowest water levels in the tidal cycle the morphology of the intertidal zone is not entirely visible on the laser scan data. The laser does not penetrate the water that remain standing in the runnels or flowing back toward the sea trough the rip channels resulting in gaps in the elevation data. The location of these gaps correspond to the location of the objects of interest. Without interpolation the only attributes that can be determine of a channel is the width by means of the width in of the gap, and the location by means of selecting the centre of the gap. Is has to be noted that not all channels are located within these gaps, some of the more shallow channels are visible in the data. Besides these issues, the gaps proved difficult to handle in the analysis.



Previous work using similar laser scan data used linear interpolation in order to fill these gaps, this research focussed around the cross-shore bar behaviour [37]. Linear interpolation in the cross-shore direction is sufficient when the gaps that have to be interpolated are not too large (in the order of max a few meter). When these gaps increase in size the linear interpolation does not yield reasonable elevation profiles estimations. The data used in this research often has gaps in between 10 up to 20 meters in the cross-shore direction that can easily stretch for a few hundreds meters in the alongshore direction.

Figure 4.8 shows a single cross section of an elevation profile, the blue line represents the elevation data that is obtained from processing the scan data, the orange dotted line represents the linear interpolated elevation data for this gap, it is clear that this does not represent a realistic elevation profile. The red line in the figure is the result of an interpolation method that takes into account the surrounding slopes by means of a radial basis function (RBF) interpolation. In the next section the workings of this method is explained and how it has been applied, followed by a comparison with GPS measurements in order to determine how accurate this method is.

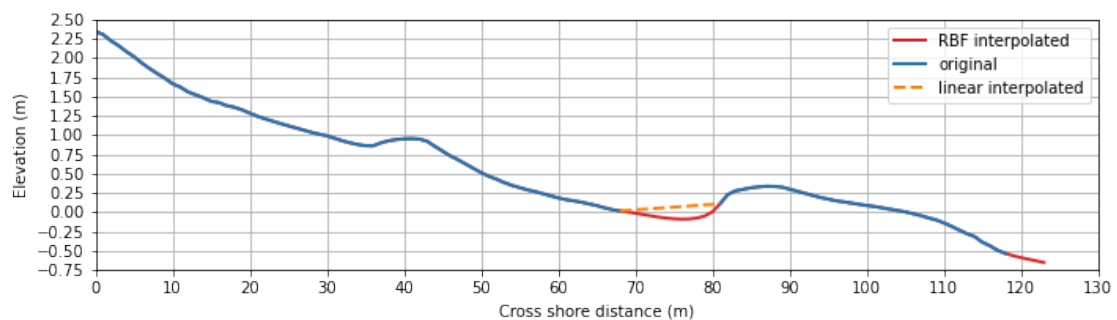


Figure 4.8: Comparison between linear interpolation (orange dotted line) of intertidal zone and a more advanced method using RBF interpolation (red line).

### 4.3.1. Radial basis function interpolation

Radial basis function (RBF) interpolation is an approximation method for construction high-order accurate interpolants of unstructured data. A main benefit of RBF interpolation is that it does not require a grid like data structure (mesh-free), where most 2D interpolation methods require a fully filled grid. In the previous post processing steps the point clouds were rasterized to a 2D grid, however, this grid is not fully filled with elevation values. Therefore, the to be interpolated dataset does not meet the requirements for most interpolation methods. The mesh-free RBF interpolation is therefore a suitable candidate. The RBF interpolation method used for this research is part of the SciPy Python library [38].

RBF interpolation makes use of the radial basis functions. A radial basis function is a real-valued function which value depends only on the (Euclidean) distance between the input and a fixed point. A few commonly used radial basis functions are: linear-, cubic-, gaussian- and multiquadric-functions. Research studying the interpolation of digital elevation models (DEM) concluded that the use of multiquadric radial basis functions provided significantly better results than the other functions [39].

The implementation of the RBF interpolation is explained on the basis of Figure 4.9. In this figure the workflow of the interpolation for a single dataset is shown. The first figure shows the 2D gridded elevation data consisting out of intertidal bars and the emerged section of the beach, elevation data in runnels and channels is not present. In the second figure a convex hull is created around the available elevation data, all points within this convex hull without elevation data will be substituted with interpolated values. The RBF interpolation is done along cross-shore sections, starting from the middle of the dataset. In order to get a representative profile it is opted to also take neighbouring grid points into account for the interpolation, this is shown in the fourth image. Even though all points within the box are taken into consideration, only the empty elevation values along the selected cross-section are substituted. This approach is chosen as if one would calculate the elevation values for the entire box, or even entire grid, the locations near the edges are prone to errors. On the other hand, only using elevation values of a single cross-section instead of the entire box can result in large deviations between interpolated



profiles of neighbouring cross-sections as only a few points are used for the interpolation. This process is repeated for every cross-section within the grid.

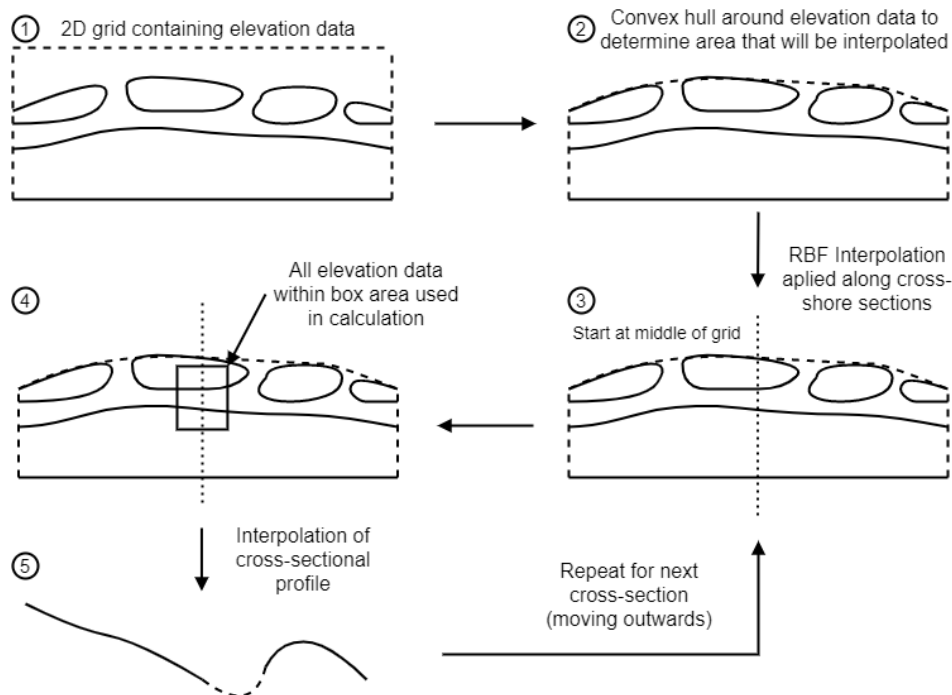


Figure 4.9: Workflow of RBF interpolation implementation. Starting with the 2D gridded elevation data for one scan an convex hull is constructed. Interpolation is done along cross-shore section, starting from the middle of the 2D grid. All elevation data within a pre defined box is used for the interpolation of a single cross-shore profile. The process is repeated until the entire area is interpolated

#### 4.3.2. Comparison with GPS data

The determine the quality of the interpolation method field measurements using GPS have been carried out. By comparing the elevation of the GPS and the interpolated scan data an error margin can be determined. This comparison is done using data from April the 13th 2021 at the beach of Noordwijk. During this day a low water of -0.84m occurred at 12:59 with mild wave conditions. A high resolution laser scan taken at 12:15 is used for the comparison and has been processed the same way as the data used in the analysis. The GPS measurements where done by walking the beach and measuring several cross sections near channels and runnels.

Figure 4.10 shows the results of the comparison between the (interpolated) scan data shown as colormap and the GPS measurements represent by the dots on the figure. The dots are coloured in respect to the deviation the the interpolated elevation profile. Green dots represent a deviation within 5 cm, yellow between 5 up to 10 cm, orange between 10 up to 15 cm and red indicated a deviation larger then 15 cm. The top figure shows shows the laser scan data before interpolation has been applied whereas the bottom figure shows the interpolated data. For small gaps is shows that the interpolated profile is largely within 10 cm accurate. For area's with larger gaps, the section between 350-450m in the alongshore direction, some larger deviations can be seen. Still, the difference does rarely exceed 15 cm.

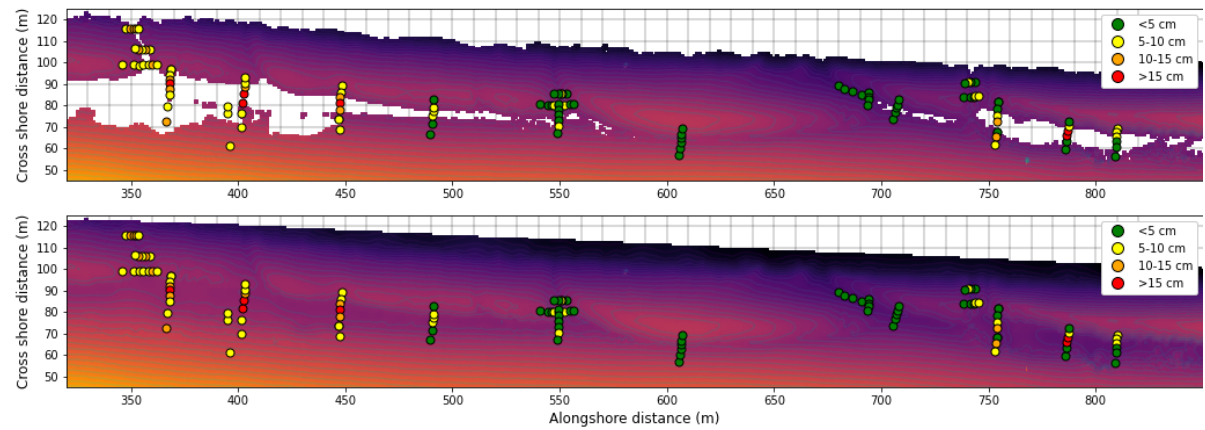


Figure 4.10: Elevation differences between GPS field measurements and RBF interpolation method. Top figure shows the non interpolated elevation mesh, bottom figure shows interpolated elevation mesh. The blue dot, present around  $x=770\text{m}$  is an elevation artifact not removed during the noise processing.

In order to have a better visual understanding of these differences 3D plots of the differences between GPS and interpolated data are created. One of these figures can be seen in Figure 4.11, more of these figures can be found in Appendix B. In these figures the interpolated data is visualized as a 3D mesh and the GPS data points are visualized using red dots. To indicate the elevation differences between the two a projection of the GPS data onto the surface mesh is calculated and visualized using green stars. The original GPS points and their projection are connected by means of a black line. From these figures it can be seen that the GPS measurement points are mostly below the interpolated elevation mesh. The mean difference between the GPS measurements and the interpolated elevation data is  $-0.05\text{m}$  with a standard deviation of  $0.06\text{m}$ .

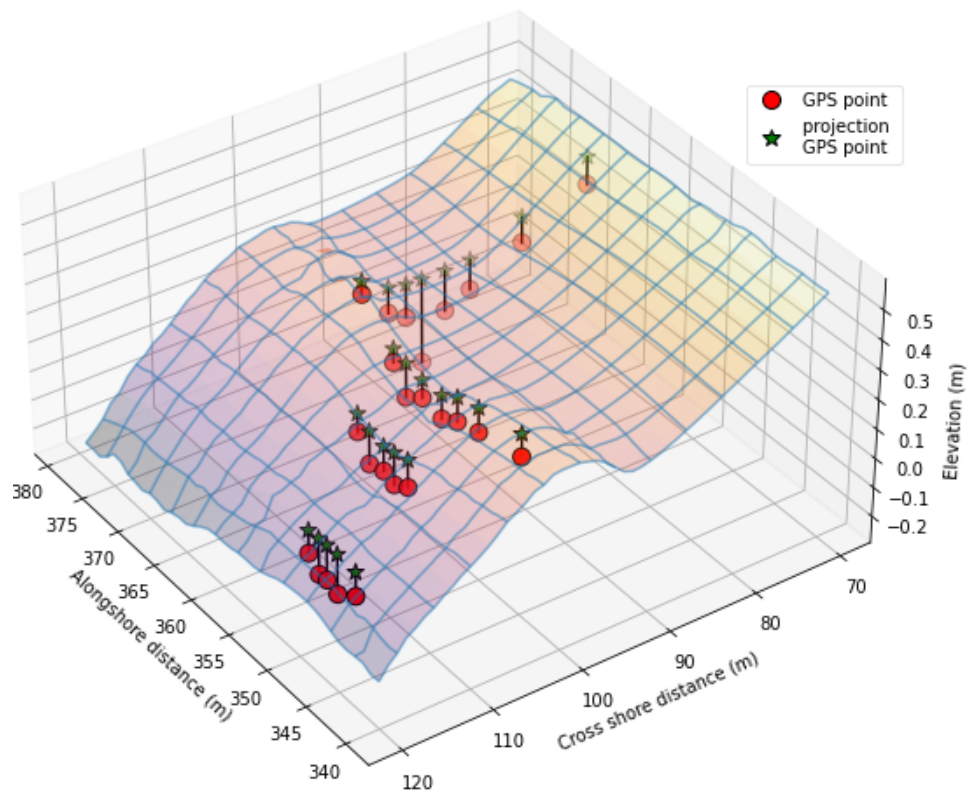


Figure 4.11: 3D comparison plot between the interpolated elevation mesh and the GPS elevation measurements (red dots). The GPS points are projected on the elevation mesh (green stars).

## 4.4. 1D Alongshore analysis

The 1D analysis aims to provide a straight forward, easy to execute analysis to assess alongshore variability of rip channels. This is achieved by simplifying the problem from a 3D situation to a 1D situation. The intertidal area is known to be very dynamic and trying to simplify the situation to a 1D case proves to be ambitious. By analysing a single alongshore elevation profile of each scan in the timeseries at a constant location in space it is deemed possible to track the movement of the channels in the alongshore direction. This process is done in several steps starting by choosing the location for the analysis, followed by detection of the actual rip channels. Finally the detected channels have to be tracked over time by grouping them based on location and movement.

### 4.4.1. Cross-shore location

In order to achieve proper detection of the rip channels it is important that the location at which the detection is executed intersects with the intertidal bar morphology. As stated previously, the intertidal morphology migrates on- and off-shore depending on the hydraulic forcing conditions. This complicates the issue of selecting a location for the alongshore cross-sections. Figure 4.12 visualises this problem by means of four fiction intertidal bars located at different distances in the cross-shore direction and three fictional alongshore lines at which the analysis is done. Analysis along the line A would only result in the detection of a rip channel between bars 1 and 2, while using line B would return the detection of a rip channel between bars 1 and 2, and bars 2 and 3. Finally, an analysis along line C would yield rip channels between bars 2 and 3, and bars 3 and 4. This example shows the importance of the cross-shore location along which the elevation profile is used for channel detection.

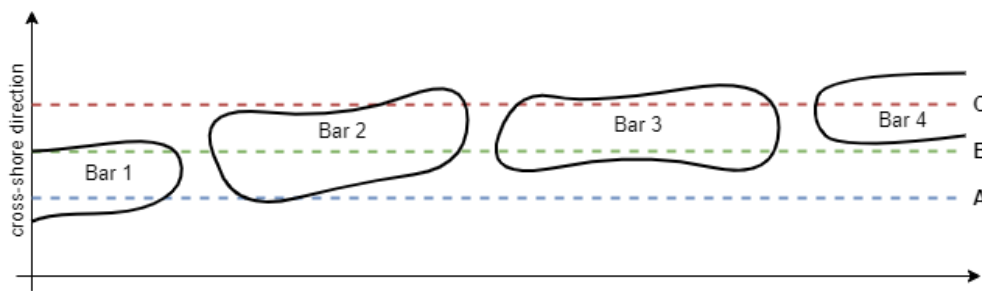


Figure 4.12: Example of intersection between three shore parallel lines (A,B,C) and four fiction intertidal bars located at different distances in the cross-shore direction.

In order to how assess the impact of the location on the detection of channels in the actual dataset it is chosen to apply the analysis for multiple cross-shore distances. Based upon visual inspection of the data it is seen that the location of the intertidal morphology is varies between 70 up to 110 meters offshore in the local reference system. The analysis is done for intervals between 70m and 100m of 5 meter.

### 4.4.2. Channel detection

Channel detection is done by analysing the elevation profile in the alongshore direction. The dips in the elevation profile, also referred to as valleys, indicate the possible presence of a rip channel. The detection of these valleys is done using peak finding algorithms available in the SciPy library for Python [38]. This algorithm compares the values, in this case elevation, of neighbouring points in order to find maxima within a signal. As it is only capable of detection maxima and not minima it is need to invert the the elevation profile in order to work. The algorithm can be fine tuned using several parameters, the most important for this use case being the relative depth of a peak, minimum width, a minimum horizontal distance between successive peaks. These parameters are tweaked in order to detect channels the most accurate while reducing the possibility of false detections. It has to be note that the detection is not 100% reliable and some channels might be skipped during detection.

Before peak detection is done, an additional processing step is applied. The elevation data contains significant amount of bumps in the order of a few centimeters. These bumps are too small to represent channels and make the detection of actual channels more difficult. The smoothing of the elevation

profile is done using a Savgol, or Savitzky–Golay, filter. A Savgol filter allows for smoothing of data without distorting the signal tendency. This is done by fitting sections of adjacent data points with a low-degree polynomial using a linear least squares method. The Savgol filter is preferred over other smoothing filters, such as a averaging and rolling mean, as it excels at preserving peaks only defined by a few data points while still using a large smoothing window.

Figure 4.13 shows the differences between an area averaged approach and the Savgol filter. The figure shows a section from an artificial generated elevation profile, the black line represent surface elevation which is relative constant and then suddenly drops. The left subfigure shows the results of the moving average approach using different window sizes. Using the moving averaged approach a small window size is required to have a good representation of the actual elevation profile, when the window size start to increase the deviation to the original profile start to increase as well. Meanwhile, the Savgol filter approach shows to be less sensitive to the increase in window size. It follow the signal tendency while smoothing out the small wiggles in the elevation profile. This property is of large importance due to the fact that the slopes at the channel locations are only defined by a few points.

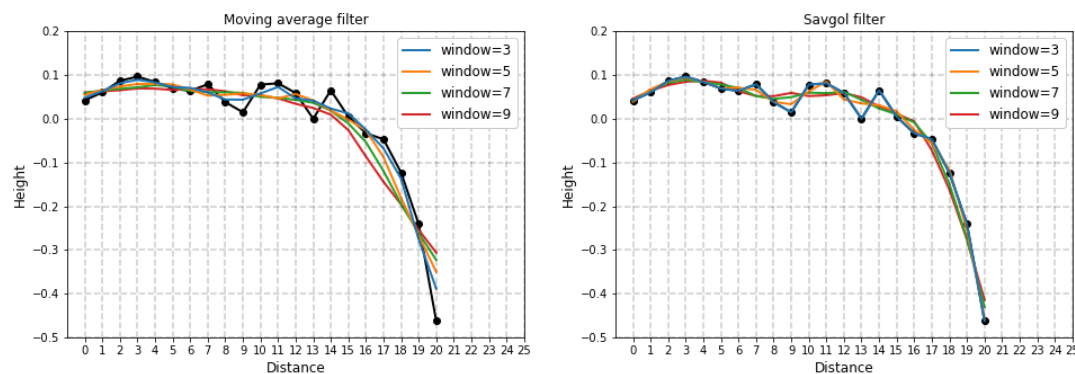


Figure 4.13: Comparison between elevation smoothing using a moving average approach (left side) and the described Savgol filter (right side). The different coloured lines indicate averaged profiles using different windows sizes.

Figure 4.14 shows the results of the channel detection for the location  $y=80\text{m}$  (offshore direction) for February 14th 2020, in the top figure the extracted alongshore elevation profile is shown and the bottom figure a top view of the entire scan is shown in which the location of the extracted section is represented by the black dashed line. In both figures the red markers indicate the location of detected channels. This channel detection method is applied to every scan and is repeated for the previous described intervals in the offshore direction.

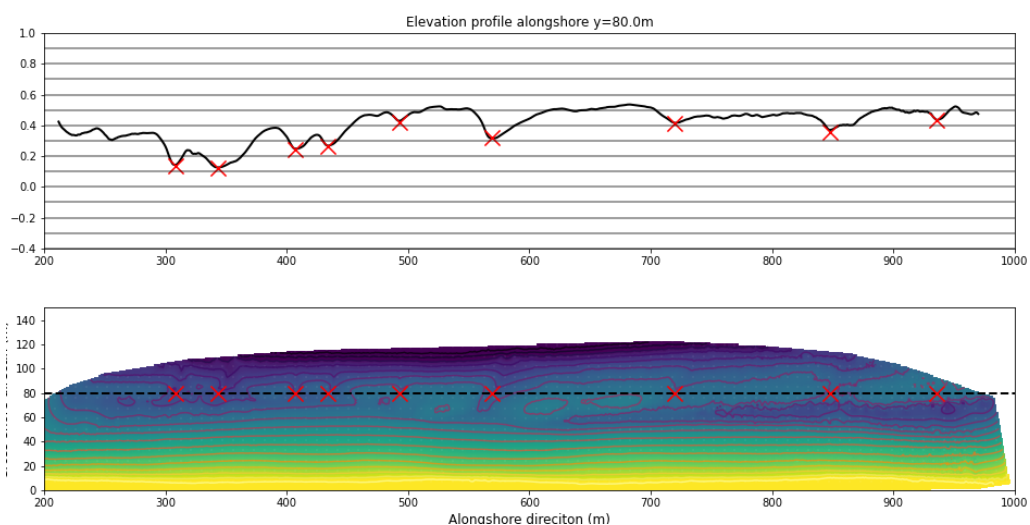


Figure 4.14: Channel detection based on elevation profile of a single alongshore cross-section. Top figure shows the elevation profile, x markers indicated detected channel. Bottom figure shows a top view of the location of the cross-section (dashed line).

For each of the detected channels additional attributes such as width and cross-sectional area are determined. Determining the correct width of a channels is not as straight forward as one might think. The width could be defined by the wet cross-section of a channel, however, this varies with water level and thus the exact time at which the scan taken. Furthermore, widths of channels that have no flowing or standing water as they might be smaller and located on the top of an intertidal bar (therefore having a higher elevation) can not be described by this method. Another option is using the local elevation surrounding the channel to determine the width. The width of the channel can be defined as the distance between the highest elevation points on the left and right side. When the slopes of the channel are very shallow this width can become very large. If the width of a rip channel is defined by the distance between adjacent bar crests, the rip would contain a significant section of the bar where no flow would occur [28]. Figure 4.15 visualizes the issue using two alongshore elevation profiles where a channel is detected. In figure 1 a relative deep channel is displayed, where in figure 2 a more shallow channel is shown. Line A is the channel width when using the highest elevations on both sides. From the figure it is seen that when dealing with shallow channels this width can become large and is not a good representation of the actual width based on visual inspection.

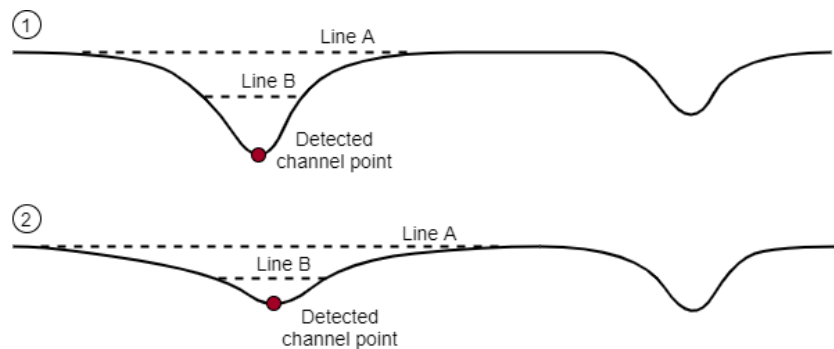


Figure 4.15: Example of problems with defining the width of a channel.

A third method, visualized by Line B in the figure, defines the width based upon the relative depth of the channel. The relative depth is the vertical distance between the detected channel point and the lowest elevation value of the highest points on the left and right. The width of the channel is chosen to correspond with the width at 50% of the relative depth. As comparison, the width of line A would correspond to 100% relative depth. The value of 50% relative depth was found to yield the best results. The cross-sectional area of a channel is determined by integration of the elevation profile below the line B.

## 4.5. 4D-Objects-By-Change analysis

With the increased availability of time series of high resolution 3D geospatial data a demand for advanced method to detect morphologic changes emerges. One of these methods is the 4D-objects-by-change (4D-OBCs) developed by Anders et al. [40]. This method distinguishes objects by detecting surface changes in the temporal domain, and finding neighbouring points with similar characteristic surface changes.

The methodology behind the 4D-OBCs method is provided in section 4.5.1 to familiarize the reader with the topic. For a detailed description of the method the reader is referred to the paper Anders [41]. Next, the application of the method to the Noordwijk dataset is explained. Section 4.5.2 describes the problems that surfaced and what caused them. The results are provided in Chapter 5.3.2.

### 4.5.1. 4D-Objects-by-change method

The 4D-OBCs approach can be split up into three steps: deriving the space-time array of surface change, identification of temporal change features and spatial segmentation. Explanation of the identification of temporal change feature and the spatial segmentation is done on the basis of Figure 4.16. This figure describes in four main steps (indicated by the numbers) how from the height change profile of a single point in the timeseries over time a spatial segment is formed.

The method uses a space-time array of surface change as input data for the segmentation. The space-time array is created by resampling the 3D point cloud for each time step within the time series to a 2D gridded data structure. For every point within this 2D grid a representative elevation value is calculated using a circular area averaged approach, comparable with the processing step described in Section 4.2.3. Using a reference elevation profile from the start of the time series the change in elevation for each time step is calculated. The space-time array of surface change describes the change at a certain point in time in relation to the start of the time series and not the previous time step.

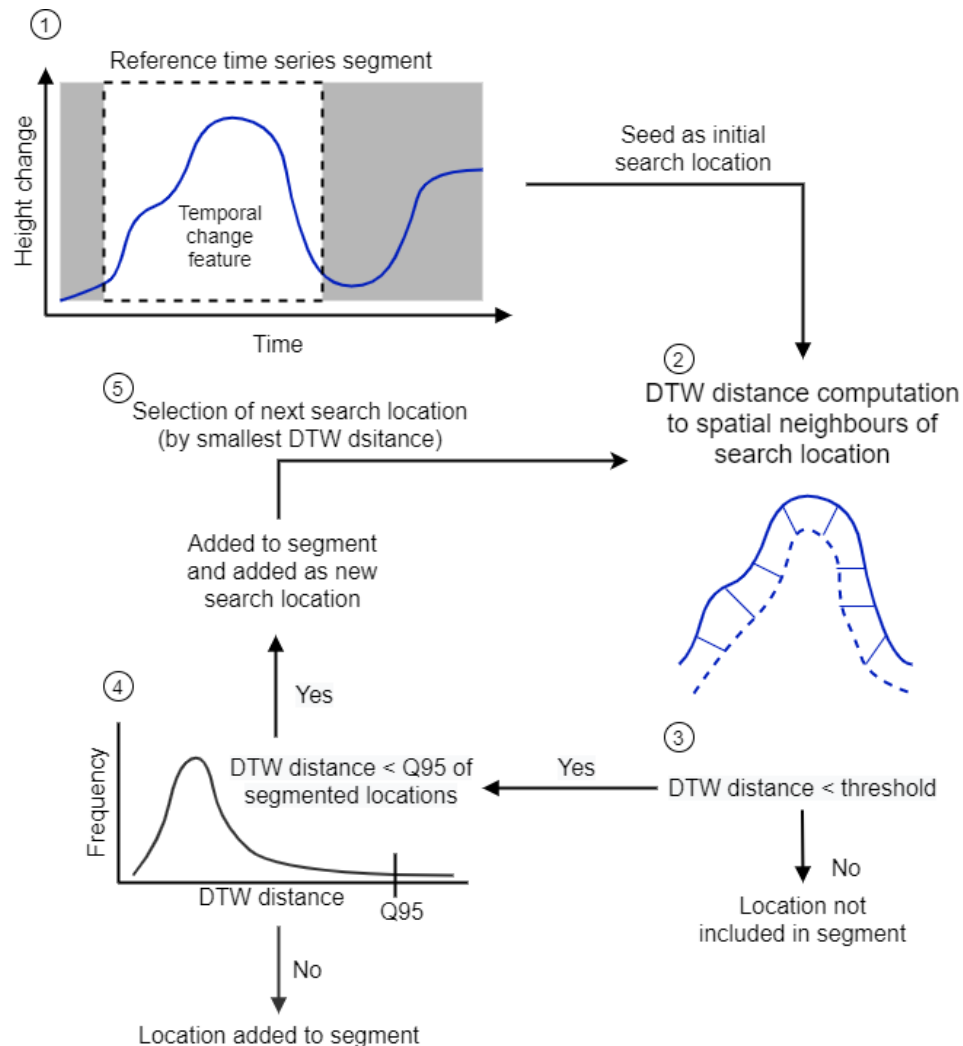


Figure 4.16: Workflow of the 4D-Objects-By-Change methods, based on Anders [41].

The first step of the flowchart shows a detected temporal change feature. A temporal change feature is found by analysing the space-time arrays for every single point within the 2D-grid. A change feature is created by grouping the successive change points where a volume increase takes place. The change point detection compares the values in a time series between the successive periods to determine the location where the signal changes shape. This approach creates segments within the time series, such a segment can be seen in the top left figure (Figure 4.16). The change feature is indicated by the area within the dashed box.

This change feature shows geomorphic change at a specific location over time. It is assumed that geomorphic changes at a given location results in similar elevation changes in the local neighbourhood. Using this assumption neighbouring points with a similar elevation history are grouped. This is done using Dynamic Time Warping (DTW) which allows finding similarities between time series by shrinking or stretching a reference time series, see step 2. By calculating the distances between the paired points



in the DTW it determined if the point is added to the segment. To be added to the segment this distance has to be below a pre-defined threshold (step 3). This is repeated for all eight neighbouring grid points.

If the point meets the requirements to be added to the segment and its DTW distance is smaller than the 95th percentile of all distances in the segment it is flagged as a new search location (step 4). From this point, the neighbouring points that are not yet a part of the segment are also being compared using the DTW distance computation. This process repeats itself until the DTW distance is larger than the 95th percentile of all DTW distances in the segment. The point is added to the segment, but does not serve as a new search location.

#### 4.5.2. Application Noordwijk data set

The 4D-OBCs method is developed around a similar data set obtained at Kijkduin, however, it was not solely applied to the intertidal zone of the beach but also more towards the backshore zone of the beach. At this emerged section of the beach gaps present in the elevation data have a different origin. They are mostly the result of the presence of temporal objects such as people, animals or vehicles. These gaps are small (in the order of meters) and could be removed by the means of a temporal averaging filter. The gaps in the Noordwijk, intertidal, dataset have a different origin as they are the result of the presence of larger water bodies. Temporal averaging could not be used as the interval within the timeseries is roughly 24 times as larger.

The 4D-OBCs methods was initially applied to the the Noordwijk data set before interpolation of the spatial gaps was done. Additionally, it was first opted to use a space-time array of absolute surface elevation instead of surface change. However, in the end it was chosen to use a variation on the surface change space-time array used in the original method. The reason for this change is discussed in detail in the discussion in Section 6.3.2

The results of the analysis using the non-interpolated elevation data returned as good a no segments in the detection steps, this behaviour was not expected. The cause for this behaviour could be traced back to the change point detection and DTW calculation. The change point detection is used to find seed candidates is done using the Python library Ruptures [42]. In this implementation change point detection is limited by gaps within the signal, cause by the spatial gaps in the data. This means that very limited seed candidates are found within the intertidal zone. When a possible seed is found a next issue can occur during the 2D segmentation growth done by means of the dynamic time warping. The calculation for the DTW distance would not yield an outcome if the time series it would compare to each other contained gaps in the elevation profile. With the dynamic nature of the intertidal morphology and the lack of elevation data at the location of runnels and channels it was found that as good as none of the elevation profiles were free of those gaps. Therefore no segment growth would take place.

Possible solutions to these problems are spatial interpolation of the data, or the usage of temporal averaging. The interpolation method used in Section 4.3 eliminates the gaps in the elevation data present due to the channels and runnels. However, it is still possible to have gaps in the elevation time series. For example, when a seed candidate is found at a certain point  $x,y$  in the 2D grid at epoch  $t_1$  it is not guaranteed that at the next epoch  $t_2$  elevation data is available in this point as it could be outside the area covered by the laser scanner for that day. Such could be the case for days where during storm conditions the wave setup was significant and the entire intertidal area was submerged. Possible option to fix this are removing the scans from the time series, using temporal averaging of the space-time elevation array, or use linear interpolation in the time series for this point. The later option is used as removal of the entire epoch could result in removing use full elevation data at other points in the grid.

Temporal averaging is used in the original method developed around the Kijkduin dataset. This dataset consists off hourly laser scans of the entire beach and not only the intertidal zone. Averaging of surface change values is done for every point in the 2D grid. Temporal averaging allows for the identification of values that differ from their temporal neighbour, but removing the likelihood they represent measurements errors [40]. Temporal averaging proves to be very use full, however, the time window used for averaging plays an important role. Due to the large time intervals within the time series used at Noordwijk in relation to Kijkduin, roughly 24h versus 1h, temporal averaging resulted in undesired surface elevation artefacts due to the significant morphological changes between successive time steps.





# 5

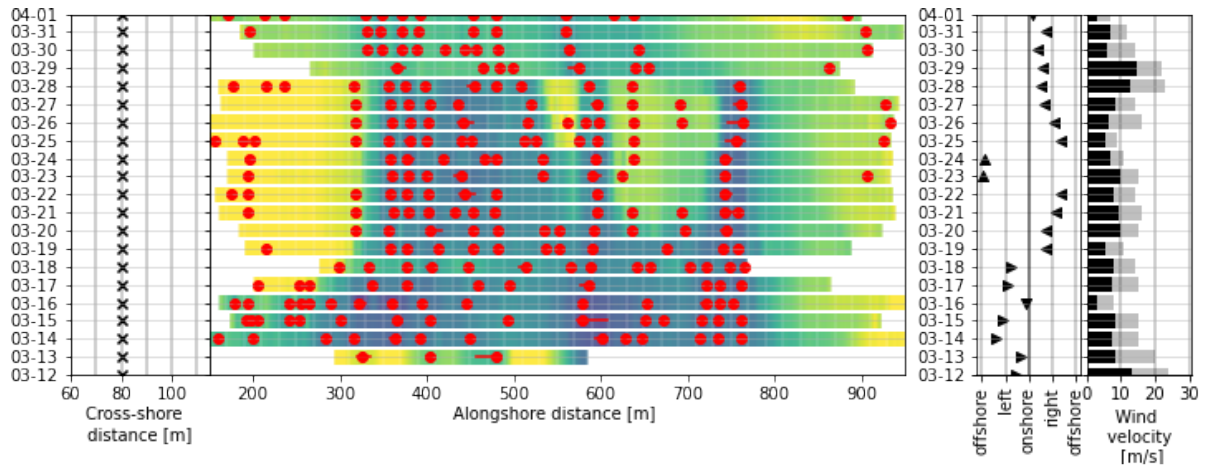
## Results 1D- and 4D-Analysis

In this chapter the results, and initial limitation, of the 1D-analysis are presented. It is followed up by the result of the improved 1D analysis showing the alongshore migration and spacing of rip channels. An overview of the results obtained by the 4D-OBCs method is presented and a comparison between the detected rip channels of both methods is provided.

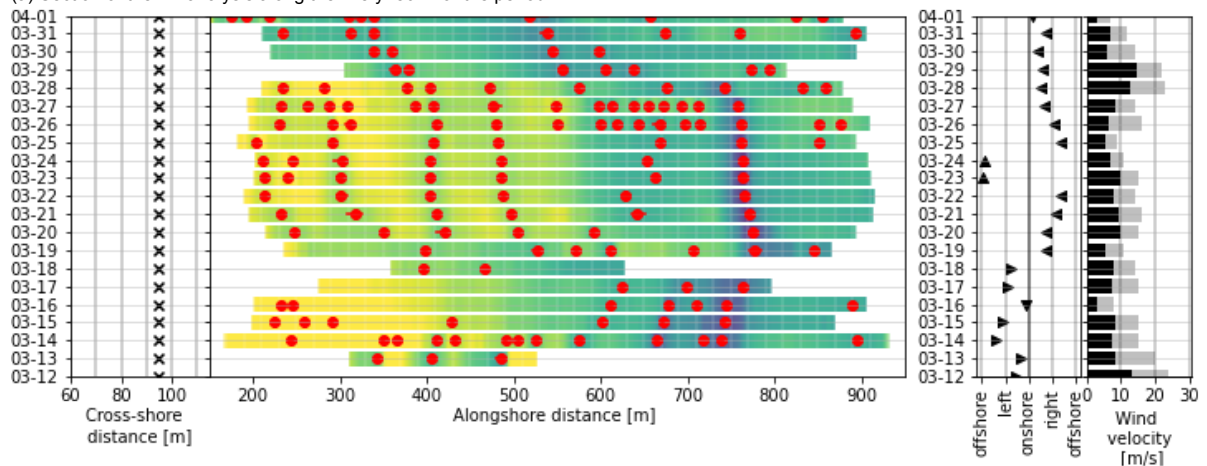
### 5.1. 1D Alongshore analysis results

By plotting the detected alongshore locations of the channels over time the alongshore variability of channels can be visualized. In section 4.4.1 the issue regarding the cross-shore movement of the intertidal zone and the stationary analysis location were addressed. The effects of the cross-shore movements are clearly visible in the results and is illustrated in Figures 5.1a and 5.1b. These figures show the analysis of a section of the time series, the full figures can be found in Appendix A. The red dots represent the detection of a channel while the colormap on the background visualises the elevation (yellow is high, blue is low), on the right side of the figure shows shore relative wind direction and magnitude.

Comparing Figure 5.1a with Figure 5.1b a clear difference can be seen. Channel detection for the location  $y=80\text{m}$  in the cross-shore direction returns lots of possible channels, however, after further inspection these detected points are located inside the runnel that is located behind the intertidal bar and channels. Low points within this section are falsely detected as channel. It should be stated that this is not the case for every single point, for instance on the right side of the figure around  $x=750\text{m}$  in the alongshore direction the detected points do correspond with a actual channel. For the channel detection along the line  $y=95\text{m}$  in the cross-shore direction a different result can be seen. First, a reduced amount of channel locations are found, and secondly, the detection corresponds better with the actual location of channels. For this cross-shore location clear channels can be distinguished that where not, or very poorly, visible for the detection along  $y=85\text{m}$ .



(a) Section of the 1D analysis along the line  $y=80\text{m}$  for the period.



(b) Section of the 1D analysis along the line  $y=95\text{m}$  for the period.

Figure 5.1: Comparison between the results of the 1D analysis along the location  $y=80$  and  $y=95$ . On the left side the cross-shore location is indicated by the black crosses. The centre figure shows detected channels (red dots) displayed on a colormap that indicates the elevation. On the right of the two figures relative to the wind a shown. The left figure displays shore relative wind directions, distinguishing between onshore, offshore, left and right. The right figure shows the daily average wind velocities (black bars) and daily maximum wind velocities (grey bars).

As stated previous, the location of the intertidal morphology varies over time and shows a pattern of migration in the on- and off-shore direction dependent on the hydraulic forcing. Looking back to the process of data selection for the period in which the laser scan data is analysed, it was chosen to use a period of varying weather conditions and thus varying forcing conditions. Therefore it can be expected that an analysis along a line constant in space yields problems. Figures 5.2a and 5.2b visualises this issue by comparing the analysis of a alongshore profile at the same location for two scans that are one month apart. In the first figure (5.2a) the alongshore line (at  $y=80\text{m}$ ) on 14th of February intersects with the intertidal bar morphology and the detection method returns multiple valid channel locations. In the second figure (5.2b) the analysis is repeated for the 14th of March and the intertidal morphology has moved offshore. An analysis along the same cross-section does return possible channels, however, on visual inspection it becomes clear that these are not the desired result. The detection returned mostly low areas within the runnel that is located behind the intertidal bar instead of the channels intersecting the intertidal bars.

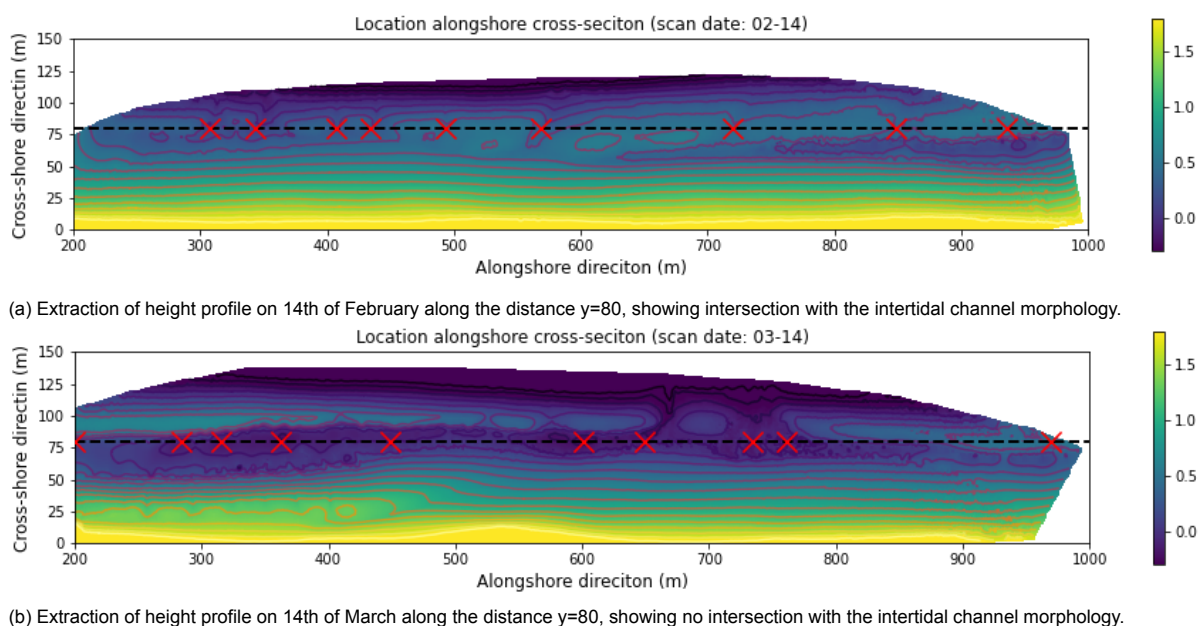


Figure 5.2: Difference between detection along the same line, with a month interval.

Using a analysis along a constant line could provide use full insight on a short timescale, such as a few weeks when the forcing conditions are relative stationary and the cross shore variability of the intertidal zone is limited. When these conditions are not met this method proves not to be accurate

## 5.2. Improved 1D alongshore analysis

It was concluded that the method of the detection of channels yields good results, but using a stationary cross-shore location over time tries to over simplify the problem to much. In this section adjustments to the 1D method are made to allow for the cross-shore movement of the intertidal zone. Additionally, the detection along a single line is extended to multiple lines to account for channel rotations.

### 5.2.1. Varying cross-shore location

The issue of shifting area of interest over time can be solved by allowing variation in the location of the alongshore cross-section where the channel detection is done. By varying the location over time in such a way that the location of analysis always intersects with the intertidal bar and channel morphology this problem is solved. Using a similar detection method to the channels it is possible to detect the crests of the intertidal bars. Figure 5.3 shows the result of this approach for the 14th of March. In the figure the location of the intertidal bar crests are shown by the red markers, the dashed line represents the average cross-shore location of these crests. By comparing this location with Figure 5.2b it is clear that

detection along the suggested line yields better results as it does intersect with the bar morphology. However, it was found that using an offset of 5 meters in the offshore direction provided even better results. This can be explained by the asymmetrical profile of intertidal bars in the cross shore direction. Intertidal bars have a steep face on the shore side and are more shallow on the seaward side, detection of the crest thus not result in finding the middle of the intertidal bar.

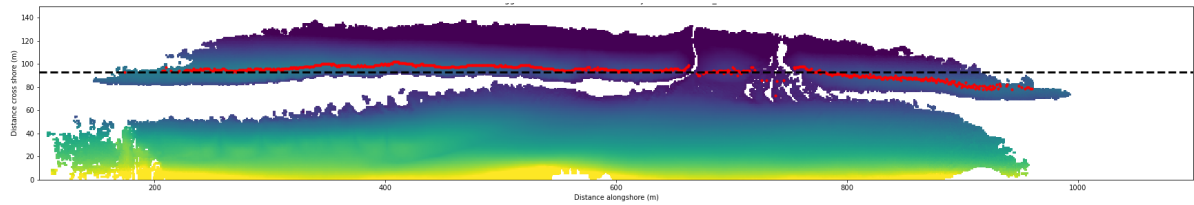


Figure 5.3: Detection of intertidal bar crests (red markers) and suggested alongshore cross-section location (dashed line) for the 14th of March 2020.

Figure 5.4 shows the cross-shore location of the intertidal ridge morphology over time, the black crosses represent the detected average cross-shore bar location for each day. From this graph it can be concluded that there is a large variability in the cross-shore direction. This illustrates the problem that arises when the analysis is done along a constant alongshore axis. For example, the alongshore line at  $y=80\text{m}$  results in good detection of channels for the start and end periods of the timeseries. However, during the period in between from 19th of February up to the first week of March an offshore migration can be seen. When the channel detection is applied for this period at the same location it returns poor detection as a result. By allowing variation in the cross-shore location at which the channel detection is done, this issue can be solved. This method eliminates the cross-shore variability from the analysis and simplifies the problem even more.

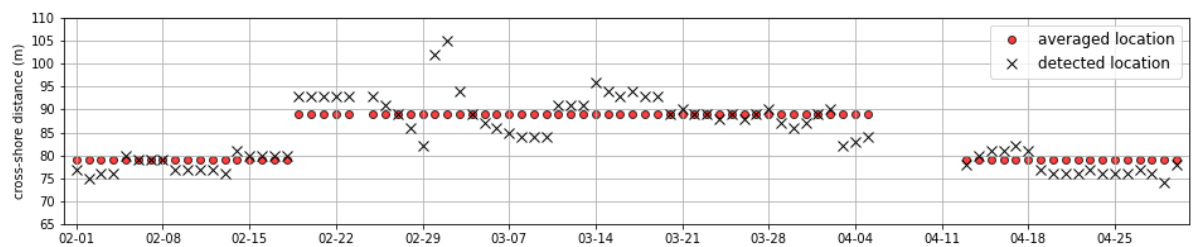


Figure 5.4: Detected cross-shore locations of the intertidal bar morphology for each day in the time series represented by the crossed markers. Three clear sections can be distinguished. The cross-shore locations used for analysis based on these findings are shown by the grey dots.

A possibility would be to use the detected cross-shore bar crest locations as input for the location of the alongshore analysis. This would result in a good detection of the channels as the two always intersect. However, allowing for two large variations in the location can result in good channel detection but can also result in wrong interpretation of the detection. In order to clarify this issue it is visualized in Figure 5.5. In this figure a side by side comparison is made between the detection of a channel and its width. The alongshore location and width of the channel are identical in both figures, when ignoring the cross-shore location of the channel one could say that based upon this detection no change has taken place. However, looking at the total picture it is clear that significant changes took place, besides the offshore directed movement of the bar the channel orientation changed. Therefore it is chosen to vary the location of the alongshore analysis based upon visual analysis of the results of the cross-shore bar crest detection. In Figure 5.4 three sections are classified. First, the period up to 18th of February where the intertidal morphology was located around 80 meters offshore in the local reference system. Second, the period up to 5th of April where relative large amounts of variation is seen a cross-shore location at 90 meters is selected for the analysis. And finally the third section, where the intertidal bars migrated back towards the shore, the analysis is again located around 80 meters offshore. In the figure the location is represented by the rounded markers.

From Figure 5.5 it also becomes clear that this simple detection method is not capable of detecting the

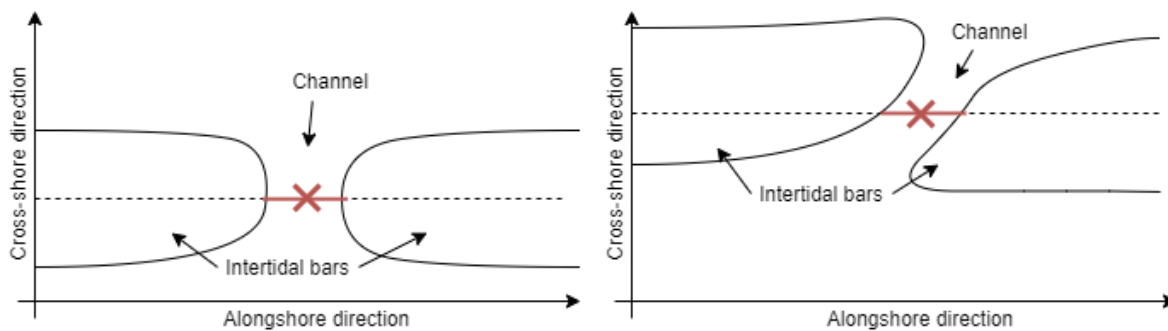


Figure 5.5: Comparison between two situations that would yield the same results when the influence of cross-shore direction is ignored. Both channels are at the same alongshore location and have the same width. Besides the influence of cross-shore location, the limitation of channel rotation detection is illustrated in the right figure.

angle of channel relative to the shoreline. In order to get an indication for this angle a channel has to be represented by at least two points. Combining this limitation with the problem of selecting the correct location for the analysis it is opted to repeat the 1D analysis at multiple location for each scan.

### 5.2.2. Extended channel detection

To account for the rotation of channels, it is chosen to repeat the detection along 15 alongshore transects for each day, the locations are still done using the suggested cross-shore location determined previously (Figure 5.4). From this suggested location the detection is done at an interval of 5 meters in the shoreward direction and 10 meters in the offshore direction due to the asymmetrical shape of the intertidal bars.

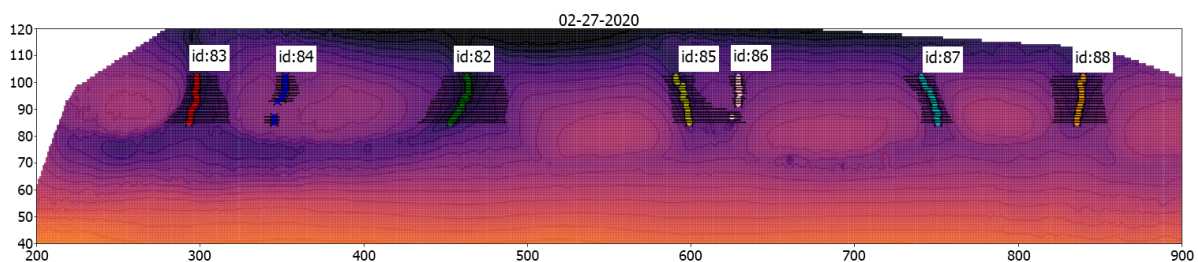


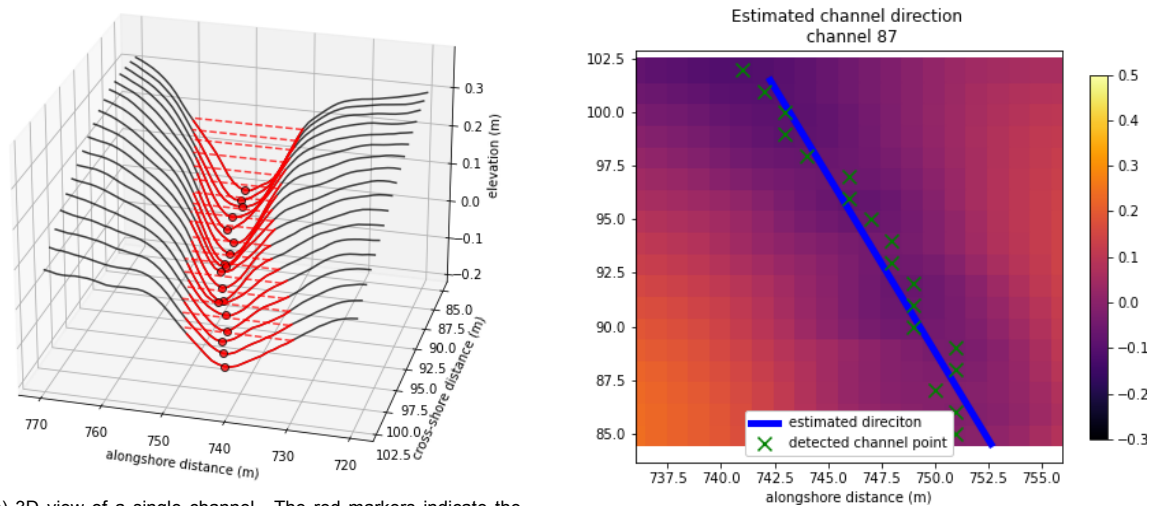
Figure 5.6: Results of the extended channel detection for the 27th of March. Nearby detected channel points are grouped and colour coded and assigned an unique identification number.

The previous detection method represented a channel using a single point, the adjusted method utilises multiple points to describe one channel. In Figure 5.6 the results of this adjusted detection method are shown, in this figure 7 different channels are visible each represented by its own colour and unique identification number. The detection returns all the channel points locations (lowest area of a channel) and their widths. The individual points are grouped to channels using a maximum distance metric. Each channel is given an unique id used to group channels over time in order to trace their alongshore movements. A 3D channel is defined by at least 5 detected channel points in the cross-shore direction.

A more in depth analysis of each single channel is done to obtain the representative depths, widths and the shore relative angle. This is explained on the basis of Figure 5.7 where a detailed view of channel number 87 (the cyan coloured channel of Figure 5.6). In the first figure (5.7a) an 3D representation of the channel detection is shown. The red markers represent the local lowest point of the elevation profile, also previously referred to as channel points. The red lined section of the elevation profiles indicate the width of the channel. The width is determined using the relative depth of a channel. The width is calculated based on 50% relative depth of the channel. Integration of this red section of the elevation profile yield the cross-sectional area of the channel. In the second figure (5.7b) the estimated direction of the channel relative to the shoreline is shown. The black crosses are the detected channel points and the green line is the result estimated direction. This direction is determined using linear regression through the detected channel points. This process is done for every channel in the time



series.



(a) 3D view of a single channel. The red markers indicate the lowest point of the channel obtained by the detection. The red dashed section of the elevation profiles indicated the width of the channel.

(b) Shore relative orientation of the channel based upon linear regression of the detected channel points.

Figure 5.7: Detailed overview of channel number 87 (from Figure 5.6). A 3D view of the detected channel is seen in the left figure. The estimated shore relative direction of the channel is shown in the right figure.

### 5.2.3. Classification of channels over time

After the detection of rip channels and determining its properties there is still need for a method to determine how long a channels has existed in time in order to asses their temporal behaviour. An attempt was made to automate this process, however, manual assessment of the channels proved more reliable. When analysing longer time series it might prove beneficial to look into improving the automation process.

Manual assessment was done by visual inspection of the time series. Channels present at the same alongshore location, or moved alongshore within reasonable distance ( $\mathcal{O}(10\text{m day}^{-1})$ ) are grouped using the unique id that has been assigned during the detection. A channel exists out of a minimum of at least two consecutive days with a detected channel. It was chosen to allow for gaps of 1 day within a group. A total of 44 channels where found to have existed for extended periods of time between February and April 2020. Figure 5.8 shows the development of this channel over time. In this figure the alongshore movement, development of the width and cross-sectional area and absolute elevation over time are shown.

For the calculation of the daily representative values for the width and depth the extended channel detection is used. For each day within the existence of the channel the median values from the extended detection for width and depth are calculated and used as representative value. This method is very rough and works only relative well for simple straight lined channels. When studying channels that adopt bifurcation like shapes an alternative method should be developed (not done at this time). The cross-sectional area is calculated in a similar fashion.

Figure 5.9 shows the location and alongshore movements of all 44 classified channels. From analysing all groups is it found that the average alongshore movement is  $-1.55\text{ m/day}$  with a standard deviation of  $0.77\text{ m/day}$ .

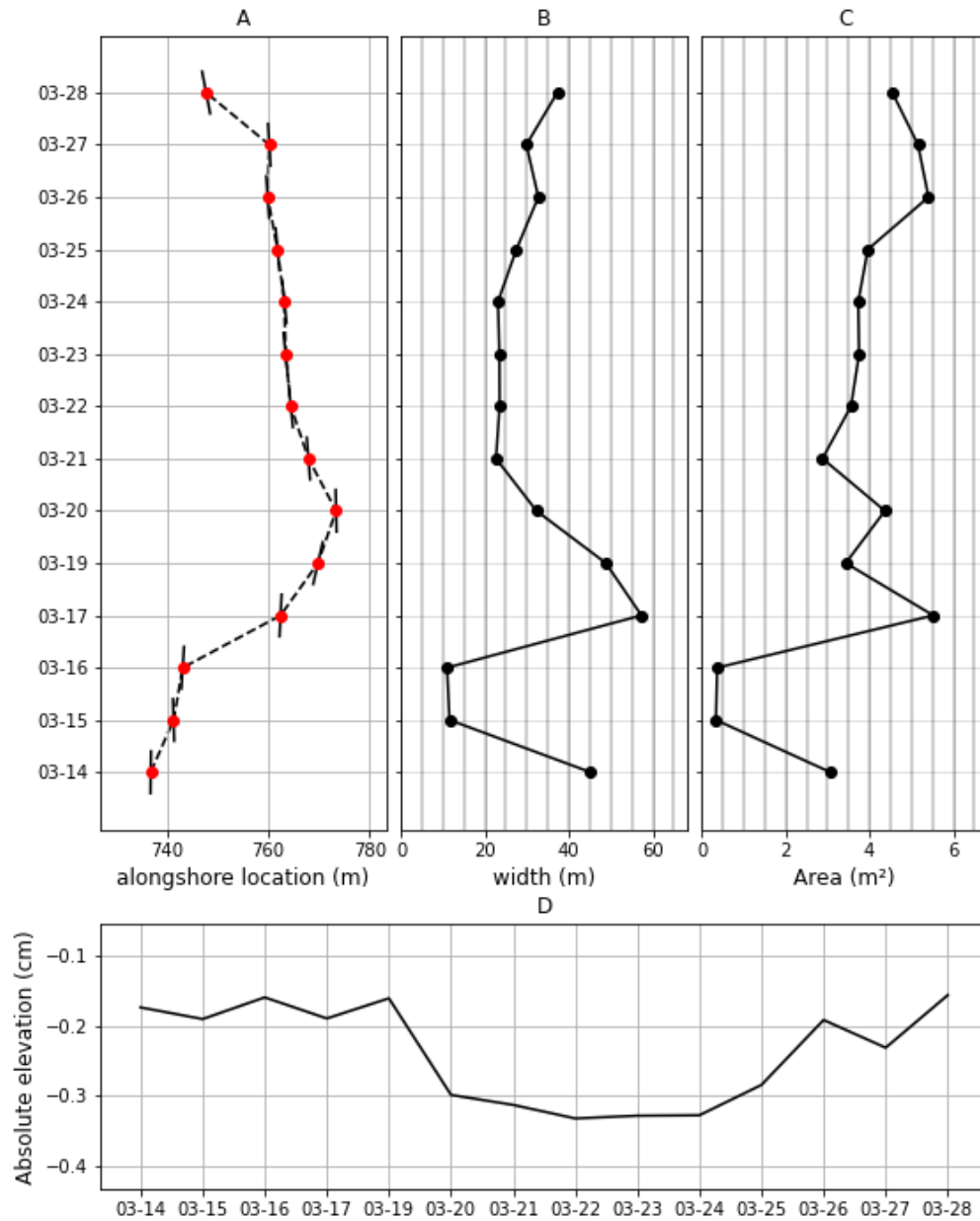


Figure 5.8: Development of a channel over time. A) Alongshore movement over time, red dots are the lowest elevation point of each channel, the black angled line represents the shore relative angle of the channel. B) Development of the width of the channel over time. C) Development of the cross-sectional area of the channel over time. D) Development of the depth of the channel over time.

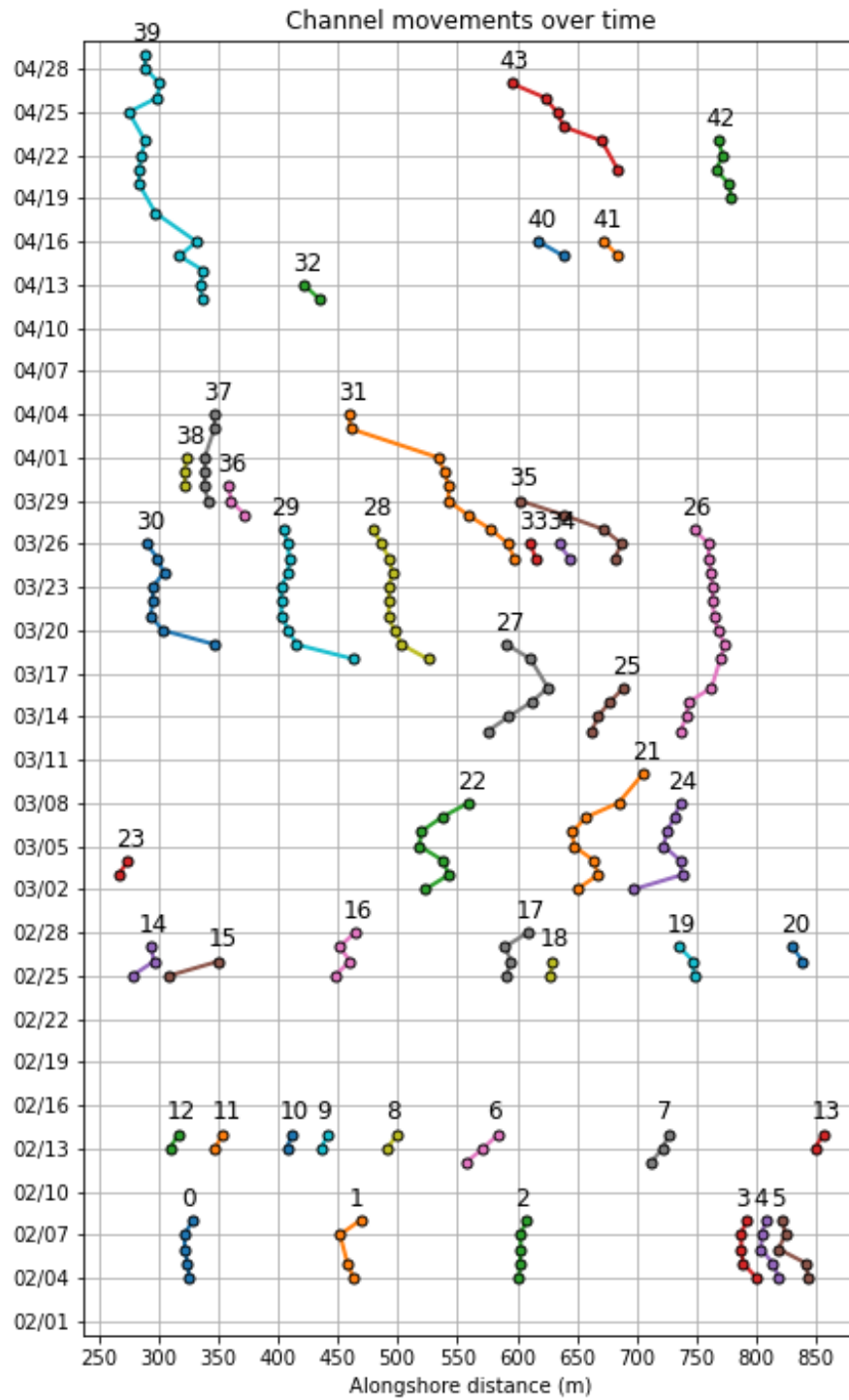


Figure 5.9: Overview of all classified channels over time. Each channels is assigned a colour and an unique identification number.



### 5.2.4. Improved 1D alongshore analysis results

The effect of varying cross-shore location is clear in the results. Visualising the alongshore locations of channels by means of a timestack now provides a better insight than previously. This timestack is shown in Figure 5.12, on the left side the jump in cross-shore location of the analysis over time is shown. The channel locations shown in the left centre figure show the improved detection of channels as the result of the varying cross-shore location of the alongshore transects. This figure does not use the detection described in Section 5.2.2 where multiple transects per epoch are used for describing the 3D shapes of channels.

Based upon the classified channels from Section 5.2.3 the rip channel spacing (distance in the alongshore spacing between two neighbouring channels) is calculated, the results are shown in Figure 5.10. The average rip channel is found to be 131 meters with a standard deviation of 91 meters.

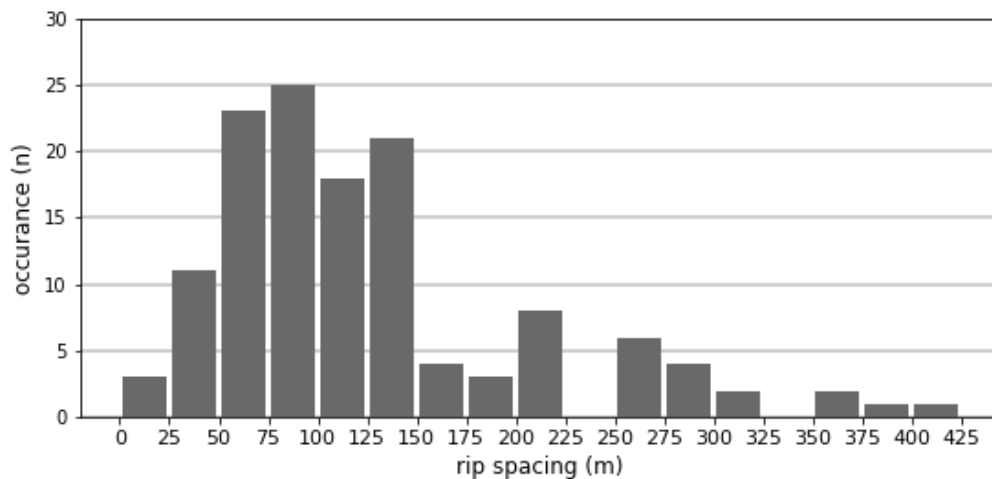


Figure 5.10: distribution of rip channel spacing.

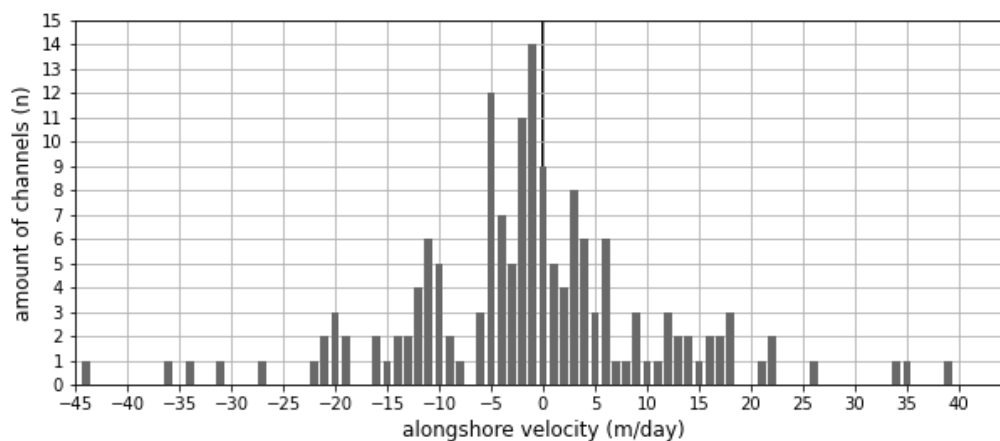


Figure 5.11: distribution of the alongshore velocities of the intertidal channels. Negative velocities correspond to movement to the left, while positive velocities indicate movement to the right (within the local reference frame).

For each channel shown in figure 5.9 the alongshore movement velocity (m/day) is calculated, the results are displayed in figure 5.11. The mean alongshore velocity is -1.55 m/day with a standard deviation of -0.77 m/day. This negative average alongshore migration velocity indicates a net movement of channels towards the left side within the local reference frame.

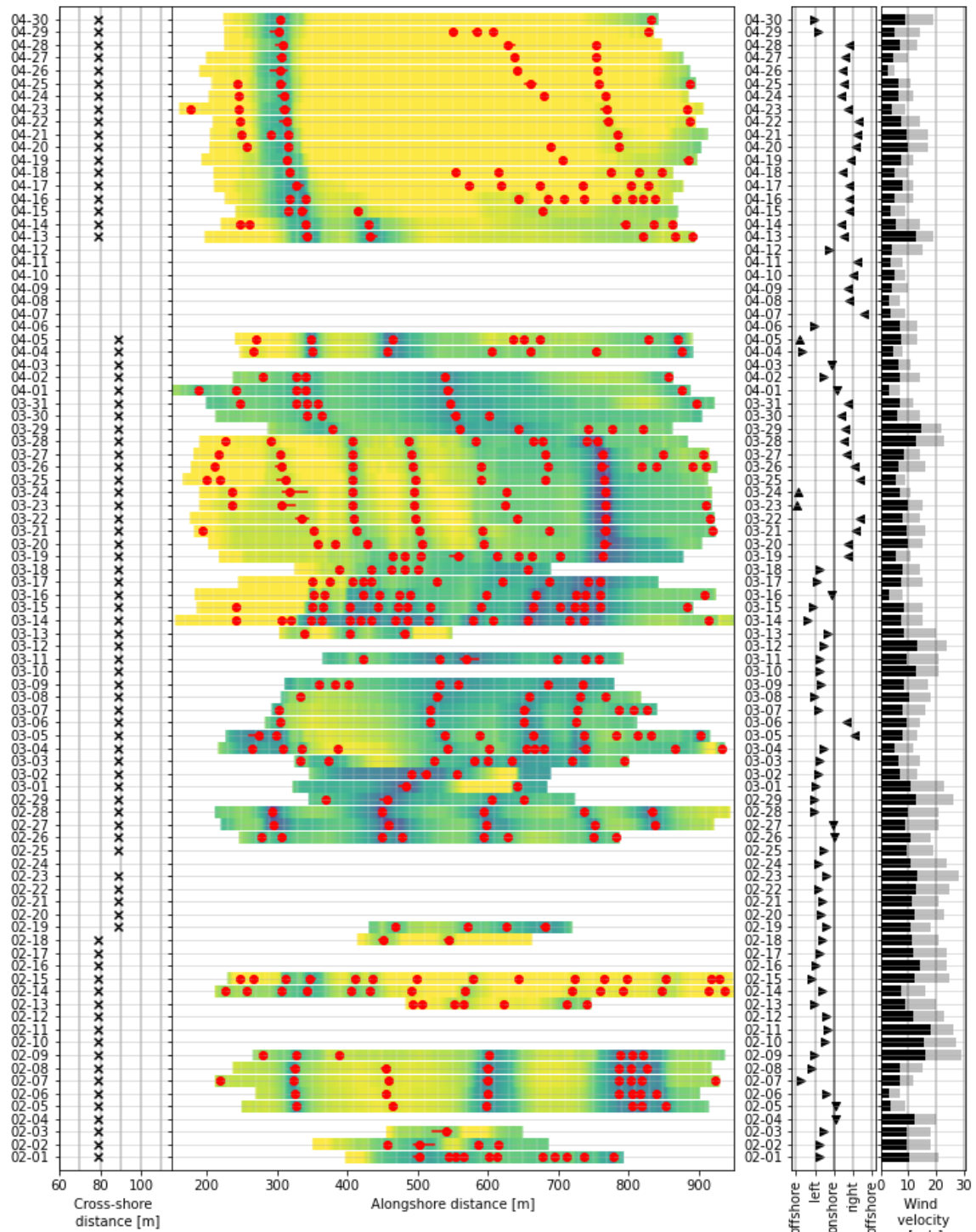


Figure 5.12: Results of the improved 1D alongshore analysis. On the left side the cross-shore location is indicated by the black crosses. The centre figure shows detected channels (red dots) displayed on a colormap that indicates the elevation. On the right of the two figures relative to the wind a shown. The left figure displays shore relative wind directions, distinguishing between onshore, offshore, left and right. The right figure shows the daily average wind velocities (black bars) and daily maximum wind velocities (grey bars).

### 5.3. 4D-Object-by-change analysis results

In this section the results of the 4D-OBCs analysis are presented. The implementation of the method as explained in 4.5.1 did not provide the expected results such as channels and runnels. Additional adjustments have been made to the input data and the way 2D-growth of objects is calculated. These changes are elaborated upon in Section 5.3.1 and the results of this change are shown in Section 5.3.2.

#### 5.3.1. Adjustments to 4D-OBCs method

From the results of the 1D analysis it became clear that channels were only observed between  $x=200$  and  $x=850$  meters alongshore in the local reference frame. The 2D data grids used in the 4D analysis are cropped to remove the additional points located outside this window. The same is done in the cross-shore direction by limiting the points in the offshore direction up to  $y=130$  instead of  $y=150$ . Using this cropping method reduced the amount of grid points for each epoch in the time series from 180.000 points down to 84.500 points which reduces the computational times significantly. Furthermore, an additional limitation for the location of seeds detection is enforced. This is done by limiting the area within the cross-shore direction where a seed can be located to ensure the objects are located in the intertidal zone. Seed search has to start between  $y=60$  and  $y=100$ m in the cross-shore direction. The combination of these limitations reduces the computational times roughly with a factor 6.

The space-time surface change array used in the analysis is not derived by calculating the differences in elevation for each epoch relative to the start of the time series. Instead the difference for each epoch relative to an averaged beach profile is calculated and used as space-time array. It is reasoned that the first epoch of a time series where large morphological changes occur is not a representative value for comparison. A point in the time series much later, when it is possible that the intertidal morphology has been subjected to significant changes, would benefit from a comparison to an averaged profile. The concept of comparing the time series to the first epoch is conceptual not wrong, but does not yield the desired results for the detection and tracking of intertidal morphology. Usage of a representative average profile proved to result in better detection of ridge-runnel features.

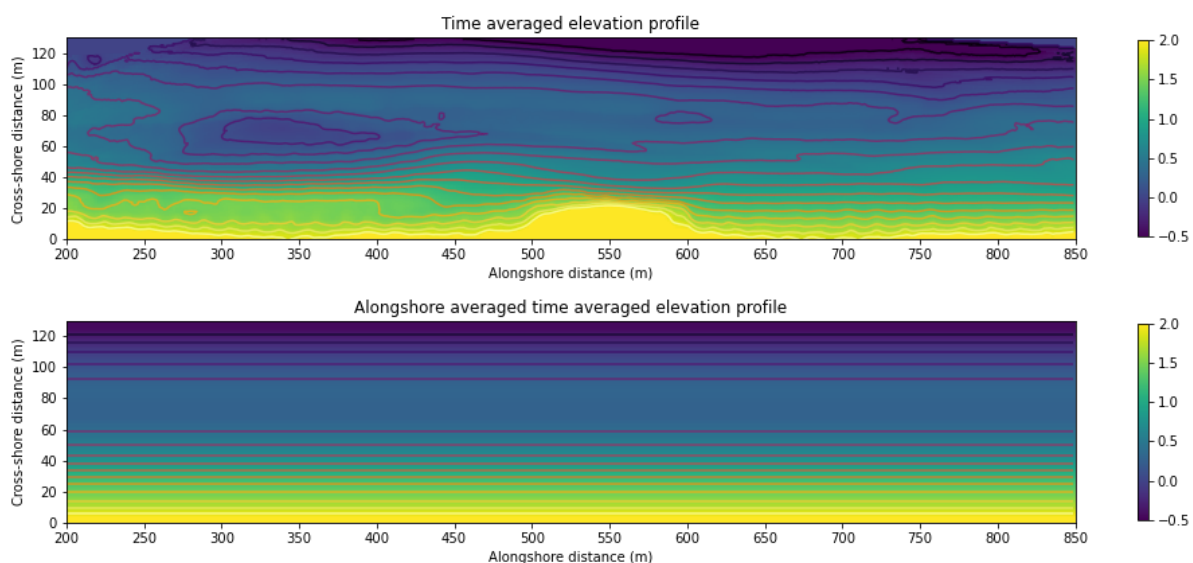


Figure 5.13: Time averaged elevation profiles of the beach at Noordwijk during the period February - April 2020. Top figure shows the average elevation for each point within the 2D grid. The bottom figure is the result of averaging this average elevation in the alongshore direction to obtain an uniform beach profile.

The average elevation profile is calculated by summation of all surface elevations for each 2D grid point and dividing this total elevation by the amount of points containing elevation data within the time series for each 2D grid point. The resulting elevation profile is shown in top image of Figure 5.13 by means of a height colour map and contour lines. The time series used for this time averaging is too short (only three months) and morphologic features that existed for extended periods during this time series are still visible. For example, the channel located at  $x=750$ ,  $y=75$  meters can still be seen and the presence

of runnel around  $x=400$ ,  $y=60$  is still present after averaging.

It is thought that this method of determining an average elevation profile yield good results when using a longer time series (a year or longer). However, on this relative small time scale of three months it is possible for morphologic features to dominated this averaging. This is the case if an intertidal ridge-runnel system is present for a significant amount of time at a stationary location.

In order to compensate for the short time series and additional averaging step is applied. In this step the cross-shore profile is averaged in the alongshore direction, the results of this averaging can be seen in the bottom image in Figure 5.13. The importance of this additional step is illustrated by means of Figure 5.14. This figure consist out of three subfigures, the top figure displays the elevation profile of one day, the middle figures shows the results of the calculated surface change when using the time averaged elevation profile and the bottom figure shows the result of this calculation when using the alongshore averaged time averaged elevation profile. Between these two last figures clear differences can be seen. In the middle figure a large area where accretion takes place is visible (yellow coloured patch), in the elevation profile for this day no morphology representing an elevation is visible at this location. Using the alongshore averaged cross-section profiles, this patch is not visible. The second averaging method proves to be better in representing the actual changes that occur. It has to be noted that in the bottom halves of both figures, between  $y=0$  and  $y=40$  some deviations are also visible. However, this area is excluded from the search area for the 4D objects.

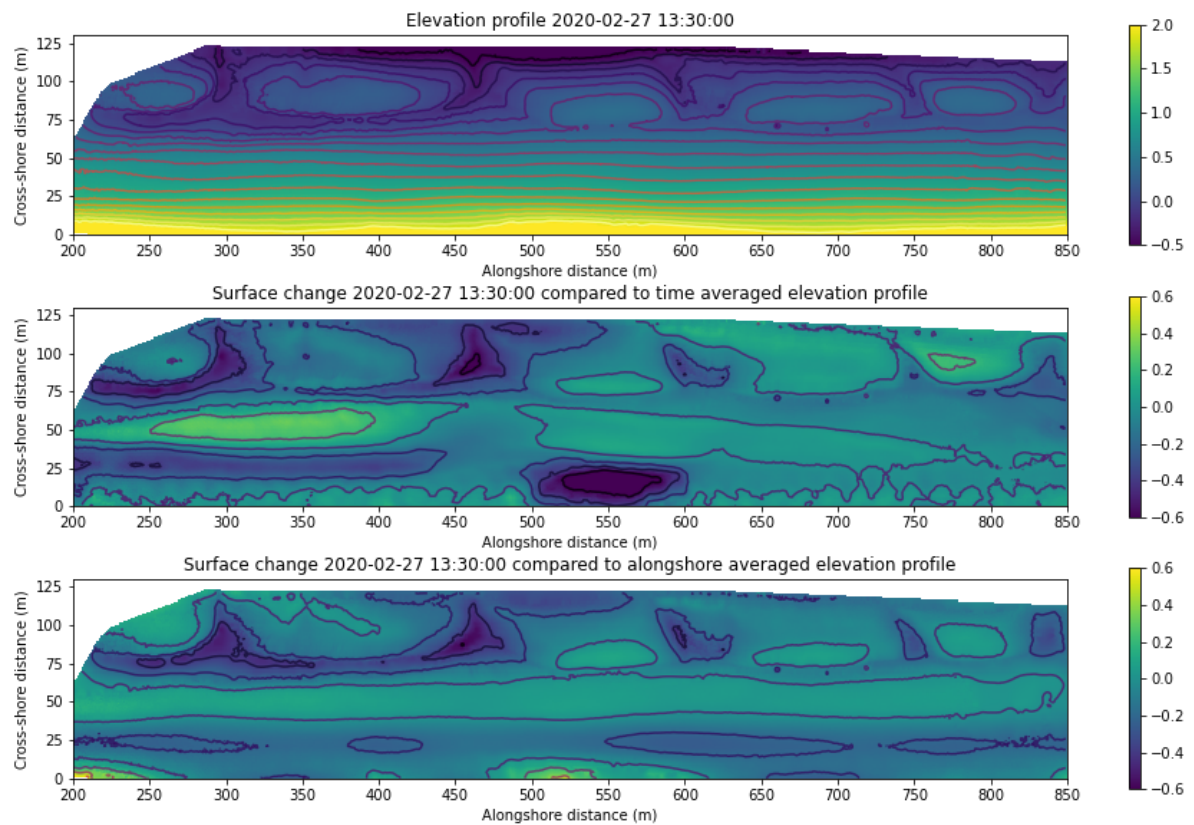


Figure 5.14: The effect of using the two different time averaged elevation profiles for the calculation of the surface change. Top figure shows the elevation profile of 27th of February. Middle figure shows the resulting surface change when using the time averaged profile as reference elevation. Bottom figure shows the surface change when using the time averaged elevation combined with the additional alongshore averaging.

Besides the changes made to the space-time array of the surface change a minor adjustment is done in the 2D segmentation growth. This adjustment influences the way surface change profiles of neighbouring points are compared to validate if they are within the threshold set for region growth. By removing a translation applied to both signals an improvement to the detection of channel and runnel morphology is achieved. The removal of this translation is related to the change made in the space-time array, the discussion in Section 6.3.2 elaborates in depth on this changes and its influence. The influence of the adjustment is illustrated by means of Figure 5.15, in the figure a difference between the distances of the two space-time arrays can be seen. The original implementation of the 2D-segmentation growth translates both signals to start at 0, the adjusted method does not use this translation. By calculation the summation of distances between paired points, as done in the DTW calculations, the difference becomes clear. In the adjusted method the calculated distance is reduced with a factor 4. For the application of the methods this implies that the a neighbouring points (comparison signal in the plots) is more likely to be within the thresholds set for the 2D-segmentation growth and thus and spatial larger 4D-OBCs can be found.

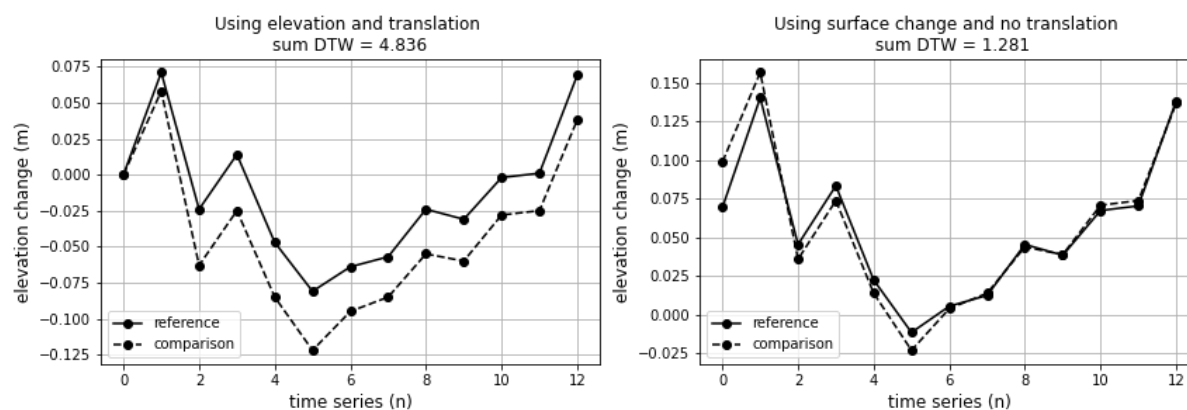


Figure 5.15: Illustration of changes made to comparison of space-time array signals of neighbouring points. Left figure shows the default method using a translation of both signals to 0. Right figure shows adjusted methods without this translation resulting in a smaller distance between paired points.

### 5.3.2. 4D-OBCs Results

The application of the 4D-OBCs method to the Noordwijk dataset resulted in the detection of 123 4D-objects. All objects are manual interpreted and are assigned to 5 pre-defined categories:

- Channel: 4D-object spatially covers a channel.
- Runnel: 4D-object spatially covers a runnel.
- Runnel-Channel combination: 4D-objects spatially covers a runnel and channel of a part of both.
- Part of a Runnel: 4D-object is located within a runnel.
- Part of a Channel: 4D-object is located within a channel.
- Other: Location of the 4D-object does not match to channel-runnel morphology.

An example of each classification category is shown in Figure 5.16. The final results of the analysis are summarized in Table 5.1.

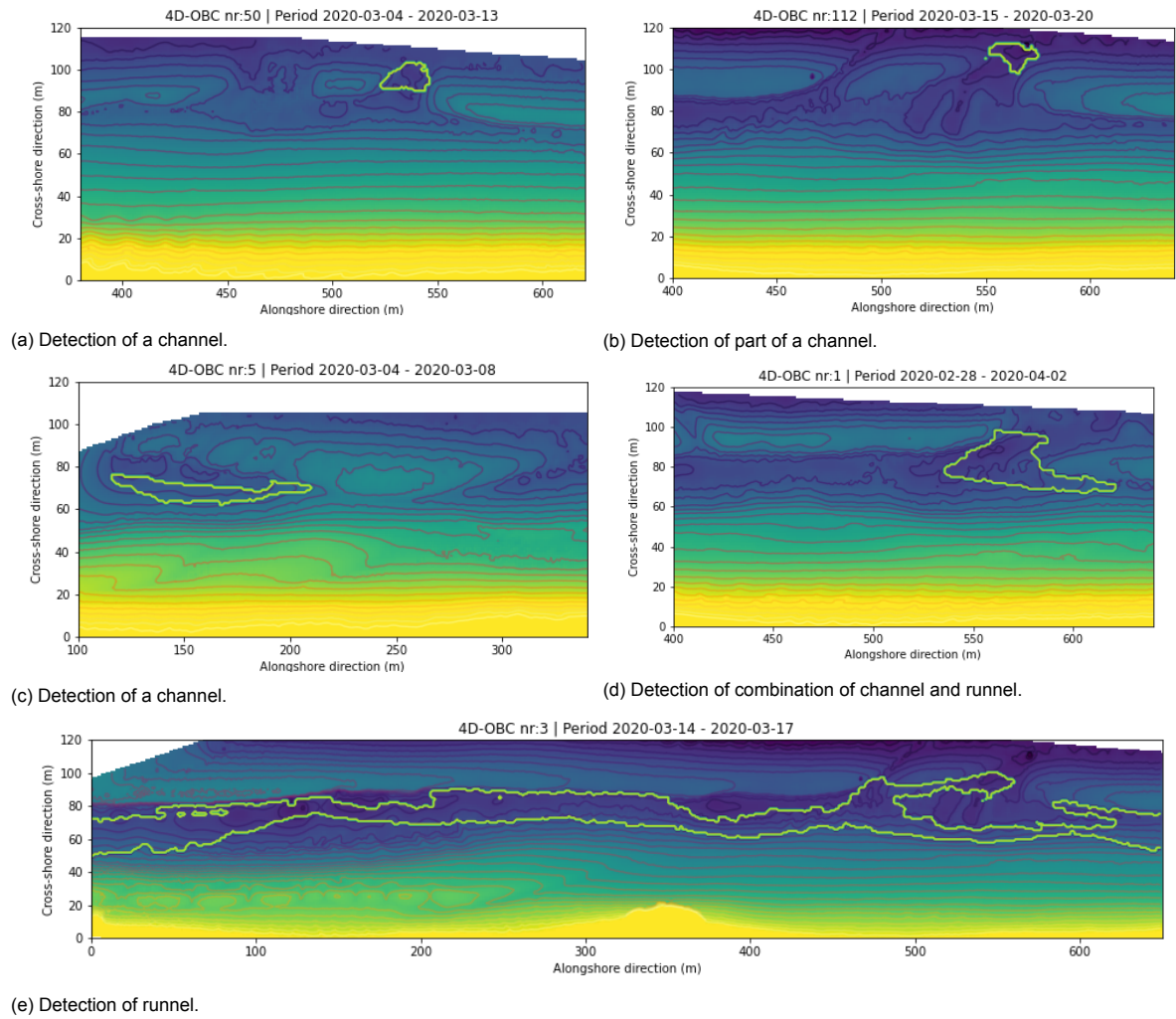


Figure 5.16: Overview of the 5 different type of 4D-OBCs that are distinguished between. All 4D-OBCs are manually interpreted and assigned to one of the defined types.

Type	Amount
Channel	5
Runnel	3
Runnel-Channel combination	14
Part of Channel	9
Part of Runnel	37
Other	55

Table 5.1: Amount of 4D-OBCs per category



## 5.4. Comparison between 1D- and 4D- Analysis

A comparison between the results of channel detection using the 1D method and the 4D-OBCs methods is made. Note that this comparison only includes channels as runnels where not part of the 1D analysis. The comparison is made by matching channels found in the 4D-OBCs method with the channels that existed for extended periods of time (result of the channel grouping) as seen in Figure 5.9.

The 1D Analysis returned a total of 44 detected channels that existed for extended periods of time within the time series. Visual inspection of the 123 4D-objects found with the 4D-OBCs method showed that 24 of the 44 previous detected channels were also found using the 4D-method. Figure 5.17 provides an overview on which channels are found by both methods. In this figure the results of the 1D- and 4D-methods are shown side by side. On the left side the channels as found using the 1D method are shown. On the right side are the results of the 4D method overlaid on top of the 1D results, each colour indicates one of the 24 4D-OBCs.

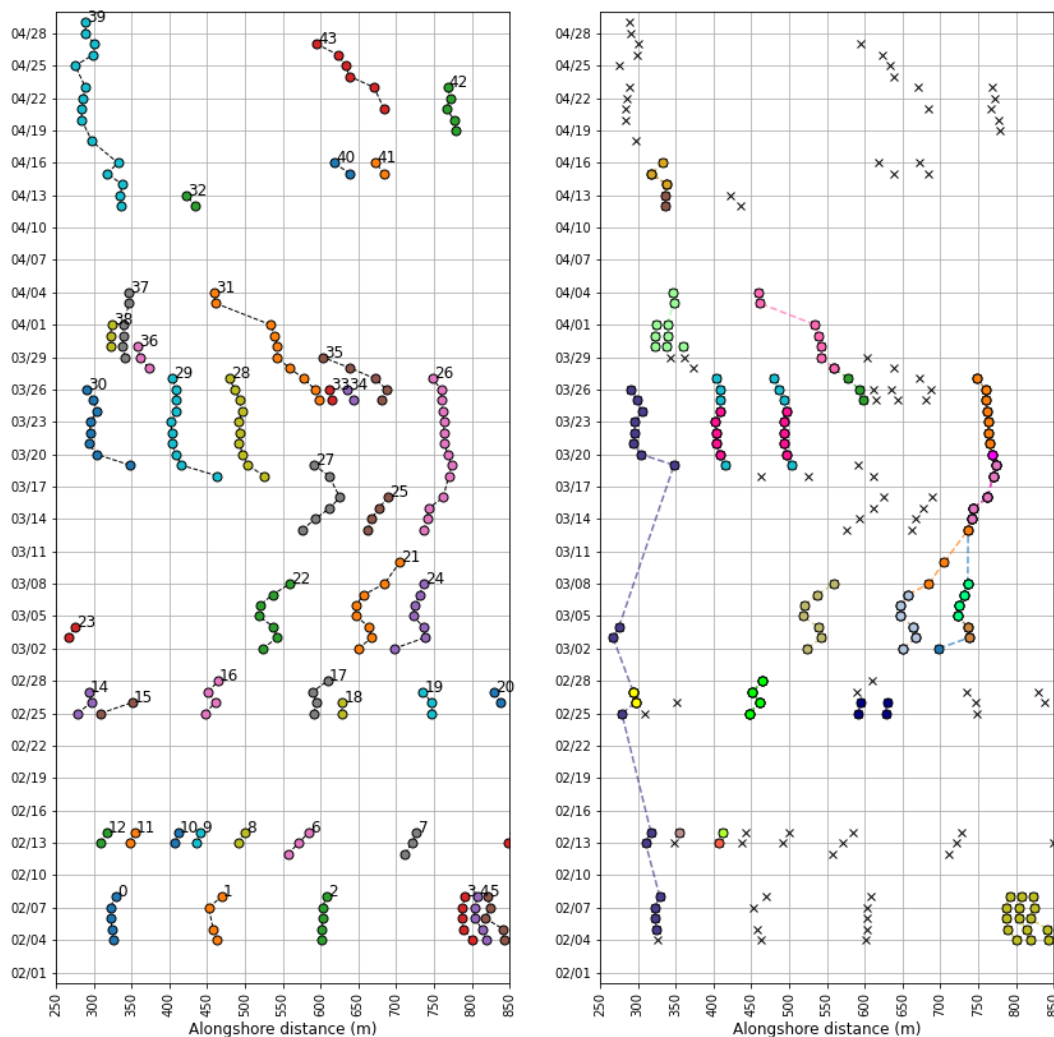


Figure 5.17: Comparison between detected channels in the 1D- and 4D-method. Left figure shows the results obtained using the 1D analysis. On the right figure the results of the 4D analysis are overlaid on top of the detected channels of the 1D analysis, indicated by the black crossed markers.

The duration of the lifetime of a channels does not have to be the same length in this comparison due to the different methods of determining the presence of a channel. Besides the time difference there is also a spatial difference, the 4D-OBCs method can return 1 object that spans the area in which multiple nearby channels can be located. An example of this can be seen by looking at the channels numbers 3,4 and 5 in the right lower corner of the figure. These channels are returned as separate entities in the

1D analysis but are regarded as one larger object-by-change in the 4D analysis. Another example of spatial differences can be seen while comparing channels numbers 28 and 29. These channels are also combined, but are also partly detected twice (cyan blue, and pink channels on right figure). This is explained by a possible difference in the rate of change within the channel(s), the 4D method will consider this as two separate objects-by-change. Furthermore, the linear interpolation of the space-time array as described in previous can result in the a channel that exists for a longer time period than detected in the 1D analysis. A example of this is the blue channel stretching along the left side of the figure.

The 4D-OBCs method did detect less channels, however it also detected two channels that where not found by the 1D method. A possible explanation for this difference is the limitation on minimum spatial size of an object enforced in the 4D-method. A minimum size of 100 grid points is used, meaning that for the 1x1m grid used in the analysis an object has an minimum of 100m<sup>2</sup>.



# 6

## Discussion

Discussion is done based on the three main steps of the research: data selection, data processing and the analysis. For each of these steps possible area's for improvement are suggested.

### 6.1. Data selection

During the process of data selection it was opted to select a period with varying weather conditions. The period spanning February, March and April 2020 met those requirements with roughly 6 weeks of windy or storm conditions and 6 weeks of mild conditions. It was found that on days where storm conditions occurred or heavy precipitation was measured the data quality was severely reduced. As consequence there were multiple gaps within the timeseries, from the 90 days that the timeseries spans only 73 contained data on the intertidal zone.

Using a period of three months showed clear alongshore variability of the intertidal rip channels. This period of three months is not representative for the variability that can occur during longer time periods such as a year. The time series of 3 months was used as starting point for this research as it was not yet known if analysis of the data would yield in good insight in the behaviour of the intertidal channels. With the established routines it is possible to extend the analysis period. However, the process of manual selection of scans, converting them to xyz-coordinates, post processing and validation is time intensive. Due to the limited time available for this research it was chosen not to extend the time series with additional months.

Another area of improvement is related to the temporal interval of the data within the time series. It was chosen to use the daily lowest water level occurring during the semi-diurnal tidal cycle. This approach assured to select the moment where the intertidal zone would be most visible. However, an argument can be made to include the 2nd low water event of each day in the time series. Using two lower water events per day would increase the temporal resolution of the time series. This higher temporal resolution allows for more accurate descriptions of the developments of the rip channels.

### 6.2. Data processing

Improvements to the data processing can be split up into three parts: noise removal, rotations, and grid spacing. The topic of interpolation is discussed separately.

#### 6.2.1. Noise and object removal

The SOR-filter used for noise removal has a few drawbacks when applied to ground based laser equipment. As explained in Section 4.2.1 the SOR-filter removes points based on distance between neighbouring points. This is a valid approach when using a dataset with a relative constant point density, but for a ground based setup where measurements are done in angular steps this point density becomes smaller over distance. Noise located close to the scanner can be skipped with this approach while completely good points can get removed by the SOR-filter as the filter threshold is constant over the

entire point cloud. Using this filter method is too harsh on data located on the outskirts of the point cloud. Using a method that takes into account the distance from a point to the laser scan and applies different filtering conditions based on this distance could yield a filtered dataset that contains more data points.

### 6.2.2. Time dependent rotations

The rotation of the point clouds to compensate for time dependent rotations was done using iterative closest point (ICP) calculations of reference area's. This concept is not new and has been applied to similar data sets with success. The application of this method to the Noordwijk dataset proved to be more difficult. During days when weather conditions were poor (rain, fog) the amount of points located within the reference area's used for the ICP calculations were severely reduced, resulting in a faulty transformation matrix and thus a poor correction. It was opted to manually correct the few occasions where this issue occurred. The development of a method for the time dependent correction was not in the scope of this research, however an improved version has come available during the timespan of this research. Even though this new method proved to be more accurate it was chosen to continue with the current corrected data.

### 6.2.3. Data rasterization

For the rasterization of the data it was chosen to use a grid with grid cells of 1x1 meter to cover the 1200x150 meter local reference system, resulting in 180.000 grid points. This 1x1 meter grid is relative coarse compared to the original density of the point cloud outputted by the scanner. The usage of a 0.5x0.5 meter grid might preserve more detail within of the original elevation values in the point cloud. Preserving these details is especially important around the edges of the dataset where interpolation takes place. The slopes of the rip channels are only described by a few points in the alongshore direction when using the 1x1m grid, using a smaller grid cell size preserves more elevation details of these slopes. However this smaller grid would result in 720.000 grid points (4 times more). Using this more detailed grid takes up significant more computational time during the analysis. During the both analysis lots of adjustments and improvements were made, using the larger grid cells the computational times are shorter and provided less downtime during calculations. However, when having an established method for analysis that has been proven to work it is suggested to repeat the analysis for a smaller grid. This step was not done during this research as time was limited.

### 6.2.4. Spatial interpolation

The interpolation of the spatial gaps within the data was originally not intended to be done during this research. However, during the application of the 4D-OBCs method it became clear that these gaps proved difficult to handle. The space-time arrays used as input data for the analysis contained too many gaps in the time series with result that seed detection returned as good as no potential location in the intertidal regions. Furthermore, interpolation could also provide better insights in the depths and widths of channels provided that the interpolation method is accurate enough. The method of interpolation applied and a comparison with GPS measurements is provided in section 4.3.

From the comparison between the interpolated height values and the GPS measurements a few observations can be made. First, the interpolated elevation profile is an underestimation of the actual elevation. Meaning that the depths of channels and runnels calculated using the interpolation are not as deep as they actually are. Figure 6.1 illustrates this by means of a histogram plot. For only 5 of the 123 measured points the difference was positive, meaning that the calculated profile is too deep. Second, from this same figure it can be concluded that the only a few points have a large deviation ( $>0.15$  m), most points are within acceptable limits ( $<0.10$  m). Taking into account the accuracy of the GPS measurements which is in  $\mathcal{O}(0.05$  m) and the accuracy of the elevation data represented in a single point within the 2D grid after processing (also  $\mathcal{O}(0.05$  m)) it is thought to give a decent representation of the real world morphology. It has to be stated that this comparison is based upon one single laser scan and the results found for this comparison might not be representative for the entire time series.

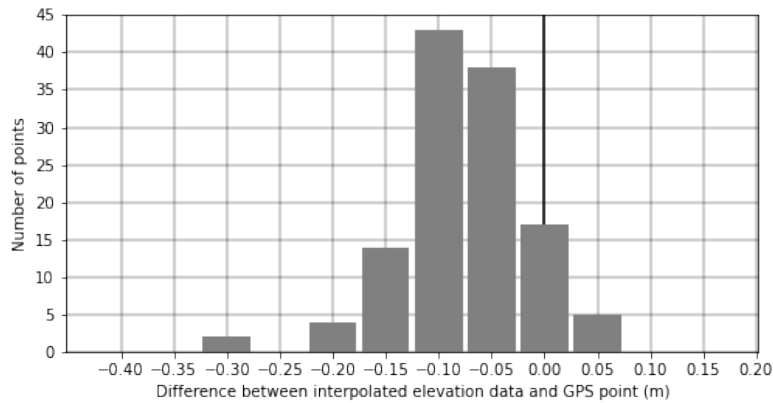


Figure 6.1: Histogram showing the distribution of deviation between GPS measurements and interpolated elevation data. Negative values indicate a GPS point having a lower absolute elevation value.

The 2D RBF-interpolation method shows promising results for the interpolation of Intertidal morphology but is not perfect. The working of the methodology is described in detail in section 4.3.1. The way the 2D approach is currently implemented can result in interpolation artefacts near the edges of the data. Near these edges the calculated elevation profiles tend to be too high. Because this area is not the main area of interest and it mainly influences the interpolation of runnels and not the channels this issue is regarded to be of little importance for the outcome of the analysis.

A final remark on the application of the RBF-method is made regarding input data. The interpolation is done using the gridded data obtained in the final step of the processing. However, the nature of the RBF-method does not require data to be on a grid like structure meaning that it would be possible to apply this method before this final processing step is done. Using the full, non gridded, dataset for the interpolation could provide a more accurate interpolation at the cost of more computational time. No comparison can be provided as this second approach has not been tried.

## 6.3. Analysis

Discussion of the analysis is split in to two parts, the first part is related to the 1D analysis method and the second part to the 4D-OBCs method.

### 6.3.1. 1D methods

The aim of the 1D method was to provide a simple straight forward means of analysis. The intertidal rip channels are assumed to only vary in the alongshore direction. This approach is an oversimplification and the detection of rip channels was only correct when the intertidal ridge-runnel morphology intersected with the location of the analysis.

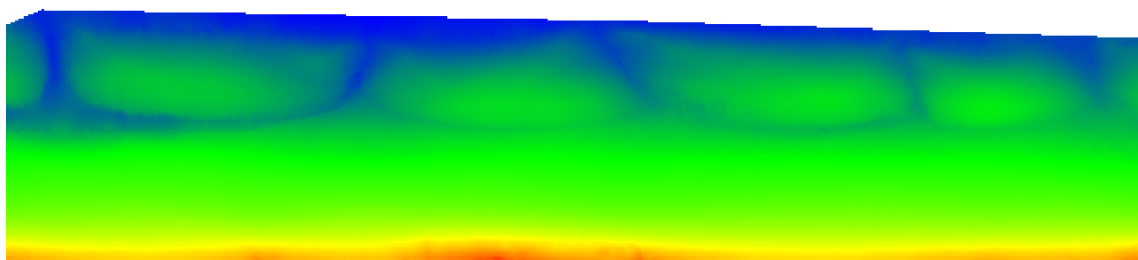
Adjusting the method to allow for these variations in the cross-shore movement was done by detection of the location of the intertidal ridge morphology. From this detection two dominant cross-shore locations were found, and the cross-shore location of the alongshore analysis was matched to these variations. This adjustment resulted in better detection of channels over the entire timeseries and provides the information about alongshore movements. However, it does not provide any data on the shore relative angle of the channels.

To detect this shore relative angle it was opted to repeat the detection process for multiple alongshore cross-sections per epoch. This method gives a better insight in the channel as a 3d object. Besides the shore relative angle an average width and depth were determined to characterize the channel and assess its changes over time.

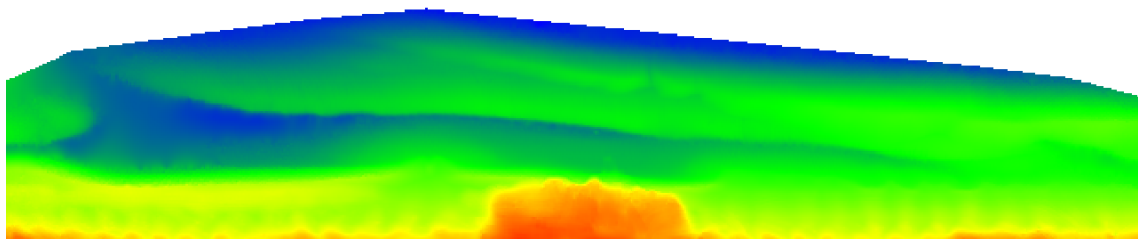
A important part of the detection of a channel is defining its width and relative depth. Defining the width of a channel base a percentage of the relative depth proved to be effective and consistent, however it has no theoretical foundation. A possible solution can be found in the work of Brander and Cowell

[28]. In this research a quadratic trend surface equation is used to describe an equilibrium profile for the surf-zone. By subtraction of this equilibrium profile from the measured elevation mesh area's are defined in rip area's and non-rip area's. The width of a rip channel is then defined by the intersection with the horizontal plane  $z=0$ . Using this, or a similar, approach has the downside that it complicates the analysis by becoming a 2D analysis method.

As stated before, 1D analysis approach works relative well and is easy to apply. However, it does have a few limitations. First of all, it only works well when the intertidal morphology is located shore parallel as the alongshore section that is being analysed is chosen to be shore parallel. During the period that has been analysed the intertidal ridge-runnel morphology was mostly oriented shore parallel and no issues occurred. Within the last epochs of the time series it can be seen that the morphology is rotating and the 1D analysis might not provide the best results. Figures 6.2a and 6.2b show the two different types of intertidal morphology that occur during the analysed time period. For such, shore inclined, intertidal ridge-runnel morphologies the 1D analysis shows shortcomings and a full fledged 2D analysis method is required.



(a) Example of shore parallel bars (27-02-2020)



(b) Example of bar morphology with an angle relative to the beach (29-04-2020)

Figure 6.2: Example of two different intertidal morphologies that are observed within the data.

Another important limitation of the current analysis is that there is no difference made between the different shapes of channels that can be seen in the data. In the analysis it is assumed that all channels are simple shapes consisting of low points located on one shore perpendicular axis. However, more advanced shapes do exist. For example bifurcations where one channel feature actually exists out of two separate channels that merge together toward the sea side. These types of channels are manually corrected by merging the corresponding channel id's assigned during detection.

### 6.3.2. 4D methods

Discussion on the application of the 4D Objects-By-Change method is done on the basis of two main topics: the space-time array containing the data on the morphology and the 2D spatial segmentation growth. These two topics proved to be the most influential when tuning the method to work as expected for the Noordwijk dataset.

The space-time array can be constructed in two manners, using surface change data or absolute elevation data. In the development of the 4D-method [41] the surface change variant is used. The surface change is calculated by subtraction of the elevation data of the first epoch, effectively meaning it offsets the entire elevation space-time array with a constant value. This indicates that the signal used for the change point detection for both methods is identical (with an offset) and yields the same results.

The usage of absolute elevation data as space-time array did not return the rip channels and runnels as would be expected by means of visual inspection. The 4D-OBCs found in the detection did not match the locations of channels and runnels but were often more located on the slopes of intertidal bars. Furthermore, the spatial extent of the objects were smaller than expected. A change to the way the surface change space-time array is calculated was implemented as explained in Section 5.3.1.

Figure 6.3 clearly illustrates the differences between the original method, using a space time-array of surface change compared to the absolute elevation at time step  $t=0$ , and the adjusted method, offsetting the surface change space time-array using the averaged elevation. In this figure the surface change over time is plotted for  $10\text{m}^2$  containing 100 grid points, the area between  $x=345\text{--}355\text{m}$  and  $y=45\text{--}55\text{m}$ . From this graph it can be seen that the surface change profile obtained using the adjusted method, the solid black lines, shows a similar signal compared to their neighbouring points. The surface change obtained using the original methods, the red lines, show a larger spread. This difference does not influence the seed detection, but is of importance for the DTW distance calculation. Another important difference is that the results of the detection of the 1D method are bound to the location of the alongshore transect where the analysis is done. The 4D method is not limited to a single transect as it can use the entire 2D grid as search locations.

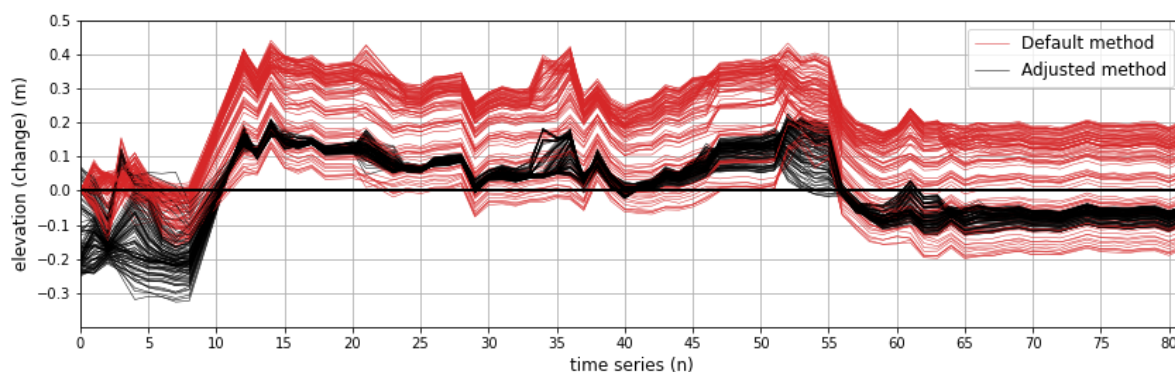
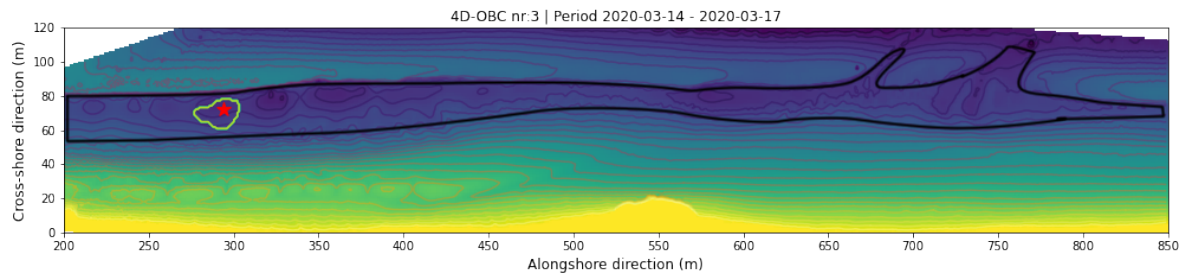


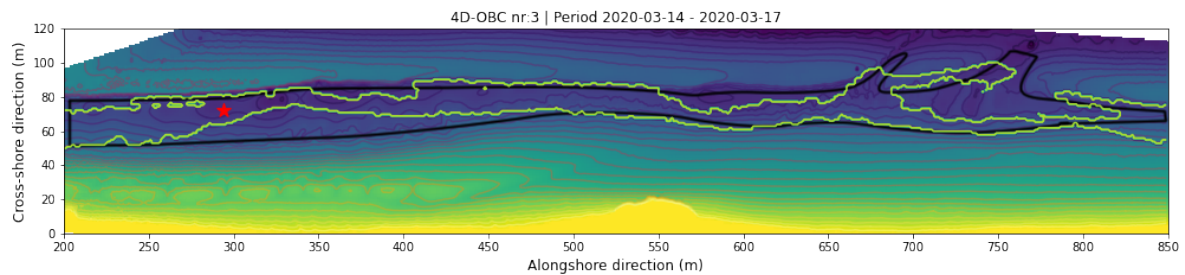
Figure 6.3: Visualization of the space-time array for 100 points within a  $10\times 10\text{m}$  area. Red lines correspond to the profiles obtained by the default method. Black lines correspond to the adjusted method. A difference in the spread between the signals can be seen.

With this adjustment the expectations are that the 2D-segmentation growth would yield larger objects. By comparing the objects grown from the same seed this impact can be assessed, Figure 6.4a and 6.4b shows an example where a clear difference is observed. In this figure the seed location is indicated by the red star, the spatial size of the object is visualized with the green contour line, the visual interpretation of the contour of runnels and channels is shown by the black line. The difference in object size is clear from the figures and confirms the expected behaviour of the adjusted method. In addition, the 4D-OBC did grow to extend over the entire runnel but does not include parts of the runnel. This is explained by the rate of surface change in these sections are larger or smaller than the rate of change of the object itself. These sections are returned as separate objects.

In the comparison between the 1D- and 4D-method a difference in the amount of detected channels was noticed. This can be explained by the fact that the 4D-method uses a minimum segment size requirement before a object is created. This minimum segment size is set at 100 grid points, and thus only features larger than  $100\text{m}^2$  are returned. This minimum requirement is used to limit the amount of 'noise' objects. However, it is possible that small channels are therefore rejected as 4D-OBCs. A possible solution could be taking into account the shape of these small features. For example, if the cross-sectional length of the objects is larger than the alongshore width the shape could indicate a possible channel.



(a) Contour plot of the maximum size of 4D-OBCs using the default detection method.



(b) Contour plot of the maximum size of 4D-OBCs using the surface change space-time array and change to the comparison of neighbouring surface profiles.

Figure 6.4: Comparison between the original and adjusted detection methods. Both objects started at the same seed location. The original method found an object that is part of the runnel, using the adjusted method the object has grown to cover the entire width of the runnel.

## 6.4. Comparison with existing research and literature

In this section the results found with the 1D-Analysis are compared to the research conducted by Quartel [9]. In their research Argus imaging technique is used to detect inter- and sub-tidal rip channels at the same section of beach at Noordwijk. The similarities between the location and the parameters used to describe intertidal rip channels, this research is used for the comparison. First a brief summary of the result of the research done by Quartel is presented, followed by a comparison with the results found in this research. Next, the differences between the results are discussed and possible explanations are provided. The section ends with a discussion on how the findings of this research correspond to the self organizing hypothesis provided in the literature chapter.

### 6.4.1. Comparison with previous research

Quartel used 15-months (during 2001-2002) of daily time averaged Argus images to describe the spatial and temporal variability of rip channels at the coast of Noordwijk. The alongshore distance covered by the Argus images is similar to that of the laser scanner (1000-1200m). The surface on these images is classified to be water, wet sand or dry sand based on colour of the images [8]. Rip channels were detected by the intersection of the dry sand alongshore bars with wet sand or water sections, resulting in the detection of 875 intertidal rip channels during 320 low tide images during the 15 month measurement period. Roughly 20% of the detected rip channels only existed for one day. The average intertidal rip spacing was found to be 243m and to be non-uniform [9]. For the alongshore movement of the rip channels a distinction between open rip channels and closed rip channels is made. Open rip channels are connected to the sea and a trough (in this research referred to as a runnel), a filled rip channel does not meet this requirements and is filled with sediments. The alongshore movements were found to be 4.6 m/day for open rip channels and 2.4 m/day for filled rip channels.

Comparing the main results from the research of Quartel shows differences in the rip channels spacing and alongshore migration rates. Using the 1D detection method a total of 375 individual rip channels were detected in a 3 month period, 168 channels only existed for one day, being 45% of the total. The average rip spacing was found to be 131 meters with a large standard deviation, indicating a non-uniform distribution. The average alongshore migration rate was found to be -1.55m/day (South-

Southwest directed). These numbers deviate from the findings of Quartel.

The difference in the length of the timeseries that are being compared, 3 months and 15 month. The amount of rip channels and their behaviour might vary during extended periods of time. Comparing averaged values of a period of 3 months with a period of 15 months could be a reason between the differences found in both results.

A more likely origin of the differences is related to the datasets and the way they are processed. The dataset used by Quartel consistent out of images, the pixels within the images represent x,y coordinates and the colour is used as indicator of state (water, wet sand, dry sand). Distinguishing of rip channels and intertidal bars is based upon contrast differences within the Argus images. In these images it is difficult to detect small rip channels that dry, or only wet for a limit time, during low tide. The data used in this research consists out of x,y,z coordinates and does not use information on the state in these points. The usages of elevation data for the detection of channels resulted in more detected channels per day. The methodology used by Quartel detected an average of 2.73 rip channels per day. The detection using elevation data resulted in an average of 5.14 rip channels per day. As the rip channel spacing is directly related to the amount of rips that are detected it is logical that the rip spacing found in this work is smaller.

A final remark is made on the years of origin of the datasets. The Argus dataset used by Quartel originates from 2001-2002 while the laser scan data is captured in 2020. During this 18 year period coastal management has changed. During the period around 2000 it was common to have sand supplementations being deposited offshore. After the completion of the Sandmotor in 2011 these supplementations have become more scarce. It could be possible that due to the construction of the Sandmotor the characteristics of the intertidal zone at the beach of Noordwijk have changes.

#### 6.4.2. Comparison with literature

In the Literature study (Chapter 2) several self-organization hypothesis on the development of the intertidal zone were explained, in this section the results are compared to the expected behaviour suggested by these hypothesis. Not all the hypothesis can be discussed as not all the required data is available. The discussion is limited to the relation between rip spacing and rip channel width, and alongshore migration direction and rate with wind and wave data.

A relation between the channel widths and alongshore distances between the channels can be seen in Figure 6.5. In this figure the distance between two channels and the averaged width of these two channels is shown as scatter plot. A linear regression, forced through 0,0 is shown with the red dashed line. From this figure it can be seen that an increases in rip spacing distance is paired with an increase in channel width. This relation is explained by the fact that when the distance between channels increases, the amount of water that flows back towards the sea through a single channels also increase. To accommodate the increased flow rates, the channel tends to become wider.

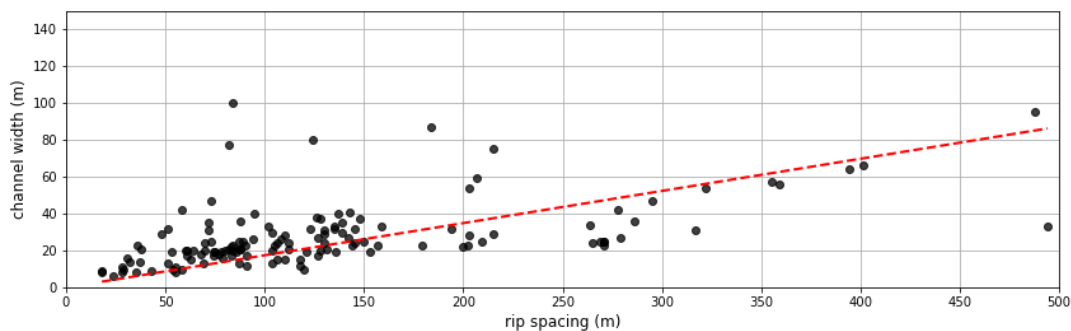


Figure 6.5: Scatter plot of the distance between two rip channels and the averaged width of those two channels. The red dashed line is the result of a linear regression through the points, forced to start at 0,0.

In Figure 6.6 the correlation between wind direction and velocity with alongshore migration rates by means of a directional are plotted. The wind direction are corrected for the shoreline orientation within the local reference system, meaning that 0° is onshore directed wind, 180° is offshore directed and



90° and 270° are from right to left, and left to right respectively. Colours are used to indicate the direction of the alongshore migration of the channels, red means a positive migration rate (to the right) and blue a negative migration rate (to the left). The intensity of the colour and size of the dot correspond to the magnitude of the migration rate.

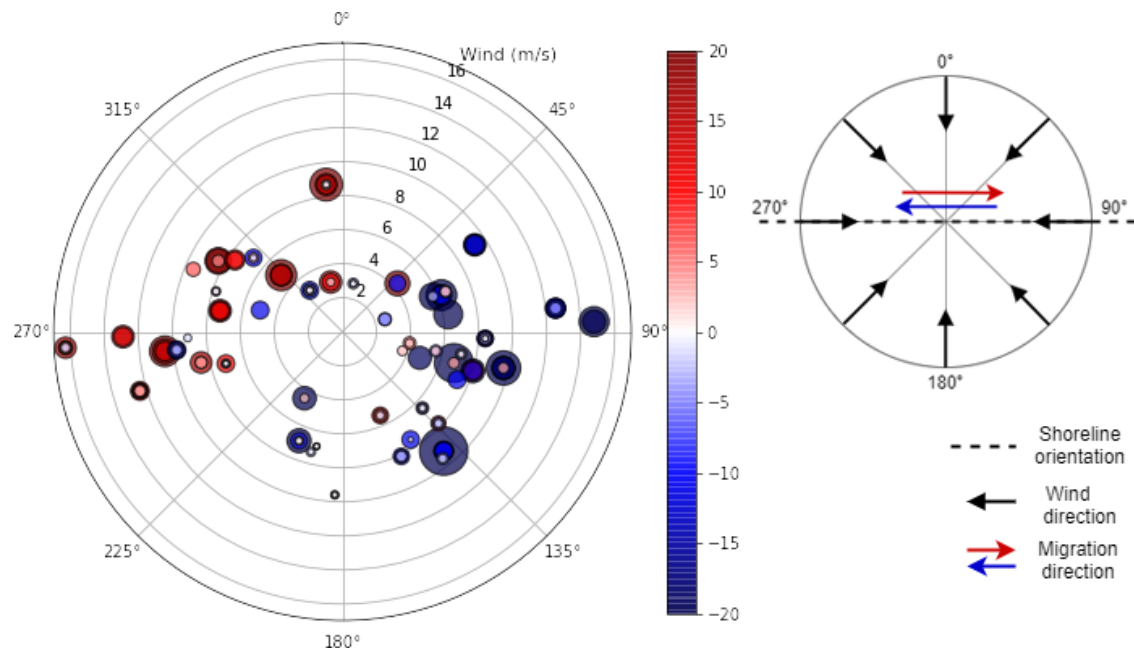


Figure 6.6: Directional plot showing the shore relative orientation of the wind and its intensity in relation to the alongshore migration rates of channels (0° is onshore directed, 90° is from the right, 180° is offshore and 270° is from the left in the local reference system). Blue dots represent negative migration rates (to the left) and red dots positive migration rates (to the right). The intensity of the colours and size of the dots are related to the migration rate. Figure on the right side elaborates on the interpretation of wind directions and alongshore movements.

From this figure it can be seen that the alongshore movement of the channels do show a correlation with the wind direction. For 68% of the alongshore movements the direction of the movement corresponds to the direction of the wind. Within the image some points can be seen where the direction does not match, for example within the range 0-180° a few (light) red dots can be seen. These dots are small and therefore have only limited migration rates. If all points with a migration rate below 1 m/day are excluded this correlation of migration direction and wind direction increases to 79%.

Due to the grid size of the rasterized data (1x1m) this exclusion of the sub 1 m/day migrations is made. It is possible that during determining the average alongshore location of a channel the lowest point of the channel (used for its location) shifts to a neighbouring grid cell even though the channel itself has not moved. In Figure 6.7 this phenomenon can be seen on the right half of the plot, quite a few small red dots are located in this section. These dots have very small migration rates (small circles, light colors) and occur during low wind velocities. In the range 180-360°, large blue dots are visible. This means that the detected migration rate does not correspond to the wind direction.

A similar plot (Figure 6.7) can be made using the wave data by plotting migration rates versus offshore wave direction (corrected for shore orientation) and wave height. The spectrum only shows onshore directed waves. The wave height and direction are the average values averaged over the period corresponding to the time span used for the calculation of the migration rate.

In this plot a similar trend is visible where the migration direction matches the incoming wave direction. For 65% of the alongshore movements the direction of the migration move along with the direction of the incoming waves, this is similar to the value found using the wind data. If all point with a migration velocity below 1 m/day are removed this value increases to 72%.

At several spots blue and red dots are located near each other (for example in between the lines 280° and 300°). This means that for similar wave direction and wave height contradicting migration rates are observed. It has to be noted that the values of the waves (direction, height, period) are at an



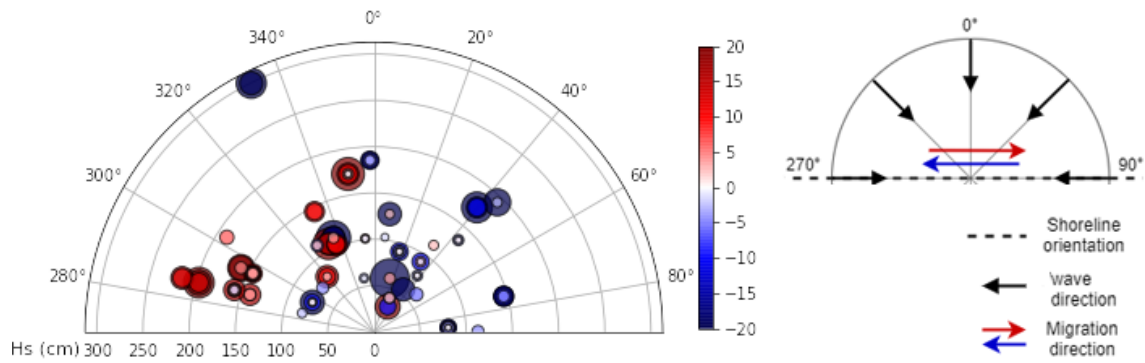


Figure 6.7: Directional plot showing the shore relative orientation of the waves and its significant wave height in relation to the alongshore migration rates of channels (0° is onshore directed, 90° is from the right, and 270° is from the left in the local reference system). Blue dots represent negative migration rates (to the left) and red dots positive migration rates (to the right). The intensity of the colours and size of the dots are related to the migration rate. Figure on the right side elaborates on the interpretation of wave directions and alongshore movements.

offshore location and are not converted to nearshore waves. The wave characteristics change when waves enter shallow water. Wave direction changes as a result of refraction (the effect of changes in wave velocity due to changing water depth). The wave directions shown in figure Figure 6.7 do not match with the wave direction nearshore.

In both figures (Figure 6.6 & 6.7) a similar observation can be made. Wind and waves coming from the right side result in a alongshore migration in the same direction (from right to left). For the wind data 77% of the points match the same direction, for the wave data this value is also 77%. If all points with a migration rate below 1 m/day are excluded these values become 82% and 86% respectively. For wind and wave coming from the left the same percentage can be calculated resulting in a correlation of 60% for wind and 57% for waves. When excluding the points with a velocity smaller than 1 m/day these values become 74% for wind and 67% for waves.

Looking into these percentages a clear difference between the correlation of wind and wave directions to the left and right is visible. A possible explanation for this difference could be the direction of the alongshore ebb current that is directed to the left side in the local reference frame. In this research the tidal alongshore currents were not taken into account and therefore this possible explanation is not researched in more detail.

## 6.5. Added value of laser scan data in the intertidal zone

One of the main limitations of studying alongshore variability in the Intertidal zone is the quality and quantity of the datasets that are available. Data obtained by field measurement campaigns often is limited in the alongshore distance (small spatial scale) and limited duration of the time series. Obtaining an intertidal dataset that covers a significant distance in the alongshore direction, while preserving a high spatial scale, for extended periods of time is labour intensive.

With the increasing usage of remote sensing techniques more extensive datasets are becoming available. Examples of the usage of these techniques can be found in the work done by Lafon et al. [10], who used satellite spot imagery to assess alongshore movement along a 35km section at the French Atlantic coast, and the already discussed work of Quartel et al. [8] using Argus. The application of remote sensing techniques for coastal monitoring provides a dataset covering a significant alongshore section of the coastline ( $O(km)$ ) for extended periods of time on a daily interval (or even shorter). However, research using these techniques distinguishes intertidal features based on colour contrast within images and does not contain any elevation data.

Laser scanning provides detailed elevation data for an alongshore coastal section (spanning  $\sim 1km$ ) for extended periods of time with a small temporal interval, creating a unique dataset combining the best properties of the field measurement (high density elevation data) and remote sensing techniques

(large spatial scales with short time intervals). Laser scanning does have its limitations: poor data quality during rain and no data available on wet sections of the beach as the laser can not penetrate the turbulent sediment rich water. The later being solved by the application of 2D-interpolation.

The usage of the 3D data provided by laser scanning allows for a more in depth analysis of intertidal features besides alongshore migration. Developments in the width and depth of rip-channels, and therefore the cross-sectional area, can be monitored over time. These cross-sectional area's can be related to the amount of water flowing through the rip-channels, which is related to the amount of sediments being transported through a channel. These last steps are not conducted within this research, more on the topic of follow up research and improvement is provided in Chapter 8 Recommendations.

Furthermore, intertidal elevation data obtained using laser scanning can prove beneficial for other studies. Brand et al. [43] provide an overview of the issues that occur when measuring sediment transport in the intertidal zone. One of main finding in their research is the need for improvements in the measurement of near bed sediment concentrations. Additionally, they suggest that continuous monitoring of beach topography by means of terrestrial laser scanning can provide valuable insights for improving sediment transport models.

## Conclusion

During the period 1 February up to 30 April 2020 laser scan data was analysed in order to assess the alongshore variability of intertidal rip channels. The temporal interval at which the intertidal zone can be analysed is related to the tidal cycle. In this 90 day period snapshots during the lowest water level each day resulting in a sufficient small temporal interval for monitoring rip-channel behaviour.

During this period varying weather conditions occurred. Days with rainfall produced low quality data with less or even no data points. On days with high onshore directed winds the resulting water level setup resulted in mostly submerged intertidal zone and therefore very limited data.

Between the 6th of April and the 13th of April no data was available due to malfunctioning equipment. From the remaining 82 days 73 days contained data on the intertidal zone after post processing. The remaining time series is processed to remove noise and 2D-interpolation is applied to spatial gaps within the laser scan data. The processed time series is analysed by means of a simple 1D analysis and the advanced 4D Objects-by-change method.

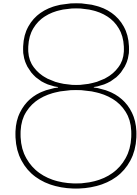
By means of detecting low lying section in alongshore elevation profiles, the 1D Analysis method detected a total 375 individual rip channels by analysis in individual days. From these individual daily detected channels 207 could be classified to be part of a morphological feature that existed for more than one epoch. Grouping individual daily channels over time based on alongshore location resulted in the detection of 44 channels that were present for more than two days. For each of these groups the alongshore movement between consecutive epochs are determined. Resulting in an average alongshore movement of -1.55m/day with a standard deviation of 0.77m/day. The rip channels spacing was found to be 131 meters with a standard deviation of 91 meters. Furthermore, a relation between the rip spacing and the width of the channels is reported.

The 4D-OBCs method was applied to the Noordwijk dataset to find erosion patterns corresponding to runnel and channel migration. By comparing daily elevation grid to an averaged mean beach elevation profile the method found 123 4D objects, these objects are manually inspected in order to classify them. From these 123 objects 78 objects could be classified to be a part of the intertidal morphology, being a runnel, channel or combination of both. The other 55 objects did not correspond to these intertidal features.

The 4D-OBCs method found 24 of the 44 channels found by the 1D method. This difference is explained by the 2D channel size limitations of 100 grid points enforced by the 4D-method. The 4D method did return additional intertidal features such as the runnels (and combinations of channels and runnel) that were not part of the 1D detection.

Comparing the alongshore migration rates and intertidal rip channels spacing with previous research conducted at the same site shows differences. The average alongshore migration rates and rip spacing were both found to be smaller. These differences are suggested to be a result of the difference in the length of the time series that are analysed, the origin of the dataset and the methods of detecting rip channels.

The usage of LiDAR measurements proves to be a valuable tool in order to obtain better insights in the alongshore variability of intertidal channels. It provides detailed elevation data on large spatial scale for extended periods of time while maintaining a small temporal interval.



# Recommendations

This chapter provides recommendations on how to improve the research and suggestions for potential follow up research. First the recommendations on improvements of the current work are provided, followed by suggestions how to proceed with the next step of the research.

## 8.1. Improvements to results

When studying the alongshore variation it is recommended to use a timeseries of at least a year long to account for seasonal variability. The Kijkduin dataset contains almost two years of laser scan data at the time of writing, using this extended dataset instead of the 3 month period would yield better insights in the alongshore variability. However, extending the length of the time series comes at the cost of longer processing times.

Within the discussion of Chapter 6 the limitations and possible improvement for each of the steps in the methodology were addressed. Improvements to the noise and object removal preserve more of the elevation details in the dataset as less non-noise point are removed by too aggressive filtering (see section 6.2). Combining this improvement with a smaller cell size for the grid used to rasterize the data could improve the overall data quality. Having a denser data grid results in having more elevation data available at the edges around the spatial gaps within the data, which could improve the accuracy of the applied RBF interpolation.

The validation of the RBF interpolation was done based on the difference between the interpolated elevation values and GPS measurements and was argued to be within acceptable limits. However, this comparison is done on the basis of only a single laser scan and it is difficult to justify that this elevation difference is within the limits for every epoch in the time series. It is suggested that a similar comparison should be done for more laser scans at different times and during different weather conditions. It might be the case that during clear weather and mild wave conditions the interpolation proves to be fairly accurate, but during stormy weather the interpolation could prove to be less accurate.

Even though the usage of the 1D method showed promising results, it is recommended to extend the detection method to a fully 2D-method. The movement of (rip) channels is not limited to the alongshore direction but moves along with the intertidal bar morphology in the cross-shore direction. A 2D method could use the concept suggested by Brander and Cowell [28] where rip channels are detected by means of a detrending method that fits an equilibrium beach profile through the elevation data. However, this raises the question on how to describe the equilibrium beach profile in the intertidal zone, furthermore, this approach would become similar to the way the 4D-Object-By-Change method was implemented for this research. It would result in a time series of surface change similar to the one derived in Section 5.3.1. Another possibility is to continue working on improvements and minor adjustments to the 4D-OBC method to obtain the desired results.

The correlation between the alongshore migration rate and wave conditions can be improved by the usage of nearshore wave data instead of the offshore wave buoy data.

## 8.2. Continuation of research

The usage of terrestrial laser scanning has proven to be a useful tool for monitoring the alongshore movement of rip channels. The unique 3D nature of the dataset allows for more detailed monitoring of the developments in width and depth of channels. In this research the development of the width and depth of the channels is analysed, however besides the relation between channel width and channel spacing no other relations are investigated. In this area a lot of knowledge can be gained.

The width and depth, and therefore the cross-sectional area, can be expected to be related to the amount of water flowing through a channel. The water flowing through the channels contains sediments and plays a role in the redistribution of sediments in the intertidal zone. Obtaining better insights in the volumes and flow rates of the water going through each channel can help with establishing sediment transport models.

Improving the detection and tracking of intertidal rip channels, and also including the runnels, is not as straightforward as it might seem. In order to get more detailed and consistent detection of those features it is needed to have a better description of the 3D-boundaries of these features. For determining flow rates and sediment transport through a channel it is needed to know in which part of the channel actual flow occurs. In this research a relative depth parameter was used to determine the borders of a channel, but this is not based on where actual flow took place. A suggestion might be to use the reflection values (present in the laser scan data) and some empirical relation between reflection and moisture content of the beach, as suggested by Di Biase et al. [44].

# Bibliography

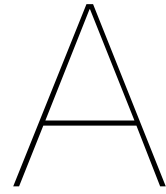
- [1] Antony R. Orme and Amalie Jo Orme. Ridge-and-runnel enigma. 78(2):169–184, 1988.
- [2] C A M King and W W Williams. The Formation and Movement of Sand Bars by Wave Action. *The Geographical Journal*, 113:70, 1949. ISSN 00167398. doi: 10.2307/1788907.
- [3] Sander Vos, Roderik Lindenbergh, and Sierd de Vries. Continuous monitoring of coastal change using terrestrial laser scanning. *Proceedings of Coastal Dynamics*, (233), 2017.
- [4] Kathelijne M Wijnberg and Aart Kroon. Barred beaches. *Geomorphology*, 48(1-3):103–120, 2002. ISSN 0169555X. doi: 10.1016/S0169-555X(02)00177-0.
- [5] Jens Figlus, Nobuhisa Kobayashi, and Christine Gralher. Ridge-runnel migration. *Coastal Engineering*, pages 1–15, 2006.
- [6] R. A. Holman and J. Stanley. The history and technical capabilities of Argus. *Coastal Engineering*, 54(6-7):477–491, jun 2007. ISSN 03783839. doi: 10.1016/j.coastaleng.2007.01.003.
- [7] Andrew Miles, Suzana Ilic, Duncan Whyatt, and Mike R. James. Characterizing beach intertidal bar systems using multi-annual LiDAR data. *Earth Surface Processes and Landforms*, 44(8):1572–1583, 2019. ISSN 10969837. doi: 10.1002/esp.4594.
- [8] S. Quartel, E. A. Addink, and B. G. Ruessink. Object-oriented extraction of beach morphology from video images. *International Journal of Applied Earth Observation and Geoinformation*, 8(4):256–269, 2006. ISSN 15698432. doi: 10.1016/j.jag.2006.01.002.
- [9] S Quartel. Temporal and spatial behaviour of rip channels in a multiple-barred coastal system. *Earth Surface Processes and Landforms*, 34(March):163–176, 2009. ISSN 01979337. doi: 10.1002/esp. URL <http://doi.wiley.com/10.1002/esp.1685>.
- [10] Virginie Lafon, H       Dupuis, H       Howa, and Jean Marie Froidefond. Determining ridge and runnel longshore migration rate using Spot imagery. *Oceanologica Acta*, 25(3-4):149–158, 2002. ISSN 03991784. doi: 10.1016/S0399-1784(02)01190-8.
- [11] Sander Vos, Mieke Kuschnerus, and Roderik Lindenbergh. Assessing the Error Budget for Permanent Laser Scanning in Coastal Areas Assessing the Error Budget for Permanent Laser Scanning in Coastal Areas. pages 1–14, 2017.
- [12] Gerhard Masselink and Jack A. Puleo. Swash-zone morphodynamics. *Continental Shelf Research*, 26(5):661–680, 2006. ISSN 02784343. doi: 10.1016/j.csr.2006.01.015.
- [13] J. A. Puleo, R. A. Beach, R. A. Holman, and J. S. Allen. Swash zone sediment suspension and transport and the importance of bore-generated turbulence. *Journal of Geophysical Research: Oceans*, 105(C7):17021–17044, 2000. ISSN 21699291. doi: 10.1029/2000jc900024.
- [14] Judith Bosboom and M.J.F Stive. *Coastal dynamics I*. Delft Academic Press, 2015.
- [15] Berry Elfrink, Daniel M. Hanes, and B. G. Ruessink. Parameterization and simulation of near bed orbital velocities under irregular waves in shallow water. *Coastal Engineering*, 53(11):915–927, 2006. ISSN 03783839. doi: 10.1016/j.coastaleng.2006.06.002.
- [16] G. Masselink, A. Kroon, and R. G.D. Davidson-Arnott. Morphodynamics of intertidal bars in wave-dominated coastal settings - A review. *Geomorphology*, 73(1-2):33–49, 2006. ISSN 0169555X. doi: 10.1016/j.geomorph.2005.06.007.

- [17] Gerhard Masselink. Formation and evolution of multiple intertidal bars on macrotidal beaches: application of a morphodynamic model. 2004. doi: 10.1016/j.coastaleng.2004.07.005.
- [18] Julian D Orford and Peter Wright. What's in a name? descriptive or genetic implications of 'ridge and runnel' topography. *Marine Geology*, 28:1–8, 1978.
- [19] Albert C. Hine. Mechanisms of berm development and resulting beach growth along a barrier spit complex. *Sedimentology*, 26(3):333–351, 1979. ISSN 13653091. doi: 10.1111/j.1365-3091.1979.tb00913.x.
- [20] Gerhard Masselink and Edward J. Anthony. Location and height of intertidal bars on macrotidal ridge and runnel beaches. *Earth Surface Processes and Landforms*, 26(7):759–774, 2001. ISSN 01979337. doi: 10.1002/esp.220.
- [21] Selma van Houwelingen, Joanna Bullard, and Gerhard Masselink. Dynamics of multiple intertidal bars over semi- diurnal and lunar tidal cycles, North Lincolnshire, England. *Earth Surface Processes and Landforms*, 33(November):1473–1490, 2007. ISSN 01979337. doi: 10.1002/esp.
- [22] Troels Aagaard, Aart Kroon, Steffen Andersen, Regin Møller Sørensen, Susanne Quartel, and Niels Vinther. Intertidal beach change during storm conditions; Egmond, The Netherlands. *Marine Geology*, 218(1-4):65–80, 2005. ISSN 00253227. doi: 10.1016/j.margeo.2005.04.001.
- [23] R. M.C. Guedes, K. R. Bryan, G. Coco, and R. A. Holman. The effects of tides on swash statistics on an intermediate beach. *Journal of Geophysical Research: Oceans*, 116(4):1–13, 2011. ISSN 21699291. doi: 10.1029/2010JC006660.
- [24] Sander Vos, Lennard Spaans, Ad Reniers, Rob Holman, Robert McCall, and Sierd de Vries. Cross-shore intertidal bar behavior along the dutch coast: Laser measurements and conceptual model. *Journal of Marine Science and Engineering*, 8(11):1–21, 2020. ISSN 20771312. doi: 10.3390/jmse8110864.
- [25] Daniel Calvete, Giovanni Coco, Albert Falqués, and Nicholas Dodd. (Un)predictability in rip channel systems. *Geophysical Research Letters*, 34(5):3–7, 2007. ISSN 00948276. doi: 10.1029/2006GL028162.
- [26] Rolf Deigaard, Nils Drønen, Jørgen Fredsøe, Jacob Hjelmager Jensen, and Mads P. Jørgensen. A morphological stability analysis for a long straight barred coast. *Coastal Engineering*, 36(3): 171–195, 1999. ISSN 03783839. doi: 10.1016/S0378-3839(99)00005-8.
- [27] R. A. Holman, G. Symonds, E. B. Thornton, and R. Ranasinghe. Rip spacing and persistence on an embayed beach. *Journal of Geophysical Research: Oceans*, 111(1):1–17, 2006. ISSN 21699291. doi: 10.1029/2005JC002965.
- [28] Robert W. Brander and Peter J. Cowell. A trend-surface technique for discrimination of surf-zone morphology: Rip current channels. *Earth Surface Processes and Landforms*, 28(8):905–918, 2003. ISSN 01979337. doi: 10.1002/esp.489.
- [29] S. T. van Houwelingen. *Cross-shore morphodynamics of intertidal sandbars*. Thesis, Loughborough University, 2005.
- [30] L. Pape, Y. Kuriyama, and B. G. Ruessink. Models and scales for cross-shore sandbar migration. *Journal of Geophysical Research: Earth Surface*, 115(3):1–13, 2010. ISSN 21699011. doi: 10.1029/2009JF001644.
- [31] Annika O'Dea, Katherine L. Brodie, and Preston Hartzell. Continuous coastal monitoring with an automated terrestrial lidar scanner. *Journal of Marine Science and Engineering*, 7(2), 2019. ISSN 20771312. doi: 10.3390/jmse7020037.
- [32] Elli Angelopoulou and John R Wright. Laser Scanner Technology Laser Scanner Technology Recommended Citation Recommended Citation. Technical report, 1999.



- [33] Sylvie Soudarissanane, Roderik Lindenbergh, Massimo Menenti, and Peter Teunissen. Scanning geometry: Influencing factor on the quality of terrestrial laser scanning points. *ISPRS Journal of Photogrammetry and Remote Sensing*, 66(4):389–399, 2011. ISSN 09242716. doi: 10.1016/j.isprsjprs.2011.01.005.
- [34] Ephraim Friedli, Robert Presl, Andreas Wieser, and Eth Zürich. Influence of atmospheric refraction on terrestrial laser scanning at long range. Technical report, 2019.
- [35] I. M.J. Van Enckevort and B. G. Ruessink. Video observations of nearshore bar behaviour. Part 1: Alongshore uniform variability. *Continental Shelf Research*, 23(5):501–512, 2003. ISSN 02784343. doi: 10.1016/S0278-4343(02)00234-0.
- [36] S. Quartel, B. G. Ruessink, and A. Kroon. Daily to seasonal cross-shore behaviour of quasi-persistent intertidal beach morphology. *Earth Surface Processes and Landforms*, 32(9):1293–1307, aug 2007. ISSN 01979337. doi: 10.1002/esp.1477. URL <http://doi.wiley.com/10.1002/esp.1477>.
- [37] Lennard Spaans. *Cross-shore morphodynamics of intertidal sandbars*. Thesis, TU Delft, 2019.
- [38] Pauli Virtanen, Ralf Gommers, Travis E. Oliphant, Matt Haberland, Tyler Reddy, David Cournapeau, Evgeni Burovski, Pearu Peterson, Warren Weckesser, Jonathan Bright, Stéfan J. van der Walt, Matthew Brett, Joshua Wilson, K. Jarrod Millman, Nikolay Mayorov, Andrew R. J. Nelson, Eric Jones, Robert Kern, Eric Larson, C J Carey, İlhan Polat, Yu Feng, Eric W. Moore, Jake VanderPlas, Denis Laxalde, Josef Perktold, Robert Cimrman, Ian Henriksen, E. A. Quintero, Charles R. Harris, Anne M. Archibald, Antônio H. Ribeiro, Fabian Pedregosa, Paul van Mulbregt, and SciPy 1.0 Contributors. SciPy 1.0: Fundamental Algorithms for Scientific Computing in Python. *Nature Methods*, 17:261–272, 2020. doi: 10.1038/s41592-019-0686-2.
- [39] Fernando J. Aguilar, Francisco Agüera, Manuel A. Aguilar, and Fernando Carvajal. Effects of terrain morphology, sampling density, and interpolation methods on grid DEM accuracy. *Photogrammetric Engineering and Remote Sensing*, 71(7):805–816, 2005. ISSN 00991112. doi: 10.14358/PERS.71.7.805.
- [40] Katharina Anders, Lukas Winiwarter, Hubert Mara, Roderik Lindenbergh, Sander E. Vos, and Bernhard Höfle. Fully automatic spatiotemporal segmentation of 3D LiDAR time series for the extraction of natural surface changes. *ISPRS Journal of Photogrammetry and Remote Sensing*, 173:297–308, 2021. ISSN 09242716. doi: 10.1016/j.isprsjprs.2021.01.015.
- [41] Katharina Anders. 4D Objects-By-Change: Spatiotemporal Segmentation of Geomorphic Surface Change from LiDAR Time Series. 2020.
- [42] Charles Truong, Laurent Oudre, and Nicolas Vayatis. Selective review of offline change point detection methods, 2020. ISSN 01651684. URL <https://doi.org/10.1016/j.sigpro.2019.107299>.
- [43] Evelien Brand, Margaret Chen, and Anne Lise Montreuil. Optimizing measurements of sediment transport in the intertidal zone. *Earth-Science Reviews*, 200(September 2018):103029, 2020. ISSN 00128252. doi: 10.1016/j.earscirev.2019.103029. URL <https://doi.org/10.1016/j.earscirev.2019.103029>.
- [44] Valeria Di Biase, Ramon F. Hanssen, and Sander E. Vos. Sensitivity of near-infrared permanent laser scanning intensity for retrieving soil moisture on a coastal beach: Calibration procedure using in situ data. *Remote Sensing*, 13(9), 2021. ISSN 20724292. doi: 10.3390/rs13091645.





## appendix A

In this appendix the full results of the 1D analysis of Chapter 5 are displayed. The figures show the timestack of channel locations over time for two different cross-shore locations, one along the cross-shore location  $y=80$  meters (Figure A.1) and one along  $y=95$  meters (Figure A.2).

Each figure consists out of four subfigures: on the left side the cross-shore location is shown, and is for this analysis constant over time. The left centre figure shows the alongshore channel locations represented by the red dotted markers, the background displays the elevation profile as a colormap in which yellow indicated high values and blue low values. The right side of the plot displays the shore relative wind direction and its daily mean and maximum amplitudes.

*As the figures are page sized the rest of this page is intendedly left blank.*

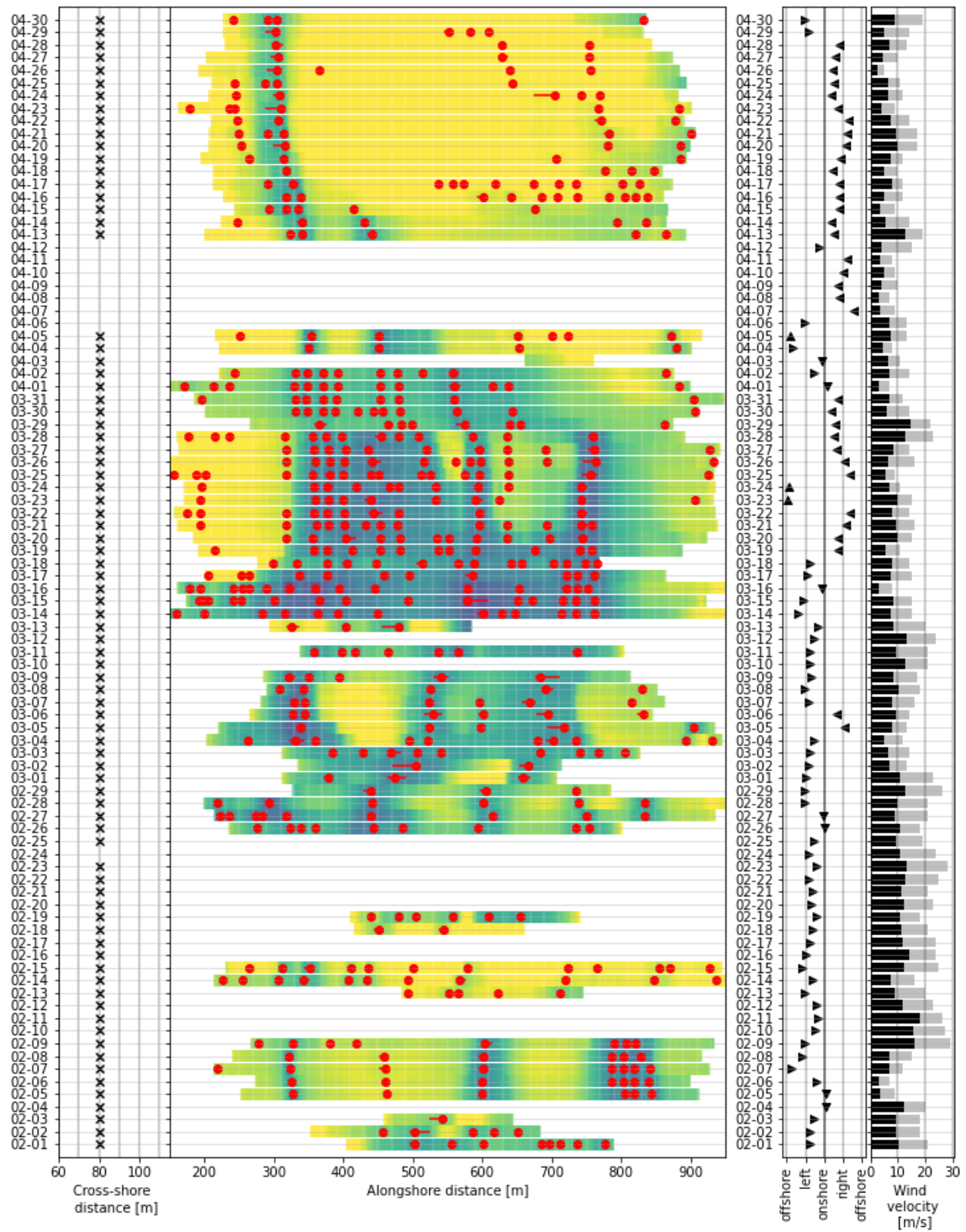


Figure A.1: The results of the 1D analysis along the cross-shore location  $y=80$  meters for the period February up till April of 2020.

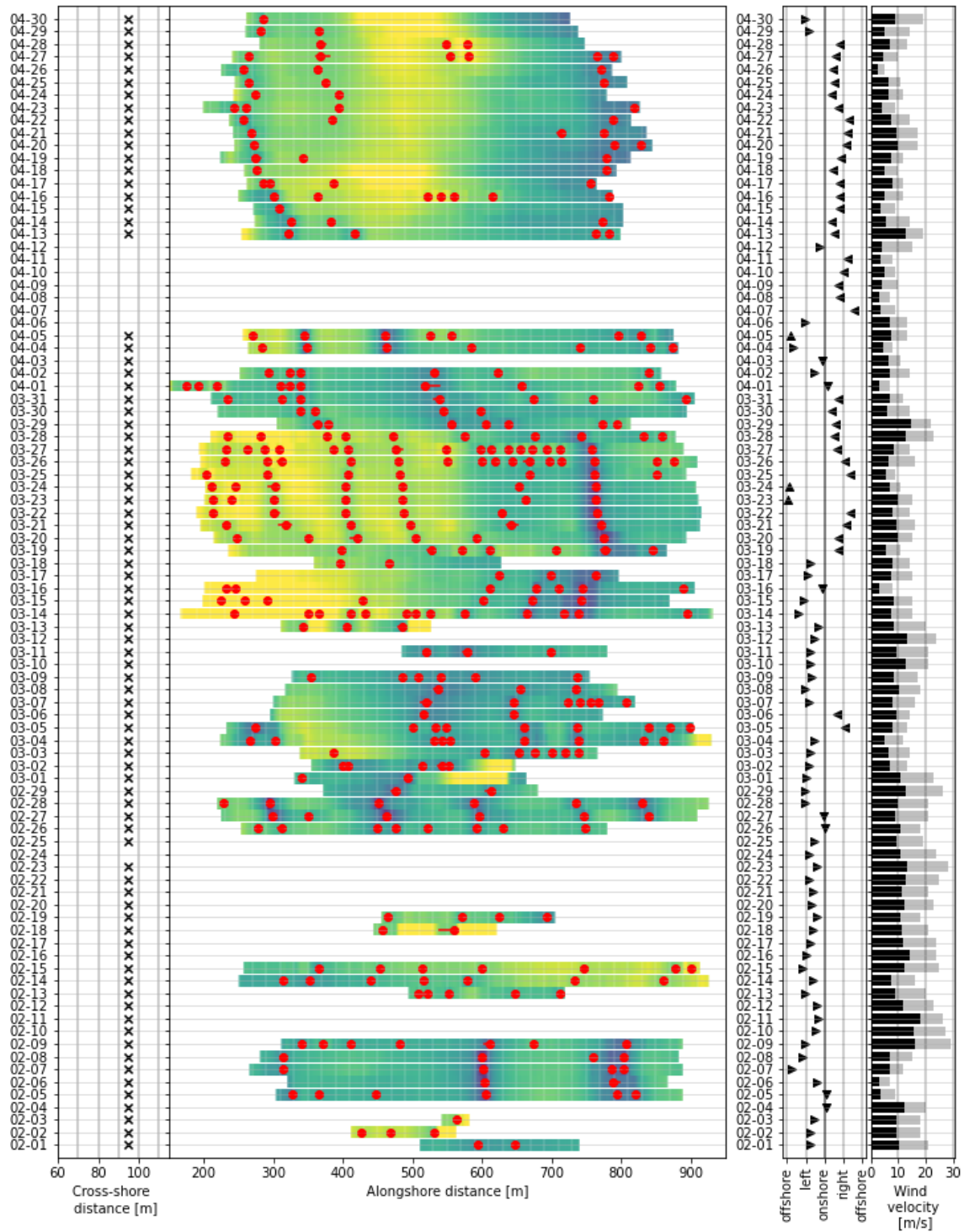


Figure A.2: The results of the 1D analysis along the cross-shore location  $y=95$  meters for the period February up till April of 2020.



# B

## appendix B

This appendix supplements Section with additional examples of comparisons between the interpolated elevation mesh and GSP measurements

